R. & M. No. 2918
(16,124)
A.R.C. Technical Report

MINISTRY OF SUPPLY

AERONAUTICAL RESEARCH COUNCIL
REPORTS AND MEMORANDA

The Calculation of the Pressure Distribution over the Surface of Two-dimensional and Swept Wings with Symmetrical Aerofoil Sections

By

J. WEBER, Dr. rer. nat.

LONDON : HER MAJESTY'S STATIONERY OFFICE
1956
PRICE 17*s* 6*d* NET

The Calculation of the Pressure Distribution over the Surface of Two-dimensional and Swept Wings with Symmetrical Aerofoil Sections

By

J. WEBER, Dr. rer. nat.

COMMUNICATED BY THE PRINCIPAL DIRECTOR OF SCIENTIFIC RESEARCH (AIR), MINISTRY OF SUPPLY

Reports and Memoranda No. 2918†

July, 1953

Summary.—A simple method is described for calculating the pressure distribution on the surface of a thick two-dimensional aerofoil section, at any incidence, in incompressible potential flow. The method has been proposed by F. Riegels and H. Wittich, Refs. 1 and 2. It is particularly suitable for practical applications, since knowledge of the section ordinates only is required. This paper gives a complete derivation of the theory including a detailed discussion of the approximations made and their effect on the accuracy of the results. The pressure distributions calculated by the present method are identical with the exact values for aerofoils of elliptic cross-section, and the numerical values for Joukowsky aerofoils agree well with the exact solutions. Calculations for a typical practical aerofoil show good agreement with the results from S. Goldstein's method, approximation III, Refs. 3 and 4.

The method is extended to sheared wings of infinite span and to the centre-section of swept wings, using the solution for zero lift from Ref. 16 and the solution for the thin wing with lift from Refs. 10 and 17.

1. *Introduction.*—The calculation of the pressure distribution over the surface of an aerofoil in inviscid flow is one of the classic problems of fluid motion theory. It has regained importance in the design of swept-wing aircraft. A large number of calculation methods have been devised for two-dimensional aerofoils, and it is now possible to choose a method which is suitable for practical application and which is not likely to be superseded in the near future. Such a method must reduce the computational work involved to a few hours, so that the method should involve only the ordinates of the given aerofoil section. Experience has shown that the possibility of ever being able to provide a single series of aerofoil sections suitable for all purposes must be ruled out, at least for swept wings. Secondly, such a method must not make exclusive use of the method of conformal transformation because it must also be applicable to cases with essentially three-dimensional flow. Therefore the method of singularities should be used since it can be readily extended to three-dimensional flow, and the terms involved are open to some physical interpretation. This latter property is particularly helpful when approximate solutions including higher order terms must be found in those cases which have a complicated flow pattern; experience has shown that the restriction to linearised theory in such cases does not often lead to adequate results.

The calculation method which provides the basis of the present paper is that of F. Riegels and H. Wittich[1,2] (1942, 1948), which is closely related to those of S. Goldstein[3,4] (1942, 1948) and B. Thwaites and E. J. Watson[5,6] (1945). The method for the two-dimensional unswept

† R.A.E. Report Aero. 2497, received 9th September, 1953.

aerofoil is explained in sections 2 and 3. Conformal transformations are used only in deriving the methods for determining the distributions of singularities, from which the velocity distributions are calculated, and secondly, in determining a few exact solutions to check the accuracy of the method. By discussing the necessary assumptions and giving an estimate of the errors in the resulting velocity distributions, it is shown that the present method is suitable for practical application.

The method is then applied to the case of the sheared wing of infinite span in section 4 and to the centre section of swept wings of large span in section 5, both with and without lift. These cases may serve as the basis of a later extension of the method to wings of any given plan-form.

A numerical method to determine the occurring integrals as sums of products of the given section ordinates and fixed coefficients, and the evaluation of these coefficients, is explained in section 6. The calculation procedure is illustrated by a worked example in section 7.

The aim of sections 2 and 3 is to provide a complete derivation of the theory. Sections 4, 5 and 7 provide most of the details needed by the reader who is only interested in the application itself.

The investigation is restricted to wings with symmetrical aerofoil sections in incompressible flow. The question of what aerofoil shapes and pressure distributions may be desirable is not considered.

2. *The Two-dimensional Aerofoil at Zero Lift.*—2.1. *General Relations.*—The aim of this and the following section is to calculate the pressure distribution on the surface of an unswept wing of infinite span. The flow around the aerofoil at incidence is here determined as the sum of two flows obtained by resolving the main stream into components parallel and normal to the chord-line. The aerofoil in a flow parallel to the chordline is treated in this section and the aerofoil in a flow normal to the chord-line is dealt with in section 3.

In any plane normal to the leading edge of the wing a system of rectangular co-ordinates x, z is used where the x-axis is along the chord with $x = 0$ at the leading edge (*see* Fig. 1). The co-ordinates are made non-dimensional by reference to the wing chord, c. The shape of the aerofoil is assumed to be known :

$$z = z(x), \qquad 0 \leqslant x \leqslant 1. \quad .. \quad .. \quad .. \quad .. \quad .. \quad .. \quad .. \quad (2\text{–}1)$$

The wing is placed in a uniform stream of velocity V_0, so that the velocity vector lies in the x, z-plane and is inclined at an angle α to the chord-line. The velocity V_0 of the main stream is resolved into its components parallel and normal to the chord-line :

$$V_{x0} = V_0 \cos \alpha \quad .. \quad .. \quad .. \quad .. \quad .. \quad .. \quad .. \quad .. \quad (2\text{–}2)$$

$$V_{z0} = V_0 \sin \alpha. \quad .. \quad .. \quad .. \quad .. \quad .. \quad .. \quad .. \quad .. \quad (2\text{–}3)$$

First we deal with the aerofoil in the uniform stream V_{x0}. This is the same problem as the aerofoil at zero lift, since we consider wings of symmetrical section shape only. The task is to determine a flow for which the given aerofoil section is a streamline, *i.e.*, a flow for which the velocity component normal to the surface is zero. This is achieved by determining a distribution of singularities at the surface of the aerofoil which produces a velocity distribution at the surface whose normal component cancels the normal velocity component of the uniform stream V_{x0}.

At the surface of the aerofoil $z(x)$, the uniform stream V_{x0} has tangential and normal components :

$$V_{t0} = \frac{V_{x0}}{\sqrt{\{1 + (dz/dx)^2\}}} \quad .. \quad .. \quad .. \quad .. \quad .. \quad .. \quad .. \quad (2\text{–}4)$$

$$V_{n0} = -\frac{V_{x0}(dz/dx)}{\sqrt{\{1 + (dz/dx)^2\}}} \quad .. \quad .. \quad .. \quad .. \quad .. \quad .. \quad .. \quad (2\text{–}5)$$

To determine the required distribution of singularities we make use of the method of conformal transformation. This is done only as an intermediate means of deriving a relation between the velocity distribution at the aerofoil surface and the section shape. It will be shown that by introducing an approximation into this relation it is possible to determine the velocity distribution without actually performing the conformal transformation.

We introduce the complex variable ζ :

$$\zeta = x + iz$$

and transform the ζ-plane conformally into a ζ^* $(= x^* + iz^*)$-plane so that the part of the ζ-plane outside the contour $z(x)$ is transformed into the ζ^*-plane outside a slit along the x^*-axis. The determination of a singularity distribution in the ζ-plane which produces a velocity distribution cancelling the normal velocity V_{n0} at the aerofoil surface is equivalent to the problem of determining a singularity distribution in the ζ^*-plane which cancels the normal velocity component $V_{n0}{}^*$ at the slit.

It is known from the theory of conformal transformations that corresponding velocity components are related by the mapping ratio $|d\zeta/d\zeta^*|$:

$$V_{n0}{}^* = V_{n0} \left|\frac{d\zeta}{d\zeta^*}\right| . \qquad \text{(2–6)}$$

The values of V_{n0} at corresponding points on the upper and lower surface of the slit are equal but of opposite sign. Such velocities can be cancelled by a source distribution at the slit. A continuous distribution of infinite source lines normal to the x, z-plane produces a velocity field which is continuous everywhere except at the position of the sources. There the velocity component normal to the sources jumps by an amount proportional to the local strength q of the sources.

The required distribution of singularities is thus a source distribution, at the slit, of strength

$$q(x^*) = -2V_{n0}{}^* . \qquad \text{(2–7)}$$

At the slit this source distribution produces the tangential velocity

$$\Delta V_t{}^*(x^*) = \frac{1}{2\pi} \int \frac{q(x^{*\prime})}{x^* - x^{*\prime}} dx^{*\prime} \qquad \text{(2–8)}$$

which corresponds to the tangential velocity ΔV_t at the surface of the aerofoil in the original ζ-plane :

$$\Delta V_t = \Delta V_t{}^* \cdot \left|\frac{d\zeta^*}{d\zeta}\right| . \qquad \text{(2–9)}$$

At the surface of the aerofoil the mapping ratio is :

$$\left|\frac{d\zeta}{d\zeta^*}\right| = \frac{ds}{dx^*} = \frac{ds}{dx} \cdot \frac{dx}{dx^*}$$

where s denotes the length of arc along the aerofoil surface. Hence,

$$\left|\frac{d\zeta}{d\zeta^*}\right| = \sqrt{\{1 + (dz/dx)^2\}} \cdot \frac{dx}{dx^*} . \qquad \text{(2–10)}$$

From equations (2–5) to (2–10) we obtain the additional velocity which the singularities produce at the aerofoil :

$$\begin{aligned}
\Delta V_t(x) &= \left|\frac{d\zeta^*}{d\zeta}\right|_x \cdot \frac{V_{x0}}{\pi} \int \left(\frac{dz/dx}{\sqrt{\{1 + (dz/dx)^2\}}}\right)_{x'(x^{*\prime})} \left|\frac{d\zeta}{d\zeta^*}\right|_{x^{*\prime}} \frac{dx^{*\prime}}{x^*(x) - x^{*\prime}} \\
&= \frac{(dx^*/dx)_x}{\sqrt{\{1 + (dz/dx)^2\}}} \cdot \frac{V_{x0}}{\pi} \int \left(\frac{dz}{dx}\right)_{x'} \frac{dx'}{dx^{*\prime}} \frac{dx^{*\prime}}{x^* - x^{*\prime}} \\
&= \frac{V_{x0}}{\sqrt{\{1 + (dz/dx)^2\}}} \cdot \frac{1}{\pi} \int_0^1 \frac{(x - x')/(x^* - x^{*\prime})}{(dx/dx^*)_x} \frac{dz}{dx'} \frac{dx'}{x - x'} . \qquad \text{(2–11)}
\end{aligned}$$

Thus the total velocity at the surface of the aerofoil in the uniform stream V_{x0} is :

$$V(x, z) = V_{t0} + \Delta V_t$$

$$= \frac{V_{x0}}{\sqrt{\{1 + (dz/dx)^2\}}} \left[1 + \frac{1}{\pi} \int_0^1 \frac{(x - x')/(x^* - x^{*\prime})}{(dx/dx^*)_x} \frac{dz}{dx'} \frac{dx'}{x - x'} \right] . \quad .. \quad (2\text{–}12)$$

For an exact determination of the integral in this equation, the relation between x^* and x is needed. *i.e.*, the transformation would have to be carried out. However, the function

$$T(x, x') = \frac{(x - x')/(x^* - x^{*\prime})}{(dx/dx^*)_x} , \quad .. \quad .. \quad .. \quad .. \quad .. \quad .. \quad .. \quad (2\text{–}13)$$

which gives the ratio between the distances of the pivotal point x and the variable point x' in the original plane $(x - x')$, and in the transformed plane $(x^* - x^{*\prime})$, related to the local mapping ratio (dx/dx^*) at the pivotal point does not differ much from unity. $T(x, x')$ is equal unity for $x' = x$ and we shall see in section 2.2 that the difference $T(x, x') - 1$ is of the order of the thickness/chord ratio t/c. Since $T(x, x')$ occurs only in the term which itself is of order t/c, an approximation for the velocity $V(x, z)$ which is correct to at least the first order in t/c may be obtained by putting

$$T(x, x') = 1. \quad .. \quad .. \quad .. \quad .. \quad .. \quad .. \quad .. \quad .. \quad .. \quad (2\text{–}14)$$

We shall discuss the accuracy of this approximation and its effect on the velocity distribution in detail in section 2.2.

With approximation (2–14) the velocity distribution (2–12) becomes :

$$V(x, z) = \frac{V_{x0}}{\sqrt{\{1 + (dz/dx)^2\}}} \left[1 + \frac{1}{\pi} \int_0^1 \frac{dz}{dx'} \frac{dx'}{x - x'} \right] . \quad .. \quad .. \quad .. \quad .. \quad (2\text{–}15)$$

This formula gives the required relation by which the velocity distribution may be determined from the given profile shape without performing the conformal transformation. A numerical method of calculating the integral

$$S^{(1)}(x) = \frac{1}{\pi} \int_0^1 \frac{dz}{dx'} \frac{dx'}{x - x'} \quad .. \quad .. \quad .. \quad .. \quad .. \quad .. \quad .. \quad .. \quad (2\text{–}16)$$

for fixed points x, as sums of products of the ordinates z at the fixed points and certain coefficients which are independent of the section shape, is described in section 6.

Before we investigate the implications of approximation (2–14), let us discuss the result in equation (2–15) in view of our aim to extend the method from the two-dimensional aerofoil to three-dimensional problems. Equations (2–12) and (2–15) are obtained from a source distribution along the slit in the transformed plane. This corresponds to a source distribution on the surface of the aerofoil in the original plane. For three-dimensional problems, the use of such surface distributions is generally out of the question since they require very complicated calculations. Since the calculations are considerably simpler when the source distributions are put on the chord-line, we interpret equation (2–15) in the following discussion as the result of a source distribution on the chord-line.

The condition that the aerofoil surface is a streamline, *i.e.*, that the total velocity component normal to the surface is zero, can be written in the form :

$$\frac{dz}{dx} = \frac{v_z(x, z)}{V_{x0} + v_x(x, z)} . \quad .. \quad .. \quad .. \quad .. \quad .. \quad .. \quad .. \quad (2\text{–}17)$$

In linear theory this condition is approximated by :

$$\frac{dz}{dx} = \frac{v_z(x, 0)}{V_{x0}} \quad .. \quad .. \quad .. \quad .. \quad .. \quad .. \quad .. \quad .. \quad .. \quad (2\text{–}18)$$

which is equivalent to the following assumptions :

(i) the velocity increment v_x is small compared with V_{x0} ;

(ii) the velocity $v_z(x, z)$ in the z-direction at the surface can be represented approximately by the velocity $v_z(x, 0)$ in the z-direction on the chord-line.

This latter approximation considerably simplifies the problem of determining a source distribution which gives the required distribution of velocity v_z. With a source distribution on the chord-line, the whole source distribution contributes to the velocity v_z at a point on the surface, but the v_z-velocity on the chordline is only dependent on the local source strength.

The required source distribution is :

$$q(x) = 2V_{x0}\frac{dz}{dx}, \quad .. \quad .. \quad .. \quad .. \quad .. \quad .. \quad .. \quad .. \quad (2\text{–}19)$$

i.e., the source strength is proportional to the local slope of the aerofoil contour.

The source distribution of the linear theory, as given by equation (2–19), satisfies the condition

$$\int_0^1 q(x)\, dx = 0 \quad .. \quad .. \quad .. \quad .. \quad .. \quad .. \quad .. \quad .. \quad .. \quad (2\text{–}20)$$

which is necessary to obtain a stagnation streamline which closes behind the source distribution, thus forming an aerofoil profile.

The source distribution of equation (2–19) also satisfies the condition that the total drag force D acting on the whole source distribution is zero. According to a theorem of A. Betz[7] (1932) about the tangential force acting on a source (which corresponds to the Kutta-Joukowsky theorem for the normal force acting on a vortex) the drag coefficient is :

$$C_D = \frac{D}{\frac{1}{2}\rho V_{x0}^2 c} = \int_0^1 \frac{V_x(x')}{V_{x0}} \frac{q(x')}{V_{x0}}\, dx' . \quad .. \quad .. \quad .. \quad .. \quad .. \quad (2\text{–}21)$$

With the approximation (i) made above : $v_x \ll V_{x0}$, i.e., $V_x = V_{x0}$, it follows :

$$C_D = 0.$$

Linear theory also makes a third assumption :

(iii) the total velocity $V(x, z)$ at the surface is represented approximately by the total V_x velocity on the chord-line.

At the chord-line, the source distribution of equation (2–19) produces a velocity v_x, along the chord, given by

$$v_x(x, 0) = \frac{V_{x0}}{\pi} \int_0^1 \frac{dz}{dx'} \frac{dx'}{x - x'} . \quad .. \quad .. \quad .. \quad .. \quad .. \quad .. \quad .. \quad (2\text{–}22)$$

The total velocity along the chord, V_x, at the chord-line, which from linear theory is also the total velocity at the surface, is thus :

$$\begin{aligned} V_x(x, 0) &= V_{x0}\left[1 + \frac{1}{\pi}\int_0^1 \frac{dz}{dx'}\frac{dx'}{x - x'}\right] \\ &= V_{x0}\,[1 + S^{(1)}(x)]. \quad .. \quad .. \quad .. \quad .. \quad .. \quad .. \quad .. \quad (2\text{–}23) \end{aligned}$$

A comparison of equations (2–15) and (2–23) gives the relation

$$V(x, z) = \frac{V_x(x, 0)}{\sqrt{\{1 + (dz/dx)^2\}}} . \quad \ldots \quad (2\text{–}24)$$

We will see in section 2.2, from calculated examples, how much the velocity distribution given by linear theory is improved on multiplying by the factor $1/\sqrt{\{1 + (dz/dx)^2\}}$. The factor is important in the stagnation region, where the approximation (i) in equation (2–18) does not hold.

Later the relation (2–24) between the velocity on the chord-line and the velocity at the surface will also be used as an approximation for the flow normal to the chord-line of the aerofoil and in the three-dimensional case. It can be interpreted by making use of the fact that the circulation around a distribution of singularities is independent of the path taken :

$$\Gamma = \oint V(x, z)\, ds = \oint V_x(x, 0)\, dx . \quad \ldots \quad (2\text{–}25)$$

In the present case $\Gamma = 0$. Equation (2–24) now means that a corresponding relation is assumed to hold locally :

$$V(x, z)\, ds = V_x(x, 0)\, dx . \quad \ldots \quad (2\text{–}26)$$

2.2. *Examples and discussion of the Accuracy of the Method.*—In deriving equation (2–15), the approximation of equation (2–14) was assumed to be admissible. We shall now check the validity of this assumption for several aerofoil shapes and determine the error in the velocity distribution resulting from this approximation by comparison with exact results. For this purpose we have actually to perform the conformal transformation. We choose the two cases of aerofoils of elliptic cross-section and Joukowsky aerofoils since for these the transformation into the slit is given by simple formulae. The ellipse and the Joukowsky profile are rather extreme cases, between which lie most practical aerofoil shapes. The usual type of aerofoil has its maximum thickness between $0{\cdot}25c$ (Joukowsky profile) and $0{\cdot}5c$ (ellipse) and has a finite trailing-edge angle† smaller than $\pi/2$, whilst Joukowsky profile and ellipse give the two extreme values of 0 and $\pi/2$. The modern type aerofoils are usually of nearly elliptical shape at the nose and up to the maximum thickness.

We begin with the elliptic aerofoil. The ellipse with axes $c = 1$ and t/c, and centre at the origin of the co-ordinate system in the ζ-plane, is transformed into a circle of radius r in the ζ_1-plane by the transformation

$$\zeta = \zeta_1 + \frac{R^2}{\zeta_1} \quad \ldots \quad (2\text{–}27)$$

with

$$R = \frac{\sqrt{\{1 - (t/c)^2\}}}{4}$$

$$r = \frac{1 + (t/c)}{4} .$$

The circle is then transformed into a slit in the ζ^*-plane by the transformation

$$\zeta^* = \zeta_1 + \frac{r^2}{\zeta_1} . \quad \ldots \quad (2\text{–}28)$$

† For sections with finite trailing-edge angle $< \pi/2$ the source distribution $q(x)$ of equation (2–19) has a finite strength at the trailing edge, which leads to a logarithmic infinity there of the integral $S^{(1)}(x)$, equation (2–16). This gives a velocity distribution with a logarithmic infinity at the trailing edge, whilst the exact value from potential theory is zero. Since the singularity is only logarithmic, its effect is negligible except for the very neighbourhood of the trailing edge where the flow conditions are considerably affected by the viscosity of the air anyhow.

We shall see later that, with the interpolation formula equation (6–4) used in the numerical method of section 6, profiles with a sharp trailing edge are replaced by profiles with a rounded trailing edge of very small radius of curvature, thus removing the singularity.

The circle in the ζ_1-plane has the equation :

$$\zeta_1 = r\,e^{i\vartheta} . \quad .. \quad .. \quad .. \quad .. \quad .. \quad .. \quad .. \quad .. \quad .. \quad (2\text{–}29)$$

Thus the real co-ordinates ξ, $\xi_1 = r\cos\vartheta$, and ξ^* for corresponding points on the ellipse, the circle and the slit are given by the relations† :

$$\xi = \left(r + \frac{R^2}{r}\right)\cos\vartheta = \tfrac{1}{2}\cos\vartheta \quad .. \quad .. \quad .. \quad .. \quad .. \quad .. \quad (2\text{–}30)$$

$$\xi^* = 2r\cos\vartheta \qquad = \frac{1 + (t/c)}{2}\cos\vartheta . \quad .. \quad .. \quad .. \quad .. \quad .. \quad (2\text{–}31)$$

This gives the relation

$$\xi = \frac{1}{1 + (t/c)} \cdot \xi^* . \quad .. \quad .. \quad .. \quad .. \quad .. \quad .. \quad .. \quad (2\text{–}32)$$

Hence,

$$T(x, x') = \frac{(\xi - \xi')/(\xi^* - \xi^{*\prime})}{(d\xi/d\xi^*)_\xi} = 1$$

and therefore the approximation (2–14) is strictly true for the whole interval of integration, and for every pivotal point x. Thus equation (2–15) gives the exact velocity distribution for the aerofoils of elliptic cross-section of any thickness/chord ratio.

This result also means that the three approximations made of linear theory, described at the end of section 2.1, are fully corrected in the case of the ellipse by multiplying $V_x(x, 0)$ by the factor $1/\sqrt{\{1 + (dz/dx)^2\}}$, as in equation (2–24).

It will prove useful later to know the explicit formula for the velocity distribution along the ellipse. Using the angle ϑ as defined by equation (2–19), the co-ordinates for the ellipse are, from equation (2–27) :

$$x = \frac{1 + \cos\vartheta}{2} \quad .. \quad .. \quad .. \quad .. \quad .. \quad .. \quad .. \quad .. \quad (2\text{–}33)$$

$$z = \tfrac{1}{2}\frac{t}{c}\sin\vartheta . \quad .. \quad .. \quad .. \quad .. \quad .. \quad .. \quad .. \quad .. \quad (2\text{–}34)$$

The integral $S^{(1)}(x)$, equation (2–16), can be calculated explicitly. It is :

$$S^{(1)}(x) = \frac{1}{\pi}\int_0^1 \frac{dz}{dx'}\frac{dx'}{x - x'} = \frac{2}{\pi}\int_0^\pi \frac{dz}{d\vartheta'}\frac{d\vartheta'}{\cos\vartheta' - \cos\vartheta}$$

$$= \frac{t}{c}\cdot\frac{1}{\pi}\int_0^\pi \frac{\cos\vartheta'\,d\vartheta'}{\cos\vartheta' - \cos\vartheta}$$

$$= \frac{t}{c} \quad .. \quad .. \quad .. \quad .. \quad .. \quad .. \quad .. \quad .. \quad .. \quad (2\text{–}35)$$

using the well-known relation (*see, e.g.*, H. Glauert[8] (1948), p. 93) :

$$\int_0^\pi \frac{\cos n\vartheta'}{\cos\vartheta' - \cos\vartheta}\,d\vartheta' = \pi\cdot\frac{\sin n\vartheta}{\sin\vartheta} . \quad .. \quad .. \quad .. \quad .. \quad .. \quad (2\text{–}36)$$

† The x-co-ordinate and the ξ-co-ordinate differ by an additive constant.

Equation (2–35), together with equation (2–23), means that in linear theory the velocity distribution along the surface of an ellipse is constant and equal to $V_{x0}(1 + t/c)$. The exact value is, from equation (2–15) :

$$V(x, z) = \frac{V_{x0}}{\sqrt{\{1 + (dz/dx)^2\}}} (1 + t/c) . \quad .. \quad .. \quad .. \quad .. \quad .. \quad .. \quad (2\text{–}37)$$

Let us now consider the Joukowsky profile. The transformation

$$\zeta = \zeta_1 + \frac{R^2}{\zeta_1} \quad .. \quad .. \quad .. \quad .. \quad .. \quad .. \quad .. \quad .. \quad .. \quad (2\text{–}38)$$

transforms the profile into a circle of radius r with the centre at $\zeta_1 = -(r - R)$ and the transformation

$$\zeta^* = \zeta_1 + (r - R) + \frac{r^2}{\zeta_1 + (r - R)} \quad .. \quad .. \quad .. \quad .. \quad .. \quad (2\text{–}39)$$

transforms the circle into a slit. The difference $r - R$ is related to the thickness/chord ratio. We introduce the parameter ε by :

$$r = (1 + \varepsilon)R . \quad .. \quad .. \quad .. \quad .. \quad .. \quad .. \quad .. \quad .. \quad (2\text{–}40)$$

It will be shown later that in linear theory :

$$\varepsilon = \frac{4}{3\sqrt{3}} \frac{t}{c} . \quad .. \quad .. \quad .. \quad .. \quad .. \quad .. \quad .. \quad .. \quad (2\text{–}41)$$

The relation between the real co-ordinates ξ and ξ^* of corresponding points along the aerofoil and the slit can be obtained from equations (2–38) to (2–40)†. We have :

$$\xi^* = 2(\xi_1 + r - R) \quad .. \quad .. \quad .. \quad .. \quad .. \quad .. \quad .. \quad (2\text{–}42)$$

$$\xi = \xi_1 + \frac{R^2\xi_1}{r^2 - (\xi_1 + r - R)^2 + \xi_1^2} \quad .. \quad .. \quad .. \quad .. \quad .. \quad (2\text{–}43)$$

$$= \left[\frac{\xi^*}{2} - (r - R)\right]\left[1 + \frac{R^2}{r^2 + (r - R)^2 - (r - R)\xi^*}\right]$$

$$\frac{\xi}{R} = \left[\frac{\xi^*}{2R} - \varepsilon\right]\left[1 + \frac{1}{1 + 2\varepsilon + 2\varepsilon^2 - \varepsilon\dfrac{\xi^*}{R}}\right] \quad .. \quad .. \quad .. \quad .. \quad (2\text{–}44)$$

with

$$-2(1 + \varepsilon) \leqslant \frac{\xi^*}{R} \leqslant 2(1 + \varepsilon) \quad .. \quad .. \quad .. \quad .. \quad .. \quad (2\text{–}45)$$

$$-2\left(1 + \frac{2\varepsilon^2}{1 + 2\varepsilon}\right) \leqslant \frac{\xi}{R} \leqslant 2 . \quad .. \quad .. \quad .. \quad .. \quad .. \quad (2\text{–}46)$$

Using equation (2–44) the function $T(x, x')$ can be calculated numerically. This has been done for profiles of 10 per cent and 20 per cent thickness/chord ratio. The results are plotted in Fig. 2. An approximate formula for $T(x, x')$ can be obtained by expressing ξ/R from equation (2–44) as a power series of ε and neglecting high order terms :

$$\frac{\xi}{R} = \frac{\xi^*}{R}(1 - \varepsilon) + \frac{\varepsilon}{2}\left(\frac{\xi^*}{R}\right)^2 - 2\varepsilon$$

$$\frac{d\xi}{d\xi^*} = 1 - \varepsilon + \varepsilon\frac{\xi^*}{R}$$

† The ξ-co-ordinates used here differ from the x-co-ordinates used otherwise in this note by additive constants.

we get

$$T(x, x') = T(\xi, \xi') = \frac{(\xi/R - \xi'/R)/(\xi^*/R - \xi^{*\prime}/R)}{(d\xi/d\xi^*)_{\xi^*}}$$

$$= 1 - \frac{\varepsilon}{2}\left(\frac{\xi^*}{R} - \frac{\xi^{*\prime}}{R}\right).$$

Finally, in x-co-ordinates referred to the chord :

$$T(x, x') = 1 - 2\varepsilon(x^* - x^{*\prime}) \quad .. \quad .. \quad .. \quad .. \quad .. \quad .. \quad .. \quad (2\text{–}47)$$

using the relation

$$c = 4R\left(1 + \frac{\varepsilon^2}{1 + 2\varepsilon}\right) \quad .. \quad .. \quad .. \quad .. \quad .. \quad .. \quad .. \quad (2\text{–}48)$$

between the chord c of the aerofoil and the radius R, which follows from equation (2–46) Equation (2–47) gives approximations for the lower and upper limits between which $T(x, x')$ varies :

$$1 - 2\varepsilon \leqslant T(x, x') \leqslant 1 + 2\varepsilon \, .$$

Fig. 2 and equation (2–47) show that the maximum error made in the integrand of equation (2–12) when using the approximation $T(x, x') = 1$ is proportional to t/c. At the pivotal point the approximation is correct and the difference $|T(x, x') - 1|$ becomes greater the further the varying point moves away from the pivotal point. This means that the contribution of the sources and sinks further away from the pivotal point is less accurately taken into account than the effect of the nearby sources. It will be shown later that the integral $S^{(1)}(x)$, equation (2–16), is of the order t/c (*see* equation (2–35) for elliptic aerofoils). The difference between the velocities calculated by the exact equation (2–12), and the approximation (2–15), is therefore of higher order than t/c.

In the following, we shall see that the error in the velocity distribution due to the approximation $T(x, x') = 1$ is considerably less than the error in the local values of the integrand. To determine the error in the velocity distribution we calculate the exact velocity distribution from the conformal transformation and compare it with the velocity distribution as given by equation (2–15). The latter is calculated by the numerical method to be described in section 6.

For the present purpose we do not determine the velocity distribution at the aerofoil by means of a source-sink distribution as in section 2, but directly from the transformation. Since the total velocity along the slit is equal to V_{x0} the velocity at the aerofoil is :

$$V = V_{x0}\left|\frac{d\zeta^*}{d\zeta}\right| .$$

The mapping ratio is given by the transformation, equations (2–38) and (2–39) :

$$V = V_{x0}\frac{|d\zeta^*/d\zeta_1|}{|d\zeta/d\zeta_1|}$$

$$= V_{x0}\frac{\left|1 - \dfrac{r^2}{(\zeta_1 + r - R)^2}\right|}{\left|1 - \dfrac{R^2}{\zeta_1^2}\right|} \, . \quad .. \quad .. \quad .. \quad .. \quad .. \quad .. \quad (2\text{–}49)$$

The circle in the ζ_1-plane which corresponds to the aerofoil has the equation

$$\zeta_1 = R_1 \, e^{i\vartheta_1} \quad .. \quad .. \quad .. \quad .. \quad .. \quad .. \quad .. \quad .. \quad .. \quad (2\text{–}50)$$

with

$$R_1 = R[\sqrt{\{1 + 2\varepsilon + (\varepsilon \cos \vartheta_1)^2\}} - \varepsilon \cos \vartheta_1] \quad \ldots \quad \ldots \quad \ldots \quad \ldots \quad (2\text{–}51)$$

From equations (2–40), (2–49) and (2–50), we obtain for the exact velocity distribution :

$$V = V_{x0} \frac{\left(\frac{R_1}{R}\right)^2 \frac{1}{1+\varepsilon} \sin \vartheta_1}{\sqrt{\left\{\sin^2 \vartheta_1 + \left[\frac{(R_1/R)^2 - 1}{2R_1/R}\right]^2\right\}}} \quad \ldots \quad \ldots \quad \ldots \quad \ldots \quad (2\text{–}52)$$

Equations (2–43), (2–48) and (2–50) give the relation between the chordwise position ξ on the aerofoil and the angle ϑ_1 :

$$\frac{\xi}{c} = \frac{1 + 2\varepsilon}{4(1 + 2\varepsilon + \varepsilon^2)} \left[\frac{R_1}{R} + \frac{1}{R_1/R}\right] \cos \vartheta_1 \quad \ldots \quad \ldots \quad \ldots \quad \ldots \quad \ldots \quad (2\text{–}53)$$

When calculating the approximate velocity distribution from equation (2–15), we need the section ordinates. These are known from the transformation. Equations (2–38), (2–48) and (2–50) give :

$$\frac{z}{c} = \frac{1 + 2\varepsilon}{4(1 + 2\varepsilon + \varepsilon^2)} \left[\frac{R_1}{R} - \frac{1}{R_1/R}\right] \sin \vartheta_1 \quad \ldots \quad \ldots \quad \ldots \quad \ldots \quad \ldots \quad (2\text{–}54)$$

For the rather extreme case of a 20 per cent thick Joukowsky aerofoil, the exact velocity distribution has been calculated numerically using equations (2–51) to (2–53). The results are given in column (*a*) of Table 1. The value $\varepsilon = 0{\cdot}1833$ was determined from equation (2–54). The values of ϑ_1 were chosen so as to give the x/c-values used in the numerical method of section 6. for $N = 16$. Table 1 also gives in column (*b*) the results of the approximate method, equation (2–15). The agreement is very good. This comparison shows that the error made in the approximation $T(x, x') = 1$ (*see* Fig. 2) does not involve any serious error in the velocity distribution.

Similar good agreement between the approximate velocity distribution calculated by the methods of conformal transformation (using the approximation III of S. Goldstein[3] (1942) and the velocity distribution calculated from equation (2–15) has been obtained for the 10 per cent thick RAE aerofoil sections 100 to 104 (*see* R. C. Pankhurst and H. B. Squire[9] (1950)). An example is shown in Fig. 3. These results prove that no further refinement of the present method is necessary.

To allow a further judgment of the accuracy of the present method, it is desirable to have another illustration of the effect of second-order terms in t/c on the velocity distribution. The Joukowsky profile gives a simple example for this. There are several possibilities of neglecting higher order terms, *e.g.*, in approximating the section shape, or in calculating the velocity distribution for the exact or the approximate section shape.

In obtaining the profile shape of the Joukowsky profile from the conformal transformation, second-order terms in ε are often neglected. This leads to a profile that is different from the exact one given by equations (2–51), (2–53) and (2–54). The approximate shape is :

$$R_1 = R[1 + \varepsilon - \varepsilon \cos \vartheta_1] \quad \ldots \quad \ldots \quad \ldots \quad \ldots \quad \ldots \quad \ldots \quad \ldots \quad (2\text{–}55)$$

$$\frac{\xi}{c} = \tfrac{1}{2} \cos \vartheta_1 \quad \ldots \quad \ldots \quad \ldots \quad \ldots \quad \ldots \quad \ldots \quad \ldots \quad \ldots \quad (2\text{–}56)$$

$$\frac{z}{c} = \tfrac{1}{2}\varepsilon(1 - \cos \vartheta_1) \sin \vartheta_1 \quad \ldots \quad \ldots \quad \ldots \quad \ldots \quad \ldots \quad \ldots \quad \ldots \quad (2\text{–}57)$$

The thickness t of the approximate profile can be determined by differentiating equation (2–57) with respect to ϑ_1. $z(\vartheta_1)$ has its maximum value for $\vartheta_1 = 120$ deg. Inserting this value into equation (2–57) we obtain

$$\frac{t}{c} = 2\frac{z_{\max}}{c} = \frac{3\sqrt{3}}{4}\varepsilon ,$$

i.e., equation (2–41). For the 20 per cent thick Joukowsky profile, equation (2–41) gives $\varepsilon = 0{\cdot}1538$, whilst the exact value from equation (2–54) is $0{\cdot}1833$.

The velocity distribution for the approximate section shape of equation (2–56) and (2–57) is from linear theory, equation (2–23) :

$$V = V_{x0}[1 + \varepsilon - 2\varepsilon \cos \vartheta_1] \quad .. \quad .. \quad .. \quad .. \quad .. \quad .. \quad (2\text{–}58)$$

since

$$S^{(1)}(\xi) = \frac{1}{\pi}\int_0^1 \frac{dz}{d\xi'}\frac{d\xi'}{\xi - \xi'} = \varepsilon\left(1 - \frac{\sin 2\vartheta_1}{\sin \vartheta_1}\right) \quad .. \quad .. \quad .. \quad .. \quad .. \quad (2\text{–}59)$$

using equation (2–36). The same result is obtained when all higher order terms in ε are neglected in equation (2–52) for the exact velocity distribution. The velocity distribution of the linear theory calculated from equation (2–58) for the 20 per cent thick Joukowsky profile is also given in Table 1, column (*c*). It is calculated for the ε-value resulting from linear theory. A comparison with the exact values in column (*a*) shows that the higher order terms have a considerable effect near the nose.

Multiplying the velocity from equation (2–58) by the factor $1/\sqrt{\{1 + (dz/dx)^2\}}$, we obtain for the approximate section shape, the velocity distribution corresponding to equation (2–15) :

$$V = V_{x0}\frac{(1 + \varepsilon)\sin \vartheta_1 - \varepsilon \sin 2\vartheta_1}{\sqrt{\{\sin^2 \vartheta_1 + \varepsilon^2(\cos 2\vartheta_1 - \cos \vartheta_1)^2\}}} . \quad .. \quad .. \quad .. \quad .. \quad (2\text{–}60)$$

Calculated values are given in column (*d*) of Table 1. A comparison of columns (*c*) and (*d*) shows the effect of the correction factor $1/\sqrt{\{1 + (dz/dx)^2\}}$. The difference between column (*b*) and (*d*) is due to the difference between the exact and the approximate section shapes.

Another approximation for the velocity distribution is obtained by retaining the terms of the lowest order in ε in the numerator and denominator of the formula for the exact velocity distribution, equation (2–52) :

$$V = V_{x0}\frac{(1 + \varepsilon)\sin \vartheta_1 - \varepsilon \sin 2\vartheta_1}{\sqrt{\{\sin^2 \vartheta_1 + \varepsilon^2(1 - \cos \vartheta_1)^2\}}} . \quad .. \quad .. \quad .. \quad .. \quad (2\text{–}61)$$

Equation (2–61) leads, of course, to two different values for the velocity distribution depending on which value of ε is used.

The ε value of the approximate section shape, equation (2–41), gives the values of column (*e*), the exact ε those of column (*f*). The results obtained from equation (2–61) show much larger variations from the exact values of column (*a*) than do the approximate values of column (*b*) calculated by the present method. This confirms that equation (2–15) gives an approximation for the velocity distribution at the surface of a symmetrical aerofoil at zero lift which takes the higher order terms well into account.

3. *The Two-dimensional Aerofoil at Incidence.*—3.1. *General Relations.*—As the next step towards our aim of calculating the velocity distribution on the surface of a two-dimensional wing at any given incidence we consider the aerofoil in a uniform stream V_{z0} normal to the chordline.

First we recapitulate the theory of the thin aerofoil, *i.e.*, the flat plate, which is an obstacle in the flow V_{z0} but not in the flow V_{x0}. In the following we require the velocity field in the neighbourhood of the plate as well as along it. This is easily determined by means of the complex

potential function for the flow around the plate. To obtain the potential function we transform the plate $-\frac{1}{2} \leqslant \xi \leqslant \frac{1}{2}$ in the ζ-plane into a circle in the ζ_1-plane :

$$\zeta = \zeta_1 + \frac{R^2}{\zeta_1}, \qquad R = \tfrac{1}{4} \quad .. \quad .. \quad .. \quad .. \quad .. \quad .. \quad .. \quad (3\text{–}1)$$

and the circle into a vertical slit in the ζ_2-plane :

$$\zeta_2 = \zeta_1 - \frac{R^2}{\zeta_1}. \quad .. \quad .. \quad .. \quad .. \quad .. \quad .. \quad .. \quad .. \quad (3\text{–}2)$$

Combining equations (3–1) and (3–2) :

$$\zeta_2 = \sqrt{(\zeta^2 - 4R^2)} = \sqrt{(\zeta^2 - \tfrac{1}{4})}. \quad .. \quad .. \quad .. \quad .. \quad .. \quad .. \quad (3\text{–}3)$$

The uniform stream, in the ζ_2-plane, which is not disturbed by the vertical plate, has the complex potential function :

$$F(\zeta_2) = \phi + i\psi = -iV_{z0}\zeta_2. \quad .. \quad .. \quad .. \quad .. \quad .. \quad .. \quad .. \quad (3\text{–}4)$$

It follows from equations (3–3) and (3–4) that the function

$$F_1(\zeta) = -iV_{z0}(\zeta^2 - \tfrac{1}{4})^{\frac{1}{2}} \quad .. \quad .. \quad .. \quad .. \quad .. \quad .. \quad .. \quad (3\text{–}5)$$

represents one possible flow around the horizontal plate. The velocity field of this flow is given by the relation :

$$\frac{dF_1(\zeta)}{d\zeta} = V_{\xi 1} - iV_{z1} = -iV_{z0}\frac{\zeta}{\sqrt{(\zeta^2 - \frac{1}{4})}}.$$

The velocity is infinite at both ends of the plate. Physical reasons do not allow an infinite velocity at the trailing edge in viscous flow. To represent the limiting case of vanishing viscosity, we require a flow pattern which fulfils the Kutta-Joukowsky condition of smooth outflow at the trailing edge.

A flow with finite velocity at the trailing edge, $\zeta = \frac{1}{2}$, is obtained by adding a flow with circulation around the plate, for which the plate is a streamline. Such a flow is obtained from the flow around the circle and the transformation of the circle into the plate, equation (3–1) :

$$\begin{aligned} F_2 &= i\frac{\Gamma}{2\pi}\ln\zeta_1 \\ &= i\frac{\Gamma}{2\pi}\ln\left[\tfrac{1}{2}\{\zeta + \sqrt{(\zeta^2 - \tfrac{1}{4})}\}\right]. \quad .. \quad .. \quad .. \quad .. \quad .. \quad (3\text{–}6) \end{aligned}$$

The potential for the general flow around the plate is then

$$F = F_1 + F_2 = -iV_{z0}\sqrt{(\zeta^2 - \tfrac{1}{4})} + i\frac{\Gamma}{2\pi}\ln\left[\tfrac{1}{2}\{\zeta + \sqrt{(\zeta^2 - \tfrac{1}{4})}\}\right]$$

and the velocity field is given by

$$\frac{dF}{d\zeta} = V_\xi - iV_z = -iV_{z0}\frac{\zeta}{\sqrt{(\zeta^2 - \frac{1}{4})}} + i\frac{\Gamma}{2\pi}\frac{1}{\sqrt{(\zeta^2 - \frac{1}{4})}}. \quad .. \quad .. \quad (3\text{–}7)$$

The velocity is zero at $\zeta = \frac{1}{2}$ if

$$\frac{\Gamma}{2\pi} = \frac{V_{z0}}{2}$$

so that

$$V_\xi - iV_z = \pm V_{z0}\sqrt{\left\{\frac{\frac{1}{2} - \zeta}{\frac{1}{2} + \zeta}\right\}}. \quad .. \quad .. \quad .. \quad .. \quad .. \quad .. \quad .. \quad (3\text{–}8)$$

At the plate the velocity in the usual co-ordinate system is :

$$V = \pm V_{z0}\sqrt{\left\{\frac{1 - x}{x}\right\}} \quad .. \quad .. \quad .. \quad .. \quad .. \quad .. \quad .. \quad (3\text{–}9)$$

the positive sign holds for the upper surface and the negative sign for the lower surface.

The velocity component normal to the plate is zero, since the plate is a streamline. The tangential velocity is of opposite sign on upper and lower surface. Such a flow pattern can be represented by a distribution of vortices (*i.e.*, infinite vortex lines normal to the x-z plane) at the position of the plate, the strength γ of which is equal to the jump in the tangential velocity when going from the upper surface to the lower surface.

$$\gamma(x) = V_{US} - V_{LS} \,. \qquad \text{(3–10)}$$

The flow around the plate is thus equal to the flow obtained by superposing a vortex distribution at the plate, of strength

$$\gamma(x) = 2V_{z0}\sqrt{\left\{\frac{1-x}{x}\right\}} \qquad \text{(3–11)}$$

on the uniform stream V_{z0}. This vortex distribution produces a v_z-component at the plate

$$v_z(x, 0) = -\frac{1}{2\pi}\int_0^1 \gamma(x')\,\frac{dx'}{x - x'} \qquad \text{(3–12)}$$

which for $\gamma(x)$ of equation (3–11) is constant along the plate, and equal to $-V_{z0}$.

We will now deal with the flow around a thick aerofoil. Again, our aim is to represent the aerofoil by a distribution of singularities which produces at the surface of the aerofoil a normal velocity distribution cancelling the normal velocity component of the uniform stream V_{z0}. To determine the required singularities we might again try to use the conformal transformation of the ζ-plane into the ζ^*-plane, which transforms the aerofoil contour into a slit. It will be shown in section 3.2 that the velocity component V_{z0}^* normal to the slit, which corresponds to the normal component V_{n0} of the uniform stream V_{z0} in the ζ-plane, is, for a general aerofoil, not constant along the slit. This means that we cannot use the vortex distribution $\gamma(x)$ of the flat plate, given in equation (3–11). Furthermore, a vortex distribution along the slit corresponds to a vortex distribution on the surface of the thick aerofoil. To allow a simple extension of the method for the two-dimensional aerofoil to three-dimensional problems, we wish to represent the aerofoil by singularities on the chord-line.

We shall determine the vortex distribution which represents the thick aerofoil as the distribution (3–11) for the flat plate and an additive term $\Delta\gamma(x)$ which depends on the section shape. We start, therefore, with the vortex distribution of equation (3–11) on the chord-line and calculate the velocity induced by it on the surface of the thick aerofoil. We obtain an approximation for the velocity field in the neighbourhood of the chord-line by expanding the right-hand side of equation (3–8) into a power series with respect to z and neglecting all higher order terms :

$$\begin{aligned} V_\xi - iV_z &= \pm V_{z0}\sqrt{\left\{\frac{\frac{1}{4} - \xi^2 - z^2 - iz}{(\frac{1}{2} + \xi)^2 + z^2}\right\}} \\ &= \pm V_{z0}\sqrt{\left\{\frac{\frac{1}{2} - \xi}{\frac{1}{2} + \xi}\right\}} - iV_{z0}\,\frac{z \,.\, \frac{1}{2}}{(\frac{1}{2} + \xi)\sqrt{(\frac{1}{4} - \xi^2)}}. \qquad \text{(3–13)} \end{aligned}$$

In the usual co-ordinate system the total V_z-velocity is :

$$V_z(x, z) = V_{z0} + v_z(x, z) = V_{z0}\,\frac{z}{x\sqrt{\{1 - (1 - 2x)^2\}}}. \qquad \text{(3–14)}$$

Equation (3–13) implies that for the vortex distribution of the flat plate the approximation

$$v_x(x, z) = v_x(x, 0) = \pm\frac{\gamma(x)}{2} \qquad \text{(3–15)}$$

is correct, if we consider only linear terms in z. (This relation corresponds to the approximation

$$v_z(x, z) = v_z(x, 0) = \pm\frac{q(x)}{2}$$

for source distributions.)

The condition that the aerofoil surface is a streamline can be written in the form (as in equation (2–17)) :

$$\frac{dz}{dx} = \frac{V_z(x, z)}{v_x(x, z)} .$$

Using the approximation (3–15) for any vortex distribution this condition can be approximated by :

$$V_z(x, z) = \frac{\gamma(x)}{2} \frac{dz}{dx} . \qquad \ldots\ldots\ldots\ldots\ldots\ldots\ldots\ldots \quad (3\text{–}16)$$

A comparison of the required V_z-velocity, equation (3–16), with the V_z-velocity produced by the vortex distribution of the flat plate, equation (3–14), shows that we need a correction $\Delta\gamma(x)$ to the vortex distribution (3–11) :

$$\gamma(x) = 2V_{z0} \sqrt{\left\{\frac{1-x}{x}\right\}} + \Delta\gamma(x) , \qquad \ldots\ldots\ldots\ldots\ldots\ldots \quad (3\text{–}17)$$

which produces the additional velocity component Δv_z, where

$$\Delta v_z(x, z) = \frac{\gamma(x)}{2} \frac{dz}{dx} - V_{z0} \frac{z}{x\sqrt{\{(1-(1-2x)^2\}}} . \qquad \ldots\ldots\ldots\ldots\ldots \quad (3\text{–}18)$$

It is, of course, again desirable to take for $\Delta\gamma(x)$ a vortex distribution on the chord-line. With $\Delta\gamma(x)$ being only a correction term, some further approximations in equation (3–18) are permissible. First, we make the approximation

$$\Delta v_z(x, z) = \Delta v_z(x, 0) ,$$

i.e., we determine a vortex distribution $\Delta\gamma(x)$ which produces the required Δv_z-velocity on the chord-line. Secondly, we make the approximation

$$\frac{\gamma(x)}{2} \frac{dz}{dx} = V_{z0} \sqrt{\left\{\frac{1-x}{x}\right\}} \frac{dz}{dx}$$

since $\Delta\gamma(x)$ is small compared with the basic term $2V_{z0}\sqrt{\{(1-x)/x\}}$. We will see later that the ratio between the two terms is of the order t/c. We obtain thus from equations (3–12) and (3–18) for $\Delta\gamma(x)$ the equation :

$$-\frac{1}{2\pi} \int_0^1 \Delta\gamma(x') \frac{dx'}{x - x'} = \Delta v_z(x, 0)$$

$$= V_{z0} \sqrt{\left\{\frac{1-x}{x}\right\}} \left(\frac{dx}{dz} - \frac{2z(x)}{1-(1-2x)^2}\right) . \qquad (3\text{–}19)$$

To solve this equation we treat the general problem of determining a vortex distribution along a flat plate which produces a velocity distribution with given components normal to the plate. For this purpose we transform the slit $-\frac{1}{2} \leqslant \xi \leqslant \frac{1}{2}$ in the ζ-plane into a circle in the ζ_1-plane by equation (3–1), and make use of the fact that in potential flow with given normal velocity $v_n^{(1)}$ at the circle, the tangential velocity $v_t^{(1)}$ is determined by the Poisson integral :

$$v_t^{(1)} = -\frac{1}{2\pi} \int_0^{2\pi} v_n^{(1)} \cot \frac{\vartheta_1' - \vartheta_1}{2} d\vartheta_1' + \text{const} . \qquad \ldots\ldots\ldots\ldots \quad (3\text{–}20)$$

The normal velocity $v_n^{(1)}$ in the ζ_1-plane is determined by the Δv_z velocity in the ζ-plane :

$$v_n^{(1)} = \Delta v_z \left|\frac{d\zeta}{d\zeta_1}\right| = 2 \sin\vartheta_1 \, \Delta v_z \ldots \qquad \ldots\ldots\ldots\ldots\ldots\ldots \quad (3\text{–}21)$$

where $\zeta_1 = \frac{1}{4} e^{i\vartheta_1}$ .. .. (3–22)

represents the circle. From the relations

$$\Delta v_\xi = - v_t^{(1)} \left| \frac{d\zeta_1}{d\zeta} \right| = - \frac{v_t^{(1)}}{2 \sin \vartheta_1}$$

and

$$\Delta\gamma = 2\Delta v_\xi$$

it follows that

$$\Delta\gamma = \frac{1}{\sin \vartheta_1} \frac{1}{\pi} \int_0^{2\pi} \Delta v_z \sin \vartheta_1' \cot \frac{\vartheta_1' - \vartheta_1}{2} d\vartheta_1' - \frac{\text{const}}{\sin \vartheta_1} .$$

Since

$$\cot \frac{\vartheta_1' - \vartheta_1}{2} = \frac{\sin \vartheta_1' + \sin \vartheta_1}{\cos \vartheta_1 - \cos \vartheta_1'}$$

we obtain, for symmetrical aerofoils for which $\Delta v_z(\vartheta_1) = \Delta v_z(2\pi - \vartheta_1)$:

$$\Delta\gamma = \frac{2}{\pi} \frac{1}{\sin \vartheta_1} \int_0^{\pi} \Delta v_z \sin \vartheta_1' \frac{\sin \vartheta_1' \, d\vartheta_1'}{\cos \vartheta_1 - \cos \vartheta_1'} - \frac{\text{const}}{\sin \vartheta_1} .$$

The angle ϑ_1 can be replaced by the chordwise co-ordinate ξ. From equations (3–1) and (3–22) :

$$\xi = \tfrac{1}{2} \cos \vartheta_1$$

so that

$$\Delta\gamma = \frac{2}{\pi} \frac{1}{\sqrt{\{1 - (2\xi)^2\}}} \int_{-\frac{1}{2}}^{+\frac{1}{2}} \Delta v_z \sqrt{\{1 - (2\xi')^2\}} \frac{d\xi'}{\xi - \xi'} - \frac{\text{const}}{\sqrt{\{1 - (2\xi)^2\}}} .$$

We are again only interested in a flow with finite velocity at the trailing edge, which means $\Delta\gamma(\xi = \frac{1}{2}) = 0$. This condition determines the value of the constant. Thus

$$\Delta\gamma = \frac{2}{\pi} \frac{1}{\sqrt{\{1 - (2\xi)^2\}}} \int_{-\frac{1}{2}}^{+\frac{1}{2}} \Delta v_z(\xi') \sqrt{\{1 - (2\xi')^2\}} \left\{ \frac{1}{\xi - \xi'} - \frac{1}{\frac{1}{2} - \xi'} \right\} d\xi'$$

which can be written as

$$\Delta\gamma = \frac{2}{\pi} \frac{1}{\sqrt{\{1 - (2\xi)^2\}}} \int_{-\frac{1}{2}}^{+\frac{1}{2}} \Delta v_z(\xi') \sqrt{\{1 - (2\xi')^2\}} \frac{1 - 2\xi}{1 - 2\xi'} \frac{d\xi'}{\xi - \xi'}$$

$$= \frac{2}{\pi} \sqrt{\left\{ \frac{1 - 2\xi}{1 + 2\xi} \right\}} \int_{-\frac{1}{2}}^{+\frac{1}{2}} \Delta v_z(\xi') \sqrt{\left\{ \frac{1 + 2\xi'}{1 - 2\xi'} \right\}} \frac{d\xi'}{\xi - \xi'} .$$

The vortex distribution which produces a given Δv_z is therefore given by the equation :

$$\Delta\gamma(x) = \frac{2}{\pi} \sqrt{\left\{ \frac{1 - x}{x} \right\}} \int_0^1 \Delta v_z(x') \sqrt{\left\{ \frac{x'}{1 - x'} \right\}} \frac{dx'}{x - x'} \quad .. \quad .. \quad .. \quad .. \quad (3–23)$$

in the usual co-ordinate system. Thus the additional vortex distribution is, from equations (3–19) and (3–23) :

$$\Delta\gamma(x) = V_{z0} \frac{2}{\pi} \sqrt{\left\{ \frac{1 - x}{x} \right\}} \int_0^1 \left[\frac{dz}{dx'} - \frac{2z(x')}{1 - (1 - 2x')^2} \right] \frac{dx'}{x - x'} . \quad .. \quad .. \quad (3–24)$$

So that the total vortex distribution which represents a thick aerofoil is :

$$\gamma(x) = 2V_{z0}\sqrt{\left\{\frac{1-x}{x}\right\}}\left\{1 + \frac{1}{\pi}\int_0^1 \left[\frac{dz}{dx'} - \frac{2z(x')}{1-(1-2x')^2}\right]\frac{dx'}{x-x'}\right\}. \quad .. \quad 3\text{–}25)$$

From the known vortex distribution we determine the velocity at the surface of the thick aerofoil by using the approximate relation (2–24) or (2–26) between the velocity on the chord-line and the velocity on the surface. The total velocity on the chord-line is :

$$V_x(x, 0) = \pm \tfrac{1}{2}\gamma(x) .$$

Hence, the velocity on the aerofoil, in a uniform stream V_{z0} normal to its chord-line, is :

$$V(x, z) = \pm \frac{V_{z0}}{\sqrt{\{1 + (dz/dx)^2\}}}\sqrt{\left\{\frac{1-x}{x}\right\}}\left\{1 + \frac{1}{\pi}\int_0^1 \left[\frac{dz}{dx'} - \frac{2z(x')}{1-(1-2x')^2}\right]\frac{dx'}{x-x'}\right\}. \quad .. \quad (3\text{–}26)$$

The accuracy of this approximate solution is discussed in section 3.2.

Having calculated the velocity distributions along the aerofoil produced by uniform streams parallel and normal to the chord-line, we can now determine the total velocity on the surface of a symmetrical aerofoil in a uniform stream V_0 inclined at an angle α to the chord-line. Since the velocity components of the main flow parallel and normal to the chord-line are

$$V_{x0} = V_0 \cos\alpha$$

$$V_{z0} = V_0 \sin\alpha$$

we obtain by combining the results of equations (2–15) and (3–26) :

$$V(x, z) = \frac{V_0}{\sqrt{\{1 + (dz/dx)^2\}}}\left\{\cos\alpha\left[1 + \frac{1}{\pi}\int_0^1 \frac{dz}{dx'}\frac{dx'}{x-x'}\right]\right.$$

$$\left. \pm \sin\alpha\sqrt{\left\{\frac{1-x}{x}\right\}}\left[1 + \frac{1}{\pi}\int_0^1 \left[\frac{dz}{dx'} - \frac{2z(x')}{1-(1-2x')^2}\right]\frac{dx'}{x-x'}\right]\right\}. \quad (3\text{–}27)$$

The positive sign holds for the upper surface, the negative sign for the lower surface.

For convenience, we use the notation of equation (2–16)

$$S^{(1)}(x) = \frac{1}{\pi}\int_0^1 \frac{dz}{dx'}\frac{dx'}{x-x'},$$

and

$$S^{(2)}(x) = \frac{dz}{dx}, \quad .. \quad .. \quad .. \quad .. \quad .. \quad .. \quad .. \quad .. \quad .. \quad (3\text{–}28)$$

$$S^{(3)}(x) = \frac{1}{\pi}\int_0^1 \left[\frac{dz}{dx'} - \frac{2z(x')}{1-(1-2x')^2}\right]\frac{dx'}{x-x'}. \quad .. \quad .. \quad .. \quad .. \quad (3\text{–}29)$$

The equation for the velocity distribution then reads :

$$\frac{V(x, z)}{V_0} = \frac{\cos\alpha[1 + S^{(1)}(x)] \pm \sin\alpha\sqrt{\left\{\frac{1-x}{x}\right\}}[1 + S^{(3)}(x)]}{\sqrt{\{1 + [S^{(2)}(x)]^2\}}}. \quad .. \quad .. \quad (3\text{–}30)$$

A method for calculating the functions $S^{(1)}(x)$, $S^{(2)}(x)$ and $S^{(3)}(x)$ numerically at certain fixed points x_ν along the chord, when the ordinates of the aerofoil section at the fixed points x_μ are given, is described in section 6. The functions are approximated by sums of products of the ordinates and certain coefficients, which are independent of the section shape :

$$S^{(1)}(x_\nu) = \sum_{\mu=1}^{N-1} s_{\mu\nu}^{(1)} z_\mu \qquad \ldots \qquad (3\text{–}31)$$

$$S^{(2)}(x_\nu) = \sum_{\mu=1}^{N-1} s_{\mu\nu}^{(2)} z_\mu \qquad \ldots \qquad (3\text{–}32)$$

$$S^{(3)}(x_\nu) = \sum_{\mu=1}^{N-1} s_{\mu\nu}^{(3)} z_\mu + s_{N\nu}^{(3)} \sqrt{\frac{\varrho}{2c}} \qquad \ldots \qquad (3\text{–}33)$$

where ρ is the radius of curvature at the leading edge. The coefficients $s_{\mu\nu}^{(1)}$, $s_{\mu\nu}^{(2)}$, $s_{\mu\nu}^{(3)}$ are determined in section 6 and calculated values are given in Tables 3 to 12. In most cases it is advisable to use Tables 7 to 9, taking 16 points along the chord.

Using Bernoulli's equation for incompressible flow the pressure coefficient along the surface of a two-dimensional aerofoil at incidence α is :

$$C_p = \frac{p - p_0}{\frac{1}{2}\rho V_0^2} = 1 - \left(\frac{V}{V_0}\right)^2$$

$$= 1 - \frac{\{\cos\alpha\,[1 + S^{(1)}(x)] \pm \sin\alpha \sqrt{\left\{\frac{1-x}{x}\right\}}[1 + S^{(3)}(x)]\}^2}{1 + [S^{(2)}(x)]^2} . \qquad \ldots \qquad (3\text{–}34)$$

At high incidence the pressure distribution on the upper surface has a high suction peak near the nose of the aerofoil and changes rapidly along the chord. In this case it is advisable, for practical calculations, to write equation (3–34) in the following form :

$$C_p = 1 - \frac{\{\cos\alpha\,[1 + S^{(1)}(x)]\,\sqrt{x} \pm \sin\alpha\,\sqrt{(1-x)}[1 + S^{(3)}(x)]\}^2}{x + \frac{1}{4}\left(\frac{dz}{d\sqrt{x}}\right)^2} . \qquad \ldots \qquad (3\text{–}35)$$

The chordwise load distribution, *i.e.*, the difference between the pressure coefficients on the upper and lower surface of the aerofoil is, from equation (3–34) :

$$\Delta C_p = C_{p\,\mathrm{US}} - C_{p\,\mathrm{LS}}$$

$$= -\,4\cos\alpha\sin\alpha \sqrt{\left\{\frac{1-x}{x}\right\}} \frac{[1 + S^{(1)}(x)][1 + S^{(3)}(x)]}{1 + [S^{(2)}(x)]^2} . \qquad \ldots \qquad \ldots \qquad (3\text{–}36)$$

The factor $\dfrac{[1 + S^{(1)}(x)][1 + S^{(3)}(x)]}{1 + [S^{(2)}(x)]^2}$ gives the correction to the flat-plate distribution due to the non-zero thickness of the aerofoil. The term $[1 + S^{(1)}(x)]$ takes into account the fact that the vortices are put into a flow with the velocity $V_0[1 + S^{(1)}(x)]$, instead of V_0 as for the thin wing. The term $[1 + S^{(3)}(x)]$ takes into account the fact that the vortex distribution for the thick wing differs from that for the thin wing. The term $\dfrac{1}{1 + [S^{(2)}(x)]^2}$ is the usual correction term to allow for the difference between the velocities at the chord-line and on the surface. The first two terms increase the load over the forward part of the aerofoil and decrease it over the rear part. The third term reduces the infinite suction at the leading edge of the thin wing to finite values.

From the load distribution, the coefficients of the normal force and the pitching moment can be obtained by integration :

$$C_N = -\int_0^1 \Delta C_p \, dx = -2\int_0^1 \Delta C_p \sqrt{x}\, d\sqrt{x} \quad \ldots \quad (3\text{–}37)$$

$$C_m = \int_0^1 \Delta C_p (x - 0{\cdot}25)\, dx = 2\int_0^1 \Delta C_p (x - 0{\cdot}25)\sqrt{x}\, d\sqrt{x}\,. \quad \ldots \quad (3\text{–}38)$$

The lift coefficient and the drag coefficient are related to the coefficients of normal force and tangential force by the equations :

$$C_L = C_N \cos\alpha - C_T \sin\alpha \quad \ldots \quad (3\text{–}39)$$

$$C_D = C_N \sin\alpha + C_T \cos\alpha\,. \quad \ldots \quad (3\text{–}40)$$

Since the drag in potential flow is zero,

$$\text{i.e., } C_D = 0\,, \quad \ldots \quad (3\text{–}41)$$

we have :

$$C_T = -\tan\alpha\, C_N \quad \ldots \quad (3\text{–}42)$$

$$C_L = \frac{C_N}{\cos\alpha}\,. \quad \ldots \quad (3\text{–}43)$$

3.2. *Examples and Discussion of the Accuracy of the Method.*—To check the validity of the approximations made in deriving equation (3–26) for the velocity distribution along the aerofoil in a uniform stream normal to its chord-line, we again calculate the exact distributions for aerofoils of elliptic cross-section and for Joukowsky profiles, and compare them with the approximate results.

The exact velocity distribution can be determined from the velocity distribution of the flat plate, equation (3–8), using the transformations given in equations (2–27) and (2–28) which transform the flat plate in the ζ^*-plane into an ellipse in the ζ-plane. To the velocity distribution of the flat plate

$$V(x^*, 0) = \pm V_{z0}\sqrt{\left\{\frac{c^*/2 - \xi^*}{c^*/2 + \xi^*}\right\}}$$

corresponds the velocity along the ellipse :

$$V(x, z) = \pm V_{z0}\sqrt{\left\{\frac{c^*/2 - \xi^*}{c^*/2 + \xi^*}\right\}}\left|\frac{d\zeta^*}{d\zeta}\right|. \quad \ldots \quad (3\text{–}44)$$

Thus, using equations (2–10) and (2–32), we obtain, for the exact velocity along the surface of elliptical aerofoils in a flow normal to the chord the equation :

$$V(x, z) = \pm V_{z0}\sqrt{\left\{\frac{1 - x}{x}\right\}}\frac{1 + t/c}{\sqrt{\{1 + (dz/dx)^2\}}}. \quad \ldots \quad (3\text{–}45)$$

To determine the approximate distribution from equation (3–26), we calculate the term $S^{(3)}(x)$, equation (3–29). It follows from equations (2–16), (2–33), (2–34), (2–35), (2–36), (3–29), that :

$$\begin{aligned} S^{(3)}(x) &= S^{(1)}(x) - \frac{2}{\pi}\int_0^1 \frac{z(x')}{1 - (1 - 2x')^2}\frac{dx'}{x - x'} \\ &= t/c - \frac{1}{\pi}\cdot\frac{t}{c}\int_0^\pi \frac{d\vartheta'}{\cos\vartheta - \cos\vartheta'} \\ &= t/c\,. \quad \ldots \quad (3\text{–}46) \end{aligned}$$

This means that equation (3–26) gives the velocity distribution of equation (3–45). In the case of elliptic aerofoils equation (3–26) is therefore exact. It has already been shown in section 2.2 that equation (2–15) gives the exact velocity distribution for a flow parallel to the chord. These two results mean that equations (3–27) or (3–30) give the exact distribution for elliptical aerofoils at any incidence α.

The pressure coefficient for aerofoils of elliptical cross-section at any incidence α to the uniform stream V_0 is therefore :

$$C_p = 1 - \left(1 + \frac{t}{c}\right)^2 \frac{\left\{\cos\alpha \pm \sin\alpha \sqrt{\left(\frac{1-x}{x}\right)}\right\}^2}{1 + \left(\frac{dz}{dx}\right)^2}$$

$$= 1 - \left(1 + \frac{t}{c}\right)^2 \frac{\left\{\cos\alpha \pm \sin\alpha \sqrt{\left(\frac{1-x}{x}\right)}\right\}^2}{1 + \left(\frac{t}{c}\right)^2 \frac{(1-2x)^2}{1-(1-2x)^2}} \quad . \quad . \quad . \quad . \quad . \quad (3\text{–}47)$$

The chordwise load distribution is

$$\Delta C_p = - \frac{4 \cos\alpha \sin\alpha \left(1 + \frac{t}{c}\right)^2}{1 + \left(\frac{t}{c}\right)^2 \frac{(1-2x)^2}{1-(1-2x)^2}} \sqrt{\left(\frac{1-x}{x}\right)} \quad . \quad . \quad . \quad . \quad . \quad (3\text{–}48)$$

To obtain the lift coefficient we integrate the load distribution :

$$C_N = \int_0^1 - \Delta C_p \, dx = 4 \cos\alpha \sin\alpha \left(1 + \frac{t}{c}\right)^2 . J$$

with

$$J = \int_0^1 \sqrt{\left(\frac{1-x}{x}\right)} \frac{x - x^2}{[1 - (t/c)^2](x - x^2) + \frac{1}{4}(t/c)^2} \, dx .$$

The integral J can be written in the form

$$J = \frac{1}{1-(t/c)^2} \int_0^1 \sqrt{\left(\frac{1-x}{x}\right)} \left[1 + \frac{1}{4} \frac{(t/c)^2}{\sqrt{\{1-(t/c)^2\}}} \left\{ \frac{1}{x - \frac{1}{2}\left[1 + \frac{1}{\sqrt{\{1-(t/c)^2\}}}\right]} \right.\right.$$

$$\left.\left. - \frac{1}{x - \frac{1}{2}\left[1 - \frac{1}{\sqrt{\{1-(t/c)^2\}}}\right]} \right\} \right] dx .$$

Using the relations

$$\int_0^1 \sqrt{\left\{\frac{1-x}{x}\right\}}\,dx = \frac{\pi}{2}$$

$$\int_0^1 \frac{1}{x-a}\sqrt{\left\{\frac{1-x}{x}\right\}}\,dx = -\pi\left[1-\sqrt{\left\{\frac{1-a}{-a}\right\}}\right]$$

for $a < 0$ or $a > 1$

we obtain

$$J = \frac{\pi}{2}\frac{1}{1+t/c}$$

and finally,

$$C_N = 2\pi(1+t/c)\cos\alpha\sin\alpha$$
$$C_L = 2\pi(1+t/c)\sin\alpha\,. \qquad \ldots\ \ldots\ \ldots\ \ldots\ \ldots\ \ldots\ \ldots \quad (3\text{–}49)$$

The last relation states that, for the same incidence, a greater lift is acting on the thick aerofoil than on the thin one. The same is true for ordinary aerofoils with sharp trailing edge. For these the correction factor to the lift of the thin aerofoil can be approximated by $1 + 0{\cdot}8\,t/c$:

$$C_L = 2\pi(1+0{\cdot}8\,t/c)\sin\alpha\,. \qquad \ldots\ \ldots\ \ldots\ \ldots\ \ldots\ \ldots \quad (3\text{–}50)$$

To make a comparison between the exact velocity distribution and the approximation of equation (3–26), for the Joukowsky profile, we first determine the exact distribution again using equation (3–44). The mapping ratio $|d\zeta^*/d\zeta|$ has been determined from the transformations (2–38) and (2–39) in equations (2–49) to (2–52). It follows from equations (2–40), (2–42), (2–45), (2–50) that

$$\frac{c^*/2-\xi^*}{c^*/2+\xi^*} = \frac{1+\varepsilon-\left(\frac{R_1}{R}\cos\vartheta_1+\varepsilon\right)}{1+\varepsilon+\left(\frac{R_1}{R}\cos\vartheta+\varepsilon\right)}.$$

The exact velocity distribution along the Joukowsky profile in a uniform stream normal to its chord-line is therefore :

$$V = V_{z0}\sqrt{\left\{\frac{1-\frac{R_1}{R}\cos\vartheta_1}{1+2\varepsilon+\frac{R_1}{R}\cos\vartheta_1}\right\}}\,\frac{\left(\frac{R_1}{R}\right)^2\frac{1}{1+\varepsilon}\sin\vartheta_1}{\sqrt{\left\{\sin^2\vartheta_1+\left[\frac{(R_1/R)^2-1}{2R_1/R}\right]^2\right\}}}\,. \quad \ldots \quad (3\text{–}51)$$

Some values calculated for the 20 per cent thick aerofoil are given in column (*a*) of Table 2.

Values for the approximate velocity distribution of the present method, equation (3–26), have been calculated by the numerical method of section 6, using the ordinates of the exact section shape given by equations (2–53) and (2–54). The comparison of the approximate values in column (*b*) with the exact values in column (*a*) shows good agreement, especially in the front part of the aerofoil. This implies that equations (3–34) and (3–35) give a good approximation to the suction peak.

Similar agreement is obtained for the 10 per cent thick sections RAE 100 to 104 between the results of the present method, equation (3–36), and the approximation III of the method by S. Goldstein, based on conformal transformation (*see* R. C. Pankhurst and H. B. Squire [9] (1950)). This is illustrated by an example given in Fig. 3.

To show again the effect of higher order terms in t/c, for the example of the Joukowsky profile, the results of some further approximations, corresponding to those of section 2.2, are given in Table 2. We consider first the approximate section shape, equations (2–56), (2–57). The integral $S^{(3)}(x)$, equation (3–29), is :

$$S^{(3)}(x) = S^{(1)}(x) - \frac{2}{\pi} \int_{-\frac{1}{2}}^{+\frac{1}{2}} \frac{z(\xi')}{1 - (2\xi'/c)^2} \frac{d\xi'}{\xi - \xi'}$$

$$= S^{(1)}(x) - \frac{\varepsilon}{\pi} \int_0^{\pi} \frac{1 - \cos \vartheta_1'}{\cos \vartheta_1 - \cos \vartheta_1'} \, d\vartheta_1'$$

$$= - \varepsilon \frac{\sin 2\vartheta_1}{\sin \vartheta_1} \quad .. \quad .. \quad .. \quad .. \quad .. \quad .. \quad .. \quad .. \quad (3\text{–}52)$$

using equations (2–36) and (2–59). The approximation to the velocity distribution V/V_{z0}, which corresponds to approximation (2–60) for V/V_{x0}, is thus by equations (2–56) and (3–26) :

$$V = V_{z0} \tan \frac{\vartheta_1}{2} \cdot \frac{\sin \vartheta_1 - \varepsilon \sin 2\vartheta_1}{\sqrt{\{\sin^2 \vartheta_1 + \varepsilon^2 (\cos 2\vartheta_1 - \cos \vartheta_1)^2\}}} \cdot \quad .. \quad .. \quad .. \quad (3\text{–}53)$$

Some values calculated from equation (3–53) are given in column (*d*) of Table 2. The differences between the values in columns (*b*) and (*d*) are only due to the difference between exact and approximate section shape, since both are based on equation (3–26).

To show the total effect of the non-zero thickness, the velocity distribution of the thin wing, equation (3–9), is also given in Table 2, column (*c*). This distribution is again the result from linear theory for the thick wing.

The approximate velocity distribution, corresponding to equation (2–61), is obtained by retaining only the terms of lowest order in ε in numerator and denominator of the formula for the exact distribution, equation (3–51) :

$$V = V_{z0} \tan \frac{\vartheta_1}{2} \cdot \frac{\sin \vartheta_1 - \varepsilon \sin 2\vartheta_1}{\sqrt{\{\sin^2 \vartheta_1 + \varepsilon^2 (1 - \cos \vartheta_1)^2\}}} \cdot \quad .. \quad .. \quad .. \quad .. \quad (3\text{–}54)$$

Velocity distributions have been calculated from equation (3–54) for the ε-value of the approximate section shape, equation (2–41), and for the exact ε. They are given in columns (*e*) and (*f*) of Table 3. A comparison of the results in columns (*e*) and (*f*) with the exact values in column (*a*) shows generally greater differences than between columns (*b*) and (*a*). This means that the approximate solution of the present method, equation (3–26), takes the higher order terms well into account.

To illustrate the accuracy of the present method, it may be of interest to compare it with a further approximation for the flow around the aerofoil in the uniform stream V_{z0}. The aerofoil in the ζ-plane is transformed into a slit in the ζ^*-plane, and at the slit an approximate vortex distribution is determined which cancels the normal velocity component resulting from the uniform stream V_{z0}.

The uniform stream V_{z0} has tangential and normal velocity components at the aerofoil :

$$V_{t0} = V_{z0} \frac{dz/dx}{\sqrt{\{1 + (dz/dx)^2\}}} \quad .. \quad .. \quad .. \quad .. \quad .. \quad .. \quad .. \quad (3\text{–}55)$$

$$V_{n0} = V_{z0} \frac{1}{\sqrt{\{1 + (dz/dx)^2\}}} \cdot \quad .. \quad .. \quad .. \quad .. \quad .. \quad .. \quad .. \quad (3\text{–}56)$$

The corresponding normal component at the slit in the ζ^*-plane is, with equation (2–10) :

$$V_{n0}^* = V_{n0}\left|\frac{d\zeta}{d\zeta^*}\right|$$

$$= V_{z0}\frac{dx}{dx^*} . \qquad \ldots\ldots\ldots\ldots\ldots\ldots\ldots\ldots \quad (3\text{–}57)$$

V_{n0}^* is exactly constant along the slit only for the elliptical aerofoil.

A vortex distribution which produces the V_{n0}^* distribution given by equation (3–57) could be determined by equation (3–23). To obtain a simple solution, let us approximate the varying V_{n0}^* distribution for the general aerofoil by a constant :

$$V_{n0}^* = V_{z0}\left(\frac{dx}{dx^*}\right)_{x_0} \qquad \ldots\ldots\ldots\ldots\ldots\ldots\ldots\ldots \quad (3\text{–}58)$$

where x_0 is any point along the chord, $0 < x_0 < 1$†. The vortex distribution of the flat plate, equation (3–11),

$$\gamma^* = 2V_{z0}\left(\frac{dx}{dx^*}\right)_{x_0}\sqrt{\left\{\frac{1 - x^*/c^*}{x^*/c^*}\right\}}$$

cancels the velocity $V_{n0}^* = V_{z0}(dx/dx^*)_{x_0}$. It produces at the slit the tangential velocity

$$\Delta V_t^* = \pm\frac{\gamma^*}{2} .$$

This corresponds to a tangential velocity at the aerofoil :

$$\Delta V_t = \Delta V_t^*\frac{d\zeta^*}{d\zeta}$$

$$= \pm\frac{(dx^*/dx)_x}{\sqrt{\{1 + (dz/dx)^2\}}}\,V_{z0}\left(\frac{dx}{dx^*}\right)_{x_0}\sqrt{\left\{\frac{1 - x^*/c^*}{x^*/c^*}\right\}}$$

which with the same approximation as in equation (3–58) becomes

$$\Delta V_t = \pm\frac{V_{z0}}{\sqrt{\{1 + (dz/dx)^2\}}}\sqrt{\left\{\frac{1 - x}{x}\right\}} .$$

The total velocity is

$$V_t = V_{t0} + \Delta V_t$$

$$= \frac{V_{z0}}{\sqrt{\{1 + (dz/dx)^2\}}}\left[\pm\sqrt{\left\{\frac{1 - x}{x}\right\}} + \frac{dz}{dx}\right] . \qquad \ldots\ldots\ldots\ldots \quad (3\text{–}59)$$

For aerofoils with finite radius at the trailing edge this velocity is not zero there. To obtain such a velocity distribution, we add a flow with circulation around the slit in the ζ^*-plane. From equations (3–6) and (3–7) :

$$\Delta V_{t1}^* = \text{const}\,\frac{1}{\sqrt{(x^*/c^*)}\,\sqrt{(1 - x^*/c^*)}}$$

and

$$\Delta V_{t1} = \text{const}\,\frac{dx^*/dx}{\sqrt{\{1 + (dz/dx)^2\}}}\,\frac{1}{\sqrt{(x^*/c^*)}\,\sqrt{(1 - x^*/c^*)}} .$$

† To illustrate the accuracy of this approximation the following limits are given. For the 10 per cent thick Joukowsky profile :

$$0{\cdot}81 < \frac{dx}{dx^*} < 1{\cdot}08$$

and for the 20 per cent thick profile :

$$0{\cdot}70 < \frac{dx}{dx^*} < 1{\cdot}18$$

With the above approximations :

$$\Delta V_{t1} = \text{const} \frac{1}{\sqrt{\{1 + (dz/dx)^2\}}} \frac{1}{\sqrt{x}\sqrt{(1-x)}} . \quad .. \quad .. \quad .. \quad .. \quad (3\text{–}60)$$

Finite velocity at the trailing edge is obtained, if

$$\text{const} = - V_{z0} \left(\frac{dz}{dx} \sqrt{(1-x)} \right)_{x=1} . \quad .. \quad .. \quad .. \quad .. \quad .. \quad .. \quad (3\text{–}61)$$

Adding the additional velocity ΔV_{t1} to the velocity given by equation (3–59) gives the total velocity for the elliptical aerofoil :

$$V = V_{z0} \frac{1}{\sqrt{\{1 + (dz/dx)^2\}}} \left[\pm \sqrt{\left\{ \frac{1-x}{x} \right\}} \pm \frac{t}{c} \sqrt{\left\{ \frac{1-x}{x} \right\}} \right] .$$

This is the same result as in equation (3–45), as was to be expected since the approximations made are correct for the elliptical aerofoil. In the general case, the approximation for the velocity distribution reads :

$$V = V_{z0} \frac{1}{\sqrt{\{1 + (dz/dx)^2\}}} \left[\pm \sqrt{\left\{ \frac{1-x}{x} \right\}} + \frac{dz}{dx} - \left(\frac{dz}{dx} \sqrt{(1-x)} \right)_{x=1} \frac{1}{\sqrt{x}\sqrt{(1-x)}} \right] . \quad (3\text{–}62)$$

For the approximate section shape of the Joukowsky aerofoil, equations (2–56), (2–57), the velocity distribution reads :

$$V = V_{z0} \tan \frac{\vartheta_1}{2} \cdot \frac{\sin \vartheta_1 - \varepsilon(\sin \vartheta_1 + \sin 2\vartheta_1)}{\sqrt{\{\sin^2 \vartheta_1 + \varepsilon^2 (\cos 2\vartheta_1 - \cos \vartheta_1)^2\}}} . \quad .. \quad .. \quad .. \quad (3\text{–}63)$$

The last column in Table 2 gives the velocity distribution for the 20 per cent thick Joukowsky profile, calculated by equation (3–63). The comparison of columns (*d*) and (*g*), which both use the approximate section shape, with the exact values in column (*a*) shows that equation (3–62) gives in this case a rather poor approximation.

Since the determination of the terms $S^{(1)}(x)$, $S^{(2)}(x)$ and $S^{(3)}(x)$ by equations (3–31), (3–32) and (3–33) is easy and quick, we can conclude from the above discussions that the present method, *i.e.*, equation (3–30), is accurate enough, as well as simple, to recommend itself for practical application.

4. *The Sheared Wing of Infinite Span.*—In this section we extend the above results for the straight two-dimensional wing to the sheared wing of infinite span by adding a flow parallel to the leading edge of the wing.

The leading edge of a wing of infinite span is sheared by an angle φ in the direction of the main stream. In addition to the usual co-ordinate system x, y, z, where the x, z-plane is parallel to the main stream, we introduce a rectangular system ξ, η, z, *see* Fig. 4, where the ξ-axis is normal to the leading edge of the wing and the η-axis parallel to it. The relation between the two systems is :

$$\left. \begin{aligned} \xi &= x \cos \varphi - y \sin \varphi \\ \eta &= x \sin \varphi + y \cos \varphi \end{aligned} \right\} . \quad .. \quad .. \quad .. \quad .. \quad .. \quad .. \quad (4\text{–}1)$$

To determine the flow around the sheared wing, we split the velocity V_0 of the main stream into its components along the ξ, η, z axes :

$$\left. \begin{aligned} V_{\xi 0} &= V_0 \cos \alpha \cos \varphi \\ V_{\eta 0} &= V_0 \cos \alpha \sin \varphi \\ V_{z0} &= V_0 \sin \alpha \end{aligned} \right\} , \quad .. \quad .. \quad .. \quad .. \quad .. \quad .. \quad .. \quad (4\text{–}2)$$

consider the aerofoil in the three uniform streams $V_{\xi 0}$, $V_{\eta 0}$ and V_{z0} separately, and finally add the resulting velocities.

The sheared wing is a stream surface of the uniform stream $V_{\eta 0}$, so that no velocity increments v_η are produced.

There remain the flow components $V_{\xi 0}$ and V_{z0}. The velocity distribution at the surface of the aerofoil in these uniform streams is the same as in a two-dimensional flow around the wing normal to its leading edge, *i.e.*, a plane $\eta = \text{const.}$, and can thus be calculated from equations (2–15) and (3–26) by replacing x by ξ and inserting $V_{\xi 0}$ and V_{z0} from equation (4–2). When applying equations (2–15) and (3–26), the ordinates z are to be measured in terms of the wing chord normal to the leading edge which is smaller by the factor $\cos\varphi$ than the wing chord c measured along wing. The effective thickness/chord ratio is thus increased to $(t/c)/\cos\varphi$.

The sheared wing in the uniform stream $V_{\xi 0}$ can be represented by a distribution of source lines parallel to the leading edge of strength

$$q(\xi) = 2V_0 \cos\varphi \frac{dz}{d\xi}.$$

This is equal to

$$q(x) = 2V_0 \frac{dz}{dx}.$$

Thus the source distribution is the same as for an unswept wing of the same section shape $z(x)$ along wind, equation (2–19). This is a consequence of the fact that for any continuous source distribution in a plane the normal velocity component at the plane depends only on the local source strength, $v_z\,(z = 0) = \pm\, q/2$.

The sheared flat plate at incidence can be represented by the same vortex distribution as the unswept plate, equation (3–11). The additional vortex distribution $\Delta\gamma$, equation (3–24), which takes account of the finite thickness is increased by the factor $1/\cos\varphi$.

These considerations give for the total velocity component in the plane $\eta = 0$:

$$\frac{V_{\eta=0}\,(x,\,z)}{V_0} = \frac{\cos\alpha\cos\varphi\left[1 + \dfrac{S^{(1)}(x)}{\cos\varphi}\right] \pm \sin\alpha\sqrt{\left\{\dfrac{1-x}{x}\right\}}\left[\dfrac{1 + S^{(3)}(x)}{\cos\varphi}\right]}{\sqrt{\left\{1 + \left(\dfrac{S^{(2)}(x)}{\cos\varphi}\right)^2\right\}}}$$

$$= \frac{\cos\alpha\,[\cos\varphi + S^{(1)}(x)] \pm \sin\alpha\sqrt{\left\{\dfrac{1-x}{x}\right\}}\left[1 + \dfrac{S^{(3)}(x)}{\cos\varphi}\right]}{\sqrt{\left\{1 + \left(\dfrac{S^{(2)}(x)}{\cos\varphi}\right)^2\right\}}} \quad .. \quad .. \quad (4\text{–}3)$$

where $S^{(1)}(x)$, $S^{(2)}(x)$ and $S^{(3)}(x)$ are determined by equations (2–16), (3–28) and (3–29) and the section shape $z(x)$ in a plane parallel to the wind direction. They can be calculated from equations (3–31), (3–32) and (3–33).

The total velocity is given by adding the velocity components $V_{\eta=0}$ and $V_{\eta 0}$:

$$\frac{V}{V_0} = \sqrt{\left\{\left(\frac{V_{\eta=0}}{V_0}\right)^2 + \left(\frac{V_{\eta 0}}{V_0}\right)^2\right\}} = \sqrt{\left\{\left(\frac{V_{\eta=0}}{V_0}\right)^2 + \cos^2\alpha\sin^2\varphi\right\}}. \quad .. \quad (4\text{–}4)$$

The velocity component in the spanwise direction v_y, which is needed for instance when calculating the shape of a streamline, is given by :

$$\frac{v_y}{V_0} = \sin\varphi \left[\frac{V_{\eta=0}}{V_0} - \cos\alpha\cos\varphi\right] . \qquad (4\text{–}5)$$

The pressure coefficient in incompressible flow is from equation (4–4) :

$$C_p = 1 - \left(\frac{V}{V_0}\right)^2$$

$$= 1 - \cos^2\alpha\sin^2\varphi - \frac{\left\{\cos\alpha[\cos\varphi + S^{(1)}(x)] \pm \sin\alpha\sqrt{\left\{\frac{1-x}{x}\right\}}\left[1 + \frac{S^{(3)}(x)}{\cos\varphi}\right]\right\}^2}{1 + \left(\frac{S^{(2)}(x)}{\cos\varphi}\right)^2} \qquad (4\text{–}6)$$

and the chordwise loading :

$$\Delta C_p = -4\cos\alpha\sin\alpha\cos\varphi\sqrt{\left\{\frac{1-x}{x}\right\}}\frac{\left[1 + \frac{S^{(1)}(x)}{\cos\varphi}\right]\left[1 + \frac{S^{(3)}(x)}{\cos\varphi}\right]}{1 + \left(\frac{S^{(2)}(x)}{\cos\varphi}\right)^2} . \qquad (4\text{–}7)$$

Integration of this distribution, equations (3–37) and (3–43), gives the lift coefficient.

As an example we quote the pressure distribution on a sheared wing of elliptic cross-section, (*see* equation (3–47)) :

$$C_p = 1 - \cos^2\alpha\sin^2\varphi - \frac{\left[1 + \frac{t/c}{\cos\varphi}\right]^2\left\{\cos\alpha\cos\varphi \pm \sin\alpha\sqrt{\left(\frac{1-x}{x}\right)}\right\}^2}{1 + \left(\frac{t/c}{\cos\varphi}\right)^2\frac{(1-2x)^2}{1-(1-2x)^2}} . \qquad (4\text{–}8)$$

This gives the lift coefficient :

$$C_L = 2\pi\left(1 + \frac{t/c}{\cos\varphi}\right)\sin\alpha\cos\varphi . \qquad (4\text{–}9)$$

The above relations show that, for wings of constant thickness/chord ratio t/c along wind, the thickness corrections become larger with increasing angle of sweep. This implies that the greater the angle of sweep the more important it is to take the higher order terms in t/c into account. For this reason, we have investigated the accuracy of the present method, in sections 2.2 and 3.2, using the rather thick Joukowsky aerofoil with $t/c = 0{\cdot}2$ as an example.

When deriving a formula for the pressure coefficient of a sheared wing by first determining the linear order terms for the sheared wing and then applying a second-order correction, like equation (2–24), some doubt may arise as to whether the correction reads

$$\frac{1}{\sqrt{\{1 + (dz/dx)^2\}}} \text{ or } \frac{1}{\sqrt{\left\{1 + \left(\frac{dz/dx}{\cos\varphi}\right)^2\right\}}} .$$

This question is solved in favour of the second alternative by the above derivation since this gives the exact answer for the aerofoil of elliptic cross-section.

Since no exact solutions exist for the three-dimensional flow around swept wings, the accuracy of approximate solutions must be determined by comparison with experimental results. Part of the differences which occur are, however, due to the viscosity of the air which is neglected in the present calculations. To show the magnitude of such effects it is desirable to have a comparison between calculated and measured pressure distributions on a sheared wing, for in this two-dimensional case we know that the present method gives sufficiently accurate results.

It is difficult to study a sheared wing of infinite aspect ratio in practice, since a sheared wing spanning a wind tunnel represents the conditions on a zig-zag wing, with the tunnel walls acting as reflection plates. The flow conditions existing near mid-semispan on a swept wing of finite aspect ratio are, however, similar to those on a sheared wing of infinite span, provided the aspect ratio is not smaller than about 4. Then the station considered is not affected by the distributions of the flow near the centre and the tips. The incidence, α, to be used in calculating the pressure distribution is the effective incidence, α_e, which differs from the given geometrical incidence, α_g, by the induced angle of incidence, α_i, produced by the trailing vortices:

$$\alpha = \alpha_e = \alpha_g - \alpha_i \quad (4\text{–}10)$$

α_i has to be obtained from a calculation of the spanwise load distribution of the wing. In the following comparisons between theoretical and experimental results, the induced incidence has been calculated by the method of D. Küchemann[10] (1953). This method excludes wings of very small aspect ratio; but it is only on wings unaffected by small aspect ratio effects that conditions exist which are similar to those on an infinite sheared wing, as discussed here.

Fig. 6 shows the chordwise load distribution measured near mid-semispan on a 45-deg swept-back wing of aspect ratio 5 (from Ref. 11), together with the calculated distribution. The calculation is made for inviscid flow. The comparison shows the effect of the boundary layer, present in the real flow, which is to reduce the circulation around the wing. The viscosity effect already exists for $\alpha \to 0$, and increases with increasing incidence. The shape of the chordwise load distribution is also altered by the boundary layer, the more so the higher the incidence. Methods for calculating the pressure distributions on two-dimensional wings in viscous flow, when the growth of the boundary layer is known, have been described by J. H. Preston[12] (1949) D. Spence[13] (1952), G. G. Brebner and J. A. Bagley[14] (1952). A good approximation for small incidence can be obtained by ignoring the alteration of the shape of the chordwise load distribution and calculating the pressure distribution for a reduced effective incidence. The latter can be found from a calculated spanwise load distribution which uses the lift slope C_L/α_e of viscous flow for infinite aspect ratio. For the quoted example: $C_L/\alpha_e = 5 \cdot 00$; inviscid flow: $C_L/\alpha_g = 3 \cdot 87$; viscous flow, $R = 1 \cdot 7 \times 10^6$: $C_L/\alpha_g = 3 \cdot 63$.

A second example is given in Fig. 8, with experimental results from Ref. 15. In this case the wing is tapered. Ref. 16, which deals with the calculations of the pressure distribution on swept wings at zero lift, contains a discussion of how the three-dimensional flow around a tapered wing can be approximated by a series of 'local two-dimensional flows'. In this approximation the pressure distribution at a station free from centre and tip interference is calculated from the formulae for the sheared wing of constant chord by taking for each point along the chord its local geometric sweep $\varphi(x)$, *i.e.*, the sweep of lines joining points of constant percentage chord ('local sweep').

In Fig. 8, two calculated curves are given for the load distribution on the thick wing. In one calculation the local angle of sweep $\varphi(x)$ was used. The other calculation was made with a constant φ along the chord, *i.e.*, the angle of sweep at mid chord, $\varphi_{c/2}$. The two different chordwise load distributions give different values of C_L/α_e ($3 \cdot 87$ for $\varphi = \varphi(x)$, $4 \cdot 12$ for $\varphi = \varphi_{c/2}$) and consequently different values of C_L/α_g ($2 \cdot 79$ for $\varphi = \varphi(x)$, $2 \cdot 91$ for $\varphi = \varphi_{c/2}$). Since the experimental results are also affected by the viscosity of the air, it is not possible to conclude from this test†

† It is difficult to isolate the taper effect from experimental results on more highly tapered wings since these are wings of small aspect ratio and it is known that, with straight constant-chord wings of small aspect ratio, the chordwise load distribution differs from the two-dimensional distribution.

whether to use the local $\varphi(x)$ or the constant $\varphi_{c/2}$. To show that the effect of this uncertainty is not large compared with the effect of the finite thickness, the load distributions of thin wings are also plotted in Figs. 6 and 8.

5. *The Centre-section of a Swept Wing.*—To solve the problem of calculating the pressure distribution at any station of a swept wing, a further basic problem is the determination of the pressure distribution at the centre section of a swept wing of infinite aspect ratio.

The solution for zero lift has been dealt with in detail in Ref. 16. The problem was solved by replacing the wing by a distribution of kinked source lines. The strength of the source distribution is, in linear theory, again given by equation (2–19), since the v_z-velocity on the chord-line produced by a continuous distribution of kinked source lines is still equal to $q/2$. This implies that in linear theory the problem is a ' quasi two-dimensional ' one, since for wings of constant section shape the source strength does not vary on lines parallel to the leading edge.

It was shown that the source distribution produces a velocity component, v_x, at the chord-line of the centre-section which differs from that on the sheared wing, $\cos\varphi . S^{(1)}(x)$, by an additive term dependent on the local source strength :

$$\begin{aligned}\frac{v_x(x, z=0)}{v_0} &= \cos\varphi . S^{(1)}(x) - f(\varphi)\cos\varphi \frac{q(x)}{2V_0} \\ &= \cos\varphi . S^{(1)}(x) - f(\varphi)\cos\varphi \frac{dz}{dx} \\ &= \cos\varphi . S^{(1)}(x) - f(\varphi)\cos\varphi . S^{(2)}(x) \qquad .. \quad .. \quad .. \quad .. \quad .. \quad (5\text{–}1)\end{aligned}$$

with

$$f(\varphi) = \frac{1}{\pi}\ln\frac{1+\sin\varphi}{1-\sin\varphi} . \qquad .. \quad .. \quad .. \quad .. \quad .. \quad .. \quad .. \quad (5\text{–}2)$$

The spanwise velocity component v_y is zero by reasons of symmetry.

To obtain the velocity distribution on the surface the correction factor of the straight wing, equation (2–24), is again applied :

$$\frac{V(x, z)}{V_0} = \frac{1 + \cos\varphi . S^{(1)}(x) - f(\varphi)\cos\varphi . S^{(2)}(x)}{\sqrt{\{1 + (S^{(2)}(x))^2\}}} \qquad .. \quad .. \quad .. \quad .. \quad .. \quad (5\text{–}3)$$

and

$$C_p = 1 - \frac{\{1 + \cos\varphi . S^{(1)}(x) - f(\varphi)\cos\varphi . S^{(2)}(x)\}^2}{1 + (S^{(2)}(x))^2} . \qquad .. \quad .. \quad .. \quad .. \quad (5\text{–}4)$$

This gives only an approximate result, but the comparison with experimental results, given in Ref. 16, shows sufficient agreement for practical purposes. There are no exact solutions available to determine the accuracy of the method, nor are there known any better approximations which might be obtained by calculating the velocity components at the surface which are produced by a source distribution of constant strength along lines parallel to the leading edge. The exact solution demands source distributions of varying strength along these lines.

The infinite source strength at the leading edge, which results from the assumptions of linear theory, leads to a pressure coefficient at the leading edge different from 1. An approximate formula, giving the correct stagnation pressure at $x = 0$, is :

$$C_p = 1 - \frac{\left\{1 + \cos\varphi . S^{(1)}(x) - f(\varphi)\cos\varphi \frac{S^{(2)}(x)}{\sqrt{\{1 + (S^{(2)}(x))^2\}}}\right\}^2}{1 + (S^{(2)}(x))^2} . \qquad .. \quad .. \quad (5\text{–}5)$$

The difference between the formulae (5–4) and (5–5) is important only within the first few per cent of the chord. This is illustrated in Fig. 5, where the pressure distributions calculated from the two equations for 12 per cent thick wings with 45-deg sweepback are plotted, together with experimental results.

Measurements of the pressure coefficient on swept wings at incidence have shown that the shape of the chordwise load distribution at the centre-section differs from that of the distribution further outboard. It has been explained in Refs. 10 and 17 that this is due to the fact that the v_z-velocity produced by a distribution $\gamma(x)$ of kinked vortex lines of infinite length and constant strength along the span is no longer given by equation (3–12) but by the relation :

$$v_z(x, z) = -\frac{1}{2\pi}\left\{\int_0^1 \gamma(x')\,\frac{dx'}{x - x'} + \sigma.\gamma(x)\right\}. \qquad \text{(5–6)}$$

The term σ can be approximated with sufficient accuracy for all points along the centre-line by the constant

$$\sigma = \pi \tan\varphi\,. \qquad \text{(5–7)}$$

The term $-\frac{1}{2\pi}\sigma.\gamma(x)$ corresponds to the term $-f(\varphi)\cos\varphi\,\frac{q(x)}{2}$ in equation (5–1) for the v_x-velocity induced by a distribution of kinked source lines of infinite length.

A solution of equation (5–6) which gives the constant v_z-velocity

$$v_z = V_{z0} = V_0 \sin\alpha$$

along the chord, is the vortex distribution

$$\gamma(x) = 2V_0 \sin\alpha \cos\varphi \left(\frac{1 - x}{x}\right)^n \qquad \text{(5–8)}$$

with

$$n = \tfrac{1}{2}\left(1 - \frac{\varphi}{\pi/2}\right). \qquad \text{(5–9)}$$

As stated in Ref. 10, the vortex distribution of equation (5–8) can also be used for the centre-section of ordinary swept wings with non-uniform loading for which $\gamma(x)$ varies along the span. The vortex distribution of equation (5–8) must now replace the distribution of equation (3–11) for the unswept flat plate.

Our aim is to find a vortex distribution corresponding to equation (3–25) which also takes into account the thickness of the aerofoil. It is impossible to determine analytically a correction to the vortex distribution of equation (5–8) similar to the $\Delta\gamma(x)$ of equation (3–24) for the straight wing. Equations (5–6) and (5–7) have not yet been verified analytically for the thin wing, but only numerically for wings of finite thickness, by calculating the downwash which a vortex distribution at $z = 0$ produces at the surface of thick aerofoils. These calculations lead to σ-values in equation (5–6) which vary slightly along the chord and with the thickness/chord ratio, and the shape of the aerofoil. These variations have been ignored in equations (5–7) and (5–8).

Tentatively, therefore, we use the factor $(1 + S^{(3)}(x))$ of the two-dimensional wing to multiply the $\gamma(x)$ of equation (5–8) :

$$\gamma(x) = 2V_0 \sin\alpha \cos\varphi \left(\frac{1 - x}{x}\right)^{n(\varphi)} (1 + S^{(3)}(x)), \qquad \text{(5–10)}$$

in analogy to the procedure for the infinite sheared wing.

Finally, applying the correction factor of equation (2–24) to the velocity at the chord-line, we obtain the pressure coefficient at the centre-section of a swept wing at incidence :

$$C_p = 1 - \left(\frac{V(x,z)}{V_0}\right)^2$$

$$= 1 - \frac{\left[\begin{array}{l} \cos\alpha\left[1 + \cos\varphi.S^{(1)}(x) - f(\varphi)\cos\varphi\,\dfrac{S^{(2)}(x)}{\sqrt{\{1+(S^{(2)}(x))^2\}}}\right] \\ \pm \sin\alpha\cos\varphi\left(\dfrac{1-x}{x}\right)^{n(\varphi)}(1+S^{(3)}(x)) \end{array}\right]^2}{1+(S^{(2)}(x))^2} \quad .. \quad (5\text{–}11)$$

and for the load distribution :

$$\Delta C_p = -4\cos\alpha\sin\alpha\cos\varphi\left(\frac{1-x}{x}\right)^{n(\varphi)} \times$$

$$\times \frac{\left[1 + \cos\varphi.S^{(1)}(x) - f(\varphi)\cos\varphi\,\dfrac{S^{(2)}(x)}{\sqrt{\{1+(S^{(2)}(x))^2\}}}\right][1+S^{(3)}(x)]}{1+(S^{(2)}(x))^2} \quad .. \quad (5\text{–}12)$$

The coefficients of the normal force and the pitching moment, C_N and C_m, can be determined from the load distribution by integration (*see* equations (3–37) and (3–38)).

The relations (3–42) and (3–43) between C_T, C_N and C_L no longer hold, since equation (3–41) is no longer true. C_T can be determined by integrating the pressure distribution :

$$C_T = \oint C_p(x)\,d(z(x)). \quad .. \quad .. \quad .. \quad .. \quad .. \quad .. \quad .. \quad .. \quad (5\text{–}13)$$

By equation (3–40) a finite drag coefficient in inviscid flow is obtained for the centre-section.

When calculating the pressure coefficient near the leading edge, equation (5–11) can be written in a form similar to equation (3–35) :

$$C_p = 1 - \frac{\left[\begin{array}{l} \cos\alpha\left[1 + \cos\varphi.S^{(1)}(x) - f(\varphi)\cos\varphi\,\dfrac{\frac{1}{2}\dfrac{dz}{d\sqrt{x}}}{\sqrt{\left\{x+\frac{1}{4}\left(\dfrac{dz}{d\sqrt{x}}\right)^2\right\}}}\right]\sqrt{x} \\ \pm \sin\alpha\cos\varphi\left(\dfrac{1-x}{x}\right)^{n(\varphi)}\sqrt{x}(1+S^{(3)}(x)) \end{array}\right]^2}{x+\frac{1}{4}\left(\dfrac{dz}{d\sqrt{x}}\right)^2} \quad . \quad (5\text{–}14)$$

For positive angles of sweep, $n(\varphi) < 0{\cdot}5$ by equation (5–9), and thus

$$\lim_{x\to 0}\left(\frac{1-x}{x}\right)^{n(\varphi)}\sqrt{x} = 0$$

which means $C_p(x = 0) = 1$ for all values of α. This is not true in reality. Approximation (5–11) may be improved by replacing the term

$$\frac{\left(\frac{1-x}{x}\right)^{n(\varphi)}}{\left[1+\left(\frac{dz}{dx}\right)^2\right]^{0.5}} \text{ by } \frac{\left(\frac{1-x}{x}\right)^{n(\varphi)}}{\left[1+\left(\frac{dz}{dx}\right)^2\right]^{n(\varphi)}}$$

which is a minor correction, except in the very neighbourhood of the leading edge. Thus the final formula for the calculation of the pressure distribution at the centre-section of a swept wing reads :

$$C_p = 1 - \left\{ \cos\alpha \left[\frac{1 + \cos\varphi . S^{(1)}(x)}{\sqrt{\{1 + (S^{(2)}(x))^2\}}} - f(\varphi)\cos\varphi \frac{S^{(2)}(x)}{1 + (S^{(2)}(x))^2} \right] \right.$$

$$\left. \pm \sin\alpha\cos\varphi \left(\frac{1-x}{x}\right)^{n(\varphi)} \frac{1 + S^3(x)}{[1 + (S^{(2)}(x))^2]^{n(\varphi)}} \right\}^2 . \quad .. \quad .. \quad .. \quad (5\text{–}15)$$

To assess the accuracy of the approximations made in the above formulae, we compare calculated values with experimental results. Fig. 10 shows that the measured pressure coefficients at the leading edge ($x = 0$) agree sufficiently well with the values calculated from equation (5–15).

Fig. 7 gives a comparison of the measured and the calculated chordwise load distribution at the centre-section of a 45-deg swept-back wing of constant chord. In the calculations, equation (5–15) was used near the leading edge and equation (5–12) away from the leading edge. The relation between the geometric incidence α_g and the effective incidence α_e, which has to be used in the above formulae, was again determined from the spanwise load distributions calculated by the method of Ref. 10. The calculation given in Fig. 7 is made for inviscid flow. The comparison in Fig. 7 shows that the shape of the measured load distribution is well approximated by the calculated curve. However, the boundary layer of the viscous flow reduces the circulation, as was the case for the section near mid-semispan (*see* Fig. 6). The experiments show, in contrast to the conditions near mid-semispan, that the boundary-layer effect at the centre-section is almost independent of the incidence. If a reduced effective incidence is used in the calculation to take account of viscosity, the agreement between the calculated and the experimental load distribution is good. From this we conclude that, for wings of moderate thickness and sweep, it is not necessary to improve the thickness correction to the vortex distribution of equation (5–8). The difference in the final results between using the factor $(1 + S^{(3)}(x))$ or $(1 + S^{(3)}(x)/\cos\varphi)$ in equation (5–10), is too small to decide which term is to be preferred.

The load distributions for the thin wing are also plotted in Figs. 6 and 7. It will be seen from the figures that the thickness effect is less at the centre than at the sheared part. This was to be expected, since in the calculations the effective thickness/chord ratio is t/c at the centre, but $(t/c)/\cos\varphi$ at the sheared part ; which implies that errors in the thickness correction are less important at the centre.

The load distribution at the centre of a highly swept wing is shown in Fig. 9, this wing however being tapered. Plan-form taper has two effects at the centre-section : (i) the local sweep varies along the chord, (ii) the absolute thickness decreases when moving away from the centre. It has been discussed in Ref. 16 that the decreasing thickness brings a reduction of the velocity at the centre-section at zero lift. In the present case, this reduction is of the order of 10 per cent of the velocity increment, *i.e.*, 1 per cent of the total velocity, which means that it may be ignored when calculating the chordwise load distribution. To take account of the varying sweep, two curves are shown for the load distribution, as in Fig. 8, one calculated with the local $\varphi(x)$ and one with constant $\varphi = \varphi_{c/2}$. The exponent n is in both calculations equal to $\frac{1}{2}(1 - \varphi_{c/2}/\frac{1}{2}\pi)$. The comparison with the experimental results in Fig. 9 does not show conclusively whether $\varphi(x)$

or $\varphi_{c/2}$ gives the better agreement. This implies that we cannot decide from this test whether to take the factor $(1 + S^{(3)}(x))$ or $(1 + S^{(3)}(x)/\cos\varphi)$ in equations (5–10) and (5–11). It must be pointed out, however, that the differences between the various methods themselves, and between calculation and experiment, are small compared with the differences between the distributions at the centre and near mid-semispan. We can, therefore, conclude that the present method provides sufficiently accurate results for most practical purposes.

6. *Numerical Method.*—The calculation of the pressure distribution on a two-dimensional aerofoil by equation (3–34), on a sheared wing by equation (4–6), and at the centre-section of a swept wing by equation (5–4) for any given section shape, requires the calculation of the three functions $S^{(1)}(x)$, $S^{(2)}(x)$, $S^{(3)}(x)$. In this section a method is described for approximating these functions, at certain fixed points x_ν along the chord, by sums of products of the section ordinates at the points x_μ and certain coefficients, which can be determined once for all ; (*see* equations (3–31), (3–32) and (3–33)). These coefficients will be calculated below.

The section shape is represented approximately by an interpolation function similar to the function introduced by H. Multhopp[18] (1938) for the spanwise load distribution. Let

$$\cos\vartheta = 2x - 1. \qquad \ldots \qquad (6\text{–}1)$$

The ordinates of the aerofoil are assumed to be known at the fixed points

$$x_\mu = x(\vartheta_\mu) \text{ with } \vartheta_\mu = \frac{\mu\pi}{N} \qquad \ldots \qquad (6\text{–}2)$$

$$z_\mu = z(x_\mu) \qquad \ldots \qquad (6\text{–}3)$$

where μ is any integer $1 \leqslant \mu \leqslant N - 1$, and N is an arbitrary even number. The position of the pivotal points x_ν is given in Table 3 for $N = 8, 16, 32$. $N = 16$ has been used for the calculated examples in Tables 1 and 2 and Figs. 3 to 10.

An interpolation function which has the values z_μ at the points x_μ is

$$z(\vartheta) = \frac{2}{N} \sum_{\mu=1}^{N-1} z_\mu \sum_{\lambda=1}^{N-1} \sin\lambda\vartheta_\mu \sin\lambda\vartheta. \qquad \ldots \qquad (6\text{–}4)$$

From this approximation it follows that :

$$\frac{dz}{dx} = -\frac{2}{\sin\vartheta}\frac{dz}{d\vartheta}$$

$$= -\frac{4}{N\sin\vartheta} \sum_{\mu=1}^{N-1} z_\mu \sum_{\lambda=1}^{N-1} \lambda \sin\lambda\vartheta_\mu \cos\lambda\vartheta. \qquad \ldots \qquad (6\text{–}5)$$

Since

$$S^{(1)}(x_\nu) = \frac{1}{\pi}\int_0^1 \frac{dz}{dx'}\frac{dx'}{x_\nu - x'} = \frac{2}{\pi}\int_0^\pi \frac{dz}{d\vartheta'}\frac{d\vartheta'}{\cos\vartheta' - \cos\vartheta_\nu} \qquad \ldots \qquad (6\text{–}6)$$

by equation (2–16), we obtain, for the coefficients $s_{\mu\nu}^{(1)}$ in equation (3–31), the relation :

$$s_{\mu\nu}^{(1)} = \frac{4}{\pi N} \sum_{\lambda=1}^{N-1} \lambda \sin\lambda\vartheta_\mu \int_0^\pi \cos\lambda\vartheta' \frac{d\vartheta'}{\cos\vartheta' - \cos\vartheta_\nu}$$

using relation (2–36)

$$s_{\mu\nu}^{(1)} = \frac{4}{N\sin\vartheta_\nu} \sum_{\lambda=1}^{N-1} \lambda \sin\lambda\vartheta_\mu \sin\lambda\vartheta_\nu$$

$$= \frac{2}{N\sin\vartheta_\nu} \sum_{\lambda=1}^{N-1} \lambda[\cos\lambda(\vartheta_\mu - \vartheta_\nu) - \cos\lambda(\vartheta_\mu + \vartheta_\nu)]. \qquad \ldots \qquad (6\text{–}7)$$

Also $$\sum_{\lambda=1}^{N-1} \lambda \cos \lambda\vartheta = \frac{(N-1)\cos N\vartheta - N\cos(N-1)\vartheta + 1}{2(\cos\vartheta - 1)} \quad \ldots \quad (6\text{–}8)$$

This relation is true for $N = 2$ and can be proved by induction from $N-2$ to $N-1$. Now since

$$\sin N(\vartheta_\mu + \vartheta_\nu) = \sin N(\vartheta_\mu - \vartheta_\nu) = 0 \quad \ldots \quad (6\text{–}9)$$

$$\cos N(\vartheta_\mu + \vartheta_\nu) = \cos N(\vartheta_\mu - \vartheta_\nu) = (-1)^{\mu-\nu}, \quad \ldots \quad (6\text{–}10)$$

it follows from equations (6–7) to (6–10), that

$$s_{\mu\nu}^{(1)} = \frac{(-1)^{\mu-\nu} - 1}{N \sin\vartheta_\nu} \left\{ \frac{1}{1 - \cos(\vartheta_\mu - \vartheta_\nu)} - \frac{1}{1 - \cos(\vartheta_\mu + \vartheta_\nu)} \right\}$$

$$= \frac{(-1)^{\mu-\nu} - 1}{N} \frac{2\sin\vartheta_\mu}{[1 - \cos(\vartheta_\mu - \vartheta_\nu)][1 - \cos(\vartheta_\mu + \vartheta_\nu)]}$$

$$= \frac{(-1)^{\mu-\nu} - 1}{N} \frac{2\sin\vartheta_\mu}{(\cos\vartheta_\mu - \cos\vartheta_\nu)^2} \quad \ldots \quad (6\text{–}11)$$

For $\mu = \nu$, from equation (6–7)

$$s_{\nu\nu}^{(1)} = \frac{2}{N\sin\vartheta_\nu} \left\{ \sum_{\lambda=1}^{N-1} \lambda - \sum_{\lambda=1}^{N-1} \lambda \cos\lambda(2\vartheta_\nu) \right\}$$

$$= \frac{1}{\sin\vartheta_\nu} \left\{ N - 1 - \frac{1 - \cos 2\vartheta_\nu}{\cos 2\vartheta_\nu - 1} \right\}$$

$$= \frac{N}{\sin\vartheta_\nu} \quad \ldots \quad (6\text{–}12)$$

The coefficients $s_{\mu\nu}^{(1)}$ have been calculated from equations (6–11) and (6–12) for $N = 8$, 16 and 32, and are given in Tables 4, 7 and 10.

For high lift the pressure distribution over an aerofoil has its peak very close to the leading edge and is changing rapidly along the chord, so that the pressure coefficient is needed at points other than the fixed x_ν in that region, (*see* Table 3). The function $S^{(1)}(x)$ is a continuous function of x, which can be determined graphically at any x-value from its value at the fixed x_ν, if it is also known at $x = 0$.

The pivotal points $x = 0$ and $x = 1$, *i.e.*, $\nu = N$ and $\nu = 0$ are not included in equation (3–31) since for aerofoils with a rounded nose,

$$S^{(1)}(x=0) = \lim_{x\to 0} \int_0^1 \frac{dz}{dx'} \frac{dx'}{x - x'}$$

$$\neq \int_0^1 \frac{dz}{dx'} \frac{dx'}{-x'}.$$

In determining $S^{(1)}(x=0)$ we make use of the fact that, for aerofoils with elliptic cross-section, $S^{(1)}(x)$ is known along the whole chord ; (*see* equation (2–35)).

$$S^{(1)}(x) = \frac{t_{\text{ellipse}}}{c} = \sqrt{\left(2\,\frac{\varrho_e}{c}\right)} \quad \ldots \quad (6\text{–}13)$$

where ϱ is the nose radius. We subtract from the aerofoil ordinates those of the elliptic aerofoil with the same nose radius :

$$\Delta z = z(x) - \sqrt{\left(2\,\frac{\varrho}{c}\right)}\sqrt{(x - x^2)}\,. \qquad \text{(6–14)}$$

With conventional aerofoil sections we can assume that Δz has no term which varies linearly with x. Then :

$$\lim_{x \to 0} \int_0^1 \frac{d\Delta z}{dx'}\,\frac{dx'}{x - x'} = \int_0^1 \frac{d\Delta z}{dx'}\,\frac{dx'}{-x'}$$

$$= \sum_{\mu=1}^{N-1} s_{\mu N}^{(1)}\,\Delta z_\mu$$

with

$$s_{\mu N}^{(1)} = \frac{(-1)^\mu - 1}{N}\,\frac{2\sin\vartheta_\mu}{(1 + \cos\vartheta_\mu)^2} \qquad \text{(6–15)}$$

from equation (6–11). For the ellipse

$$z_{e\mu} = \tfrac{1}{2}\frac{t_e}{c}\sin\vartheta_\mu$$

$$\sum_{\mu=1}^{N-1} s_{\mu N}^{(1)}\,z_{e\mu} = \frac{t_e}{c}\sum_{\mu=1}^{N-1}\frac{(-1)^\mu - 1}{N}\,\frac{\sin^2\vartheta_\mu}{(1 + \cos\vartheta_\mu)^2}$$

$$= \frac{t_e}{c}\,[-(N-1)]\,.$$

Since

$$S^{(1)}(x = 0) = \sqrt{\left(2\,\frac{\varrho}{c}\right)} + \sum_{\mu=1}^{N-1} s_{\mu N}^{(1)}\,z_\mu - \sum_{\mu=1}^{N-1} s_{\mu N}^{(1)} z_{e\mu}\,.$$

we obtain finally,

$$S^{(1)}(x = 0) = N\sqrt{\left(2\,\frac{\varrho}{c}\right)} + \sum_{\mu=1}^{N-1} s_{\mu N}^{(1)}\,z_\mu\,. \qquad \text{(6–16)}$$

The term $S^{(2)}(x)$, which is equal to the slope of the profile surface dz/dx, can of course, be determined graphically from a plotting of z against x, but it can also be determined numerically at the points x_ν. From equation (6–5) we obtain a relation for the coefficients $s_{\mu\nu}^{(2)}$ in equation (3–32) :

$$s_{\mu\nu}^{(2)} = -\frac{4}{N\sin\vartheta_\nu}\sum_{\lambda=1}^{N-1}\lambda\sin\lambda\vartheta_\mu\cos\lambda\vartheta_\nu$$

$$= -\frac{2}{N\sin\vartheta_\nu}\left\{\sum_{\lambda=1}^{N-1}\lambda[\sin\lambda(\vartheta_\mu + \vartheta_\nu) + \sin\lambda(\vartheta_\mu - \vartheta_\nu)]\right\}. \qquad \text{(6–17)}$$

Now

$$\sum_{\lambda=1}^{N-1}\lambda\sin\lambda\vartheta = \frac{(N-1)\sin N\vartheta - N\sin(N-1)\vartheta}{2(\cos\vartheta - 1)}\,. \qquad \text{(6–18)}$$

This relation is true for $N = 2$ and can be proved by induction from $N - 2$ to $N - 1$. Using equation (6–9) it follows from equations (6–17) and (6–18) that :

$$s_{\mu\nu}^{(2)} = \frac{(-1)^{\mu-\nu}}{\sin\vartheta_\nu}\left\{\frac{\sin(\vartheta_\mu+\vartheta_\nu)}{1-\cos(\vartheta_\mu+\vartheta_\nu)}+\frac{\sin(\vartheta_\mu-\vartheta_\nu)}{1-\cos(\vartheta_\mu-\vartheta_\nu)}\right\}$$

$$= \frac{(-1)^{\mu-\nu}}{\sin\vartheta_\nu}\left\{\cot\frac{\vartheta_\mu+\vartheta_\nu}{2}+\cot\frac{\vartheta_\mu-\vartheta_\nu}{2}\right\}$$

$$= -2\frac{(-1)^{\mu-\nu}\sin\vartheta_\mu}{\sin\vartheta_\nu\,[\cos\vartheta_\mu-\cos\vartheta_\nu]}. \quad .. \quad .. \quad .. \quad .. \quad .. \quad (6\text{–}19)$$

For $\mu = \nu$, from equation (6–17) :

$$s_{\nu\nu}^{(2)} = -\frac{2}{N\sin\vartheta_\nu}\sum_{\lambda=1}^{N-1}\lambda\sin 2\lambda\vartheta_\nu$$

$$= \frac{1}{\sin\vartheta_\nu}\frac{\sin 2\vartheta_\nu}{1-\cos 2\vartheta_\nu}$$

$$= \frac{\cot\vartheta_\nu}{\sin\vartheta_\nu}. \quad .. \quad .. \quad .. \quad .. \quad .. \quad .. \quad .. \quad .. \quad .. \quad (6\text{–}20)$$

The coefficients $s_{\mu\nu}^{(2)}$ calculated from equations (6–19) and (6–20) for $N = 8$, 16 and 32, are given in Tables 5, 8 and 11.

In calculating the pressure distribution at high incidence by equation (3–35) the derivative of z with respect to $\sqrt{x}$, $dz/d\sqrt{x}$, is needed. This term can be determined graphically from a plotting of z against $\sqrt{x}$ or by plotting

$$\left(\frac{dz}{d\sqrt{x}}\right)_{x_\nu} = 2\sqrt{x_\nu}\,S_\nu^{(2)} \quad .. \quad .. \quad .. \quad .. \quad .. \quad .. \quad .. \quad .. \quad (6\text{–}21)$$

taking into account the relation

$$\left(\frac{dz}{d\sqrt{x}}\right)_{x=0} = \sqrt{\left(2\frac{\varrho}{c}\right)}. \quad .. \quad .. \quad .. \quad .. \quad .. \quad .. \quad .. \quad .. \quad (6\text{–}22)$$

The values of $dz/d\sqrt{x}$ determined by equation (6–21), or directly from plotting $z(\sqrt{x})$, need not fully agree since equation (6–5) is only an approximation. The magnitude of the difference can be seen by comparing the exact nose radius with the radius of the approximate section shape, equation (6–4). From equation (6–5) it follows that

$$\left(\frac{dz}{d\sqrt{x}}\right)_{x=0} = \left(\frac{dz}{d\vartheta}\right)_{\vartheta=\pi}\left(\frac{-2}{\sin\vartheta}2\sqrt{x}\right)_{x\to 0}$$

$$= -2\left(\frac{dz}{d\vartheta}\right)_{\vartheta=\pi}$$

$$= -2\sum_{\mu=1}^{N-1}(-1)^\mu\frac{\sin\vartheta_\mu}{1+\cos\vartheta_\mu}z_\mu. \quad .. \quad .. \quad .. \quad .. \quad .. \quad (6\text{–}23)$$

Now

$$-\sum_{\mu=1}^{N-1}(-1)^\mu\frac{\sin^2\vartheta_\mu}{1+\cos\vartheta_\mu} = 1{\cdot}0$$

so that for the elliptic aerofoil, $z = \frac{1}{2}(t/c)\sin\vartheta$, $(dz/d\sqrt{x})_{x=0} = t/c$, which agrees with the exact value. For the 20 per cent thick Joukowsky profile equation (6–23) gives $dz/d\sqrt{x} = 0{\cdot}2991$ whilst

the exact value from equation (2–53), (2–54) is 0·2992. For the 10 per cent thick RAE 101 section the nose radius from equation (6–23) is $\varrho/c = 0{\cdot}00760$, whilst the figure given in Ref. 9 is $\varrho/c = 0{\cdot}00763$. These figures show that for aerofoil sections which have a shape similar to an ellipse for the first few per cent of the chord, the interpolation formula (6–4) is adequate.

If there is an appreciable difference between the two values for the nose radius, one might improve the interpolation formula (6–4) by adding the term $(c_1/N)\sin N\vartheta$† :

$$z(\vartheta) = \frac{2}{N}\sum_{\mu=1}^{N-1} z_\mu \sum_{\lambda=1}^{N-1} \sin\lambda\vartheta_\mu \sin\lambda\vartheta + \frac{c_1}{N}\sin N\vartheta \quad . \quad . \quad . \quad . \quad . \quad . \quad (6\text{–}24)$$

This interpolation function gives the required values at x_μ :

$$z(\vartheta_\mu) = z_\mu$$

Thus

$$\frac{dz}{d\vartheta} = \frac{2}{N}\sum_{\mu=1}^{N-1} z_\mu \sum_{\lambda=1}^{N-1} \lambda \sin\lambda\vartheta_\mu \cos\lambda\vartheta + c_1 \cos N\vartheta \quad . \quad . \quad . \quad . \quad . \quad . \quad (6\text{–}25)$$

The constant c_1 can be chosen so that

$$\left(\frac{dz}{d\vartheta}\right)_{\vartheta=\pi} = \sum_{\mu=1}^{N-1} (-1)^\mu \frac{\sin\vartheta_\mu}{1+\cos\vartheta_\mu} z_\mu + c_1$$

$$= -\sqrt{\left(\frac{\varrho}{2c}\right)} \quad . \quad . \quad . \quad . \quad . \quad . \quad . \quad . \quad . \quad . \quad (6\text{–}26)$$

The improved interpolation function (6–24) gives the same values for $S^{(1)}(x_\nu)$ as equation (6–4), since the additional term to $S^{(1)}(x)$ is by equations (6–6) and (6–25)

$$\Delta S^{(1)}(\vartheta) = \frac{2c_1}{\pi}\int_0^\pi \cos N\vartheta' \frac{d\vartheta'}{\cos\vartheta' - \cos\vartheta} = 2c_1 \frac{\sin N\vartheta}{\sin\vartheta} \quad . \quad . \quad . \quad . \quad . \quad . \quad (6\text{–}27)$$

which is zero for $\vartheta = \vartheta_\nu$. At the leading edge, $\vartheta = \pi$, $\Delta S^{(1)}(x) = -2Nc_1$, i.e., N times the difference between the values of $\sqrt{(2\varrho/c)}$ for the given section and the interpolation function, which means $S^{(1)}(x=0)$ is given by equation (6–16).

The amendment of the interpolation function $z(\vartheta)$, given by equation (6–24), is a special case of the amendment suggested by J. Weissinger[19] (1952) for calculating the spanwise load distribution using the calculation method by H. Multhopp[18].

The interpolation function equation (6–4) gives the correct ordinates at fixed points x_μ. It may be desirable to calculate the function $S^{(1)}(x)$ from an interpolation function $z(\vartheta)$ which has the correct value z_a at one further arbitrary point x_a. Let an asterisk denote the values of z and $S^{(1)}$. obtained from equation (6–4). The new interpolation function is

$$z(\vartheta) = z^*(\vartheta) + \frac{z(\vartheta_a) - z^*(\vartheta_a)}{\sin N\vartheta_a}\sin N\vartheta \quad . \quad . \quad . \quad . \quad . \quad . \quad (6\text{–}28)$$

By equation (6–6),

$$S^{(1)}(\vartheta) = S^{(1)*}(\vartheta) + \frac{z(\vartheta_a) - z^*(\vartheta_a)}{\sin N\vartheta_a}\frac{2N\sin N\vartheta}{\sin\vartheta} \quad . \quad . \quad . \quad . \quad . \quad . \quad (6\text{–}29)$$

---

†An additive term which does not alter the section shape of equation (6–4) at the trailing edge is $(c_1/N)\sin N\vartheta.\frac{1}{2}(1-\cos\vartheta)$. To obtain the required nose radius the constant c_1 is to be determined by equation (6–26). The additive term alters the value of $S^{(1)}(x)_\mu$ slightly. It follows from equation (6–6) that the additional term to $S^{(1)}(x_\nu)$ is :

$$\Delta S^{(1)}(x_\nu) = -\frac{(-1)^\nu}{N} c_1$$

This correction can usually be neglected since c_1 is generally small.

Therefore, $\sin N\vartheta_\nu = 0$ by equation (6–2),

$$S^{(1)}(\vartheta_\nu) = S^{(1)*}(\vartheta_\nu)$$

i.e., the values of $S^{(1)}(x)$ at the points x_ν are not altered by using a further point for determining the interpolation function. This is not so for points $\vartheta \neq \vartheta_\nu$. In particular,

$$S^{(1)}(\vartheta_a) = S^{(1)*}(\vartheta_a) + [z(\vartheta_a) - z^*(\vartheta_a)]\frac{2N}{\sin\vartheta_a}.$$

This relation can be written in the form :

$$S^{(1)}(\vartheta_a) = s_{aa}^{(1)} z_a + \sum_{\mu=1}^{N-1} s_{\mu a}^{(1)} z_\mu \qquad \ldots\ldots\ldots\ldots\ldots\ldots\ldots \quad (6\text{–}30)$$

where

$$s_{aa}^{(1)} = \frac{2N}{\sin\vartheta_a} \qquad \ldots\ldots\ldots\ldots\ldots\ldots\ldots\ldots \quad (6\text{–}31)$$

$$s_{\mu a}^{(1)} = \frac{-4}{N\sin\vartheta_a} \sum_{\lambda=1}^{N-1} (N-\lambda)\sin\lambda\vartheta_\mu \sin\lambda\vartheta_a \qquad \ldots\ldots\ldots\ldots\ldots \quad (6\text{–}32)$$

by equations (3–31), (6–4) and (6–7). It follows from equation (6–8) and the relation

$$\sum_{\lambda=1}^{N-1} \cos\lambda\vartheta = \frac{\cos(N-1)\vartheta - \cos N\vartheta + \cos\vartheta - 1}{2(1-\cos\vartheta)} \qquad \ldots\ldots\ldots\ldots \quad (6\text{–}33)$$

that

$$s_{\mu a}^{(1)} = \frac{2\sin\vartheta_\mu}{N[\cos\vartheta_\mu - \cos\vartheta_a]}[\cos N\vartheta_\mu \cos N\vartheta_a - 1]$$

$$= -\frac{4\sin\vartheta_\mu}{N[\cos\vartheta_\mu - \cos\vartheta_a]} \cdot A_{\mu a} \qquad \ldots\ldots\ldots\ldots\ldots\ldots \quad (6\text{–}34)$$

where

$$A_{\mu a} = \begin{cases} \sin^2\dfrac{N\vartheta_a}{2} \text{ for } \mu \text{ even} \\ \cos^2\dfrac{N\vartheta_a}{2} \text{ for } \mu \text{ odd}. \end{cases}$$

If in particular $\vartheta_a = \{(2\varkappa + 1)/2N\}\pi$, i.e., at a pivotal point of the system with $2N$ points taken along the chord, then $A_{\mu a} = \frac{1}{2}$ for all μ and a, and the coefficients $s_{\mu a}^{(1)}$ by equation (6–34) agree with those by equation (6–11) calculated for $2N$.

We have stated in section 2.2 that the interpolation function, equation (6–4), replaces the given section by one with a finite radius ϱ_T at the trailing edge. We will now determine this radius. We have

$$\left(\frac{dz}{d\sqrt{(1-x)}}\right)_{x=1} = \sqrt{\left\{2\,\frac{\varrho_T}{c}\right\}} = 2\left(\frac{dz}{d\vartheta}\right)_{\vartheta=0}$$

$$= -2\sum_{\mu=1}^{N-1} (-1)^\mu \frac{\sin\vartheta_\mu}{1-\cos\vartheta_\mu} z_\mu . \qquad \ldots\ldots\ldots\ldots\ldots \quad (6\text{–}35)$$

For the 10 per cent thick RAE 101 section, equation (6–35) gives $\varrho_T/c = 0{\cdot}000009$, which means there is no important difference between the given section and the approximation.

Finally, we have to determine the coefficients $s_{\mu\nu}^{(3)}$ and $s_{N\nu}^{(3)}$ in equation (3–33) for the function $S^{(3)}(x_\nu)$†. From equations (2–16) and (3–29) :

$$S^{(3)}(x) = S^{(1)}(x) - \frac{2}{\pi}\int_0^1 \frac{z(x')}{1-(1-2x')^2}\frac{dx'}{x-x'}$$

$$= S^{(1)}(x) + \frac{2}{\pi}\int_0^\pi \frac{z(\vartheta')}{\sin\vartheta'}\frac{d\vartheta'}{\cos\vartheta'-\cos\vartheta}. \qquad \text{(6–36)}$$

To evaluate the integral we approximate to the value of $z(\vartheta)/\sin\vartheta$ by an interpolation function. The function

$$\frac{z(\vartheta)}{\sin\vartheta} = \sin\vartheta\left[\frac{2}{N}\sum_{\mu=1}^{N-1}\frac{z_\mu}{\sin^2\vartheta_\mu}\sum_{\lambda=1}^{N-1}\sin\lambda\vartheta_\mu\sin\lambda\vartheta\right]$$
$$-\sqrt{\left(\frac{\varrho}{2c}\right)}\frac{1}{N}\frac{\sin N\vartheta}{\sin\vartheta}\frac{1-\cos\vartheta}{2} \qquad \text{(6–37)}$$

has the required values at $\vartheta = \vartheta_\mu$, since $\sin(N\vartheta_\mu) = 0$. It also has the correct value at the leading edge, $\vartheta = \pi$:

$$\left(\frac{z(\vartheta)}{\sin\vartheta}\right)_\pi = -\left(\frac{dz}{d\vartheta}\right)_\pi = \sqrt{\left(\frac{\varrho}{2c}\right)}$$

since

$$\left(\frac{\sin N\vartheta}{\sin\vartheta}\frac{1-\cos\vartheta}{2}\right)_{\vartheta=\pi} = -N.$$

At the trailing edge, $\vartheta = 0$, equation (6–37) gives $z(\vartheta)/\sin\vartheta = 0$, which is correct for aerofoils with a sharp trailing edge.

By equations (6–36) and (6–37), we obtain, for the coefficients $s_{\mu\nu}^{(3)}$ in equation (3–33), the relation :

$$s_{\mu\nu}^{(3)} = s_{\mu\nu}^{(1)} + \frac{4}{\pi N}\frac{1}{\sin^2\vartheta_\mu}\sum_{\lambda=1}^{N-1}\sin\lambda\vartheta_\mu\int_0^\pi \sin\lambda\vartheta'\frac{\sin\vartheta'\,d\vartheta'}{\cos\vartheta'-\cos\vartheta_\nu}.$$

By means of equation (2–36) :

$$\int_0^\pi \sin\lambda\vartheta'\frac{\sin\vartheta'\,d\vartheta'}{\cos\vartheta'-\cos\vartheta_\nu} = \tfrac{1}{2}\int_0^\pi \frac{\cos(\lambda-1)\vartheta' - \cos(\lambda+1)\vartheta'}{\cos\vartheta'-\cos\vartheta_\nu}d\vartheta'$$

$$= \frac{\pi}{2}\frac{\sin(\lambda-1)\vartheta_\nu - \sin(\lambda+1)\vartheta_\nu}{\sin\vartheta_\nu}$$

$$= -\pi\cos\lambda\vartheta_\nu. \qquad \text{(6–38)}$$

Thus :

$$s_{\mu\nu}^{(3)} = s_{\mu\nu}^{(1)} - \frac{4}{N}\frac{1}{\sin^2\vartheta_\mu}\sum_{\lambda=1}^{N-1}\sin\lambda\vartheta_\mu\cos\lambda\vartheta_\nu$$

$$= s_{\mu\nu}^{(1)} - \frac{2}{N}\frac{1}{\sin^2\vartheta_\mu}\sum_{\lambda=1}^{N-1}[\sin\lambda(\vartheta_\mu+\vartheta_\nu) + \sin\lambda(\vartheta_\mu-\vartheta_\nu)] \qquad \text{(6–39)}$$

†For aerofoils with finite radius of curvature ϱ_T at the trailing edge, a further term $s_{0\nu}^{(3)}\sqrt{(\varrho_T/2c)}$ has to be added in equation (3–33). Except for the elliptic aerofoil, such aerofoils are of little practical interest.

Now $\sum_{\lambda=1}^{N-1} \sin \lambda\vartheta = \dfrac{\sin (N-1)\vartheta - \sin N\vartheta + \sin \vartheta}{2(1-\cos\vartheta)}$ .. .. (6–40)

which may be proved by induction. Using equations (6–9), (6–10) and (6–40) we obtain :

$$s_{\mu\nu}^{(3)} = s_{\mu\nu}^{(1)} - \frac{1-(-1)^{\mu-\nu}}{N\sin^2\vartheta_\mu}\left\{\frac{\sin(\vartheta_\mu+\vartheta_\nu)}{1-\cos(\vartheta_\mu+\vartheta_\nu)} + \frac{\sin(\vartheta_\mu-\vartheta_\nu)}{1-\cos(\vartheta_\mu-\vartheta_\nu)}\right\}$$

and hence

$$s_{\mu\nu}^{(3)} = s_{\mu\nu}^{(1)} + \frac{2}{N}\frac{1-(-1)^{\mu-\nu}}{\sin\vartheta_\mu}\frac{1}{\cos\vartheta_\mu - \cos\vartheta_\nu} . \quad .. .. (6–41)$$

For $\mu = \nu$, we obtain from equation (6–39)

$$s_{\nu\nu}^{(3)} = s_{\nu\nu}^{(1)} - \frac{2}{N}\frac{1}{\sin^2\vartheta_\nu}\sum_{\lambda=1}^{N-1}\sin\lambda(2\vartheta_\nu)$$

$$= s_{\nu\nu}^{(1)} - \frac{2}{N}\frac{1}{\sin^2\vartheta_\nu}\frac{\sin[(N-1)2\vartheta_\nu] + \sin 2\vartheta_\nu}{2(1-\cos 2\vartheta_\nu)}$$

$$= s_{\nu\nu}^{(1)} . \quad .. .. (6–42)$$

By equations (6–36) and (6–37), the coefficient $s_{N\nu}^{(3)}$ in equation (3–33) is :

$$s_{N\nu}^{(3)} = -\frac{1}{\pi N}\int_0^\pi \frac{\sin N\vartheta'}{\sin\vartheta'}\frac{1-\cos\vartheta'}{\cos\vartheta' - \cos\vartheta_\nu}\,d\vartheta'$$

$$= -\frac{1}{2\pi N}\int_0^\pi \frac{2\sin N\vartheta' - \sin(N-1)\vartheta' - \sin(N+1)\vartheta'}{\sin\vartheta'}\frac{d\vartheta'}{\cos\vartheta' - \cos\vartheta_\nu} . \quad .. (6–43)$$

Now

$$J_\lambda = \int_0^\pi \frac{\sin\lambda\vartheta'}{\sin\vartheta'}\frac{d\vartheta'}{\cos\vartheta' - \cos\vartheta}$$

$$= \pi\frac{1-\cos\lambda\vartheta_\nu}{\sin^2\vartheta_\nu} \qquad \text{for } \lambda \text{ even}$$

$$= \pi\frac{\cos\vartheta_\nu - \cos\lambda\vartheta_\nu}{\sin^2\vartheta_\nu} \qquad \text{for } \lambda \text{ odd} .. .. (6–44)$$

as can be proved by the relation

$$J_\lambda = J_{\lambda-2} + 2\pi\frac{\sin(\lambda-1)\vartheta_\nu}{\sin\vartheta_\nu}$$

which follows from

$$\frac{\sin\lambda\vartheta}{\sin\vartheta} = \frac{\sin(\lambda-2)\vartheta}{\sin\vartheta} + 2\cos(\lambda-1)\vartheta .$$

Therefore, using the equations

$$J_1 = 0$$

$$J_2 = 2\pi$$

N being an even number, equations (6–43) and (6–44) give

$$s_{N\nu}^{(3)} = \frac{(-1)^\nu - 1}{N} \cdot \frac{1}{1 + \cos \vartheta_\nu} . \qquad \text{(6–45)}$$

The coefficients $s_{\mu\nu}^{(3)}$ have been calculated from equations (6–41), (6–42) and (6–45) for $N = 8$, 16 and 32, and are given in Tables 6, 9 and 12.

Using these coefficients $S^{(3)}(x)$ can be calculated for the points x_ν. Since $S^{(3)}(x)$ is a continuous function, its values at points other than x_ν can be determined graphically if $S^{(3)}(x = 0)$ is known.

In determining $S^{(3)}(x = 0)$ we apply the same procedure as in determining $S^{(1)}(x = 0)$. We subtract from the given section ordinates those of an elliptic aerofoil, equation (6–14), and make use of the fact that for elliptic aerofoils

$$S^{(3)}(x) = \frac{t_{\text{ellipse}}}{c} = \sqrt{\left(2\frac{\varrho_e}{c}\right)}, \qquad \text{(6–46)}$$

(*see* equation (3–46)). For the Δz of equation (6–14) we have

$$\Delta S^{(3)}(x = 0) = \sum_{\mu=1}^{N-1} s_{\mu N}^{(3)} \Delta z_\mu$$

with

$$s_{\mu N}^{(3)} = s_{\mu N}^{(1)} + \frac{2}{N} \frac{1 - (-1)^\mu}{\sin \vartheta_\mu} \frac{1}{1 + \cos \vartheta_\mu}$$

$$= \frac{2}{N} [1 - (-1)^\mu] \frac{\cos \vartheta_\mu}{\sin \vartheta_\mu (1 + \cos \vartheta_\mu)} \qquad \text{(6–47)}$$

by equations (6–15) and (6–41). For the ellipse, $z_{e\mu} = \frac{1}{2} \frac{t_e}{c} \sin \vartheta_\mu$,

$$\sum_{\mu=1}^{N-1} s_{\mu N}^{(3)} z_{e\mu} = \frac{t_e}{c} \sum_{\mu=1}^{N-1} \frac{1 - (-1)^\mu}{N} \frac{\cos \vartheta_\mu}{1 + \cos \vartheta_\mu}$$

$$= \frac{t_e}{c} \left[1 - \frac{N}{2}\right]$$

$$= \sqrt{\left(2\frac{\varrho}{c}\right)} \left[1 - \frac{N}{2}\right] .$$

Then, from

$$S^{(3)}(x = 0) = \sqrt{\left(2\frac{\varrho}{c}\right)} + \sum_{\mu=1}^{N-1} s_{\mu N}^{(3)} z_\mu - \sum_{\mu=1}^{N-1} s_{\mu N}^{(3)} z_{e\mu}$$

we obtain finally

$$S^{(3)}(x = 0) = \frac{N}{2} \sqrt{\left(2\frac{\varrho}{c}\right)} + \sum_{\mu=1}^{N-1} s_{\mu N}^{(3)} z_\mu . \qquad \text{(6–48)}$$

7. *Calculated Example.*—To illustrate the calculation procedure a worked example will be given. We calculate by equation (4–6) the pressure distribution on a sheared wing, swept by an angle $\varphi = 45$ deg, at an incidence α. The aerofoil section parallel to the main stream is a twelve per cent thick RAE 101 section (*see* Ref. 9).

The layout of the calculation is given in Table 13, for $N = 16$, *i.e.*, we fix the section shape by its ordinates at 16 points along the chord. This number of points does not involve a great amount of computational work and gives results of sufficient accuracy for almost all practical cases.

From the given section data, with the co-ordinates x, z made dimensionless by reference to the wing chord c, the ordinates $z_\mu = z(x_\mu)$ are determined at the fixed points x_μ given in Table 3.

For determining the function $S^{(3)}(x)$ from equation (3–33) the term $\sqrt{(\varrho/2c)}$ is needed, where ϱ is the radius of curvature at the leading edge. When the nose radius is not given, the term

$$\sqrt{\frac{\varrho}{2c}} = -\left(\frac{dz}{d\vartheta}\right)_\pi$$

can be determined from a plotting of z against ϑ near the leading edge, where

$$\vartheta = \pi - \cos^{-1}(1 - 2x).$$

Such a plotting of $z(\vartheta)$ is also often advisable to obtain values of z_μ near the leading edge which are as accurate as possible. For sections which are ellipses up to the maximum thickness position $x_{\max}$,

$$\sqrt{\left(\frac{\varrho}{2c}\right)} = \frac{1}{2\sqrt{2}} \frac{t/c}{\sqrt{(x_{\max}/c)}}.$$

The functions $S^{(1)}(x)$, $S^{(2)}(x)$ and $S^{(3)}(x)$ are then calculated at the points x_ν for $\nu = 1, 2 \ldots . N - 1$ from the relations

$$S^{(1)}(x_\nu) = \sum_{\mu=1}^{N-1} s_{\mu\nu}{}^{(1)} z_\mu$$

$$S^{(2)}(x_\nu) = \sum_{\mu=1}^{N-1} s_{\mu\nu}{}^{(2)} z_\mu$$

$$S^{(3)}(x_\nu) = \sum_{\mu=1}^{N-1} s_{\mu\nu}{}^{(3)} z_\mu + s_{N\nu}{}^{(3)} \sqrt{\left(\frac{\varrho}{2c}\right)}$$

using the coefficients $s_{\mu\nu}{}^{(1)}$, $s_{\mu\nu}{}^{(2)}$, $s_{\mu\nu}{}^{(3)}$ and $s_{N\nu}{}^{(3)}$ given in Tables 7, 8 and 9. These sums are easily obtained by using a calculating machine.

The functions $S^{(1)}(x = 0)$ and $S^{(3)}(x = 0)$ at the leading edge, $\nu = 16$, are calculated from the relations

$$S^{(1)}(x = 0) = 2N \sqrt{\left(\frac{\varrho}{2c}\right)} + \sum_{\mu=1}^{N-1} s_{\mu N}{}^{(1)} z_\mu$$

$$S^{(3)}(x = 0) = N \sqrt{\left(\frac{\varrho}{2c}\right)} + \sum_{\mu=1}^{N-1} s_{\mu N}{}^{(3)} z_\mu$$

with $s_{\mu 16}{}^{(1)}$ and $s_{\mu 16}{}^{(3)}$ from Tables 7 and 9.

The pressure coefficient at the points x_ν, for a given effective incidence α, is then calculated from equation (4–6) :

$$C_p = 1 - \cos^2\alpha \sin^2\varphi - \frac{\left\{\cos\alpha\,[\cos\varphi + S^{(1)}(x)] \pm \sin\alpha \sqrt{\left(\frac{1-x}{x}\right)}\left[1 + \frac{S^{(3)}(x)}{\cos\varphi}\right]\right\}^2}{1 + \left[\frac{S^{(2)}(x)}{\cos\varphi}\right]^2}$$

where the positive sign holds for the upper surface and the negative sign for the lower surface.

If the pressure coefficient is required at points other than the fixed x_ν, the calculated values of $S^{(1)}(x_\nu)$, $S^{(2)}(x_\nu)$ and $S^{(3)}(x_\nu)$ are plotted against x_ν or preferably against $\sqrt{x_\nu}$, near the leading edge, and continuous curves $S^{(1)}(x)$, $S^{(2)}(x)$ and $S^{(3)}(x)$ are drawn. To avoid the infinity of $S^{(2)}(x) = dz/dx$ at the leading edge, the term

$$\frac{dz}{d\sqrt{x}} = 2\sqrt{x}\, S^{(2)}(x)$$

is plotted, taking into account the relation

$$\left(\frac{dz}{d\sqrt{x}}\right)_{x=0} = \sqrt{\left(2\,\frac{\varrho}{c}\right)}.$$

The pressure coefficient near the leading edge is calculated from the equation

$$C_p = 1 - \cos^2\alpha \sin^2\varphi - \frac{\left\{\cos\alpha[\cos\varphi + S^{(1)}(x)]\sqrt{x} \pm \sin\alpha\sqrt{(1-x)}\left[1 + \frac{S^{(3)}(x)}{\cos\varphi}\right]\right\}^2}{x + \frac{1}{4\cos^2\varphi}\left(\frac{dz}{d\sqrt{x}}\right)^2}.$$

If the pressure distribution is required for a given value of the normal-force coefficient C_N, the corresponding value of the effective incidence α has to be determined first. For this purpose the function

$$\frac{-\Delta C_p}{\cos\alpha\sin\alpha} = 4\cos\varphi\sqrt{\frac{1-x}{x}}\,\frac{\left[1 + \frac{S^{(1)}(x)}{\cos\varphi}\right]\left[1 + \frac{S^{(3)}(x)}{\cos\varphi}\right]}{1 + \left[\frac{S^{(2)}(x)}{\cos\varphi}\right]^2}$$

is calculated and integrated along the chord. This integration is best done from a plotting of $\frac{-\Delta C_p}{\cos\alpha\sin\alpha}\sqrt{x}$ against $\sqrt{x}$. The incidence is then determined from the relation :

$$\cos\alpha\sin\alpha = \tfrac{1}{2}\sin 2\alpha = \frac{C_N}{2\int_0^1 \frac{-\Delta C_p}{\cos\alpha\sin\alpha}\sqrt{x}\, d\sqrt{x}}.$$

LIST OF SYMBOLS

x, y, z		Rectangular co-ordinates, x-axis in direction of the main stream, y-axis spanwise ; $x = 0$ at leading edge
ξ, η, z		Rectangular co-ordinates used for sheared wing, ξ normal to leading edge, η parallel to leading edge
ζ	=	$x + iz$ complex co-ordinate in original plane
ζ^*	=	$x^* + iz^*$ complex co-ordinate in the plane where the aerofoil contour is transformed into a slit
ζ_1, ζ_2		Complex co-ordinates in transformed planes
ξ, ξ^*		Real co-ordinates in ζ or ζ^*-plane, used for flow around flat plate, ellipse and Joukowski profile ; ξ and ξ^* differ from x and x^* by an additive constant

R_1, ϑ_1		Polar co-ordinates in ζ_1-plane, *see* equation (2–50)
s		Length of arc along the aerofoil surface
$z(x)$		Aerofoil section
z_μ	=	$z(x_\mu)$ where $x_\mu = \frac{1 + \cos \vartheta_\mu}{2}$, $\vartheta_\mu = \frac{\mu\pi}{N}$
c		Wing chord
t		Maximum wing thickness
b		Wing span
ϱ		Nose radius
R		Radius of circle in ζ_1-plane into which the slit in the ζ-plane is transformed
r		Radius of circle in ζ_1-plane into which the ellipse or Joukowski profile are transformed
A		Aspect ratio
φ		Angle of sweep
$\varphi_{c/4}, \varphi_{c/2}$		Sweep of quarter-chord or semi-chord line
α		Angle of incidence
α_g		Geometric angle of incidence
α_e		Effective angle of incidence
V		Total local velocity
V_0		Velocity of main stream
V_x, V_y, V_z		Velocity components in direction of the axes
V_n, V_t		Velocity components normal and tangential to the aerofoil surface
$V_{\eta=0}$		Velocity component in plane normal to the leading edge of a sheared wing
$V_{x0}, V_{z0}, V_{n0}, V_{t0}$		Components of V_0
v_x, v_y, v_z		Velocity increments in direction of the axes
$F(\zeta)$		Complex potential function
$q(x)$		Local strength of source distribution
$\gamma(x)$		Local strength of vortex distribution
Γ		Circulation
C_p		Pressure coefficient
ΔC_p		Difference between pressure coefficients on upper and lower surface
C_N		Normal force coefficient
C_T		Tangential force coefficient
C_L		Lift coefficient
C_D		Drag coefficient

LIST OF SYMBOLS—*continued*

$f(\varphi) = \frac{1}{\pi}\ln\frac{1+\sin\varphi}{1-\sin\varphi}$

$n(\varphi)$ *See* equations (5–8), (5–9)

ε Thickness parameter for Joukowski profile, *see* equations (2–40), (2–53), (2–54)

$\vartheta = \cos^{-1}(2x-1)$

$\vartheta_\nu = \nu\pi/N$

ν Suffix indicating the pivotal point

μ Suffix indicating the inducing point

N Number of points taken along chord

$S^{(1)}(x_\nu) = \sum_{\mu=1}^{N-1} s_{\mu\nu}{}^{(1)} z_\mu$, *see* also equation (2–16)

$S^{(2)}(x_\nu) = \sum_{\mu=1}^{N-1} s_{\mu\nu}{}^{(2)} z_\mu$, *see* also equation (3–28)

$S^{(3)}(x_\nu) = \sum_{\mu=1}^{N-1} s_{\mu\nu}{}^{(3)} z_\mu + s_{N\nu}{}^{(3)}\sqrt{\left(\frac{\varrho}{2c}\right)}$, *see* also equation (3–29)

$s_{\mu\nu}{}^{(1)}$ Coefficients, *see* Tables 4, 7 and 10

$s_{\mu\nu}{}^{(2)}$ Coefficients, *see* Tables 5, 8 and 11

$s_{\mu\nu}{}^{(3)}$ Coefficients, *see* Tables 6, 9 and 12

REFERENCES

No.	*Author*	*Title, etc.*
1	F. Riegels and H. Wittich	Zur Berechnung der Druckverteilung von Profilen. Jahrbuch 1942 der deutschen Luftfahrtforschung p. I 120.
2	F. Riegels	Das Umströmungsproblem bei inkompressiblen Potentialströmungen. I. Mitteilung ; *Ing. Arch.*, Vol. XVI, p. 373. 1948. II. Mitteilung ; *Ing. Arch.*, Vol. XVII, p. 94. 1949.
3	S. Goldstein	A theory of aerofoils of small thickness. Part I. Velocity distributions for symmetrical aerofoils. A.R.C. 5804. 1942.
4	S. Goldstein	Low-drag and suction airfoils. *J. Aero. Sci.* Vol. 15, p. 189. 1948.
5	B. Thwaites	A method of aerofoil design. Part I. Symmetrical aerofoils. R. & M. 2166. May, 1945.
6	E. J. Watson	Formulae for the computation of the functions employed for calculating the velocity distribution about a given aerofoil. R. & M. 2176. May, 1945.
7	A. Betz	Singularitätenverfahren zur Ermittlung der Kräfte und Momente auf Körper in Potentialströmungen. *Ing. Arch.*, Vol. III, p. 454. 1932.

REFERENCES—*continued*

No.	*Author*	*Title etc.*
8	H. Glauert	*The elements of aerofoil and airscrew theory.* Cambridge University Press, 1948.
9	R. C. Pankhurst and H. B. Squire ..	Calculated pressure distributions for the RAE 100–104 aerofoil sections. C.P.80. March, 1950.
10	D. Küchemann	The distribution of lift over the surface of swept wings. *Aero. Quart.* Vol. IV, p. 261. 1953.
11	J. Weber and G. G. Brebner	Low-speed tests on 45-deg sweptback wings. Part I. Pressure measurements on wings of aspect ratio 5. R. & M. 2882. May, 1951.
12	J. H. Preston	The calculation of lift taking account of the boundary layer. R. & M. 2725. November, 1949.
13	D. A. Spence	Prediction of the characteristics of two-dimensional aerofoils. A.R.C. 15,504. December, 1952.
14	G. G. Brebner and J. A. Bagley ..	Pressure and boundary-layer measurements on a two-dimensional wing at low speed. R. & M. 2886. February, 1952.
15	Pt. I by Tunnel Staff of Aero Dept., R.A.E. Pt. II by G. G. Brebner	Pressure and boundary-layer measurements on a 59-deg sweptback wing at low speed and comparison with high-speed results on a 45-deg swept wing. C.P.86. Part I, February, 1949. Part II, August, 1950.
16	D. Küchemann and J. Weber ..	The subsonic flow past swept wings at zero lift without and with body. R. & M. 2908. March, 1953.
17	D. Küchemann and J. Weber ..	On the chordwise lift distribution at the centre of swept wings. *Aero. Quart.*, Vol. II, p. 146. August, 1950.
18	H. Multhopp	The calculation of the lift distribution of aerofoils. Translation: A.R.C. 8516. Die Berechnung der Auftriebsverteilung von Tragflügeln. Luftfahrtforschung Vol. 15, p. 153. 1938.
19	J. Weissinger	Über die Einschaltung zusätzlicher Punkte beim Verfahren von Multhopp. *Ing. Arch.*, Vol. XX, p. 163. 1952.

TABLE 1

Various Approximations of the Velocity Distribution V/V_{x0} along the Surface of the 20 per cent Thick Joukowsky Aerofoil in a Flow Parallel to its Chord-line

x/c	(*a*) exact equation (2–52)	(*b*) present method equation (2–15) exact $z(x)$	(*c*) linear theory equation (2–58) $\varepsilon = 0{\cdot}1538$	(*d*) equation (2–60) $\varepsilon = 0{\cdot}1538$	(*e*) equation (2–61) $\varepsilon = 0{\cdot}1538$	(*f*) equation (2–61) $\varepsilon = 0{\cdot}1833$
0	0	0	1·461	0	0	0
0·0096	0·807	0·802	1·456	0·807	0·785	0·730
0·0381	1·191	1·190	1·438	1·203	1·138	1·119
0·0843	1·322	1·320	1·410	1·336	1·257	1·274
0·146	1·347	1·345	1·372	1·354	1·285	1·319
0·222	1·323	1·321	1·325	1·324	1·273	1·312
0·309	1·275	1·273	1·272	1·270	1·239	1·276
0·402	1·214	1·212	1·214	1·206	1·193	1·225
0·500	1·149	1·147	1·154	1·140	1·140	1·164
0·598	1·084	1·082	1·094	1·077	1·085	1·104
0·691	1·024	1·022	1·036	1·020	1·031	1·035
0·778	0·971	0·969	0·983	0·968	0·980	0·975
0·854	0·926	0·924	0·936	0·926	0·935	0·921
0·916	0·891	0·889	0·898	0·891	0·897	0·877
0·962	0·865	0·863	0·870	0·866	0·869	0·844
0·990	0·850	0·848	0·852	0·851	0·852	0·824
1·000	0·845	0·844	0·846	0·846	0·846	0·817

TABLE 2

Various Approximations of the Velocity Distribution V/V_{x0} along the Surface of the 20 per cent Thick Joukowsky Aerofoil in a Flow Normal to its Chord-line

x/c	(*a*) exact equation (3–51)	(*b*) present method equation (3-26) exact $z(x)$	(*c*) thin aerofoil	(*d*) equation (3–53) $\varepsilon = 0{\cdot}1538$	(*e*) equation (3–54) $\varepsilon = 0{\cdot}1538$	(*f*) equation (3–54) $\varepsilon = 0{\cdot}1833$	(*g*) equation (3–63) $\varepsilon = 0{\cdot}1538$
0	8·610	8·650	∞	8·502	8·502	7·456	7·502
0·0096	7·344	7·344	10·153	7·326	7·128	6·534	6·460
0·0381	5·358	5·383	5·027	5·400	5·107	4·949	4·753
0·0843	3·894	3·906	3·297	3·924	3·693	3·682	3·443
0·146	2·898	2·904	2·414	2·903	2·753	2·780	2·538
0·222	2·198	2·199	1·871	2·190	2·105	2·130	1·902
0·309	1·689	1·685	1·497	1·670	1·630	1·646	1·440
0·402	1·303	1·296	1·219	1·283	1·270	1·274	1·097
0·500	1·007	0·998	1·000	0·988	0·988	0·984	0·836
0·598	0·776	0·765	0·821	0·760	0·765	0·754	0·636
0·691	0·594	0·582	0·668	0·580	0·587	0·570	0·479
0·778	0·449	0·437	0·535	0·437	0·442	0·424	0·356
0·854	0·331	0·320	0·414	0·321	0·324	0·306	0·257
0·916	0·232	0·223	0·303	0·224	0·226	0·211	0·178
0·962	0·147	0·140	0·199	0·142	0·142	0·132	0·111
0·990	0·072	0·068	0·098	0·069	0·069	0·063	0·054
1·000	0	0	0	0	0	0	0

TABLE 3

Position of the Pivotal Points

$N = 8$		$N = 16$		$N = 32$	
ν	x_ν	ν	x_ν	ν	x_ν
0	1·000	0	1·0000	0	1·0000
				1	0·9976
		1	0·9904	2	0·9904
				3	0·9785
1	0·9619	2	0·9619	4	0·9619
				5	0·9410
		3	0·9157	6	0·9157
				7	0·8865
2	0·8536	4	0·8536	8	0·8536
				9	0·8172
		5	0·7778	10	0·7778
				11	0·7357
3	0·6913	6	0·6913	12	0·6913
				13	0·6451
		7	0·5975	14	0·5975
				15	0·5490
4	0·5000	8	0·5000	16	0·5000
				17	0·4510
		9	0·4025	18	0·4025
				19	0·3549
5	0·3087	10	0·3087	20	0·3087
				21	0·2643
		11	0·2222	22	0·2222
				23	0·1828
6	0·1464	12	0·1464	24	0·1464
				25	0·1135
		13	0·08427	26	0·08427
				27	0·05904
7	0·03806	14	0·03806	28	0·03806
				29	0·02153
		15	0·00961	30	0·00961
				31	0·00241
8	0	16	0	32	0

TABLE 4

$s_{\mu\nu}^{(1)}$ *for* $N = 8$

μ	ν							
	1	2	3	4	5	6	7	8
1	20·905	−4·072	0	−0·224	0	−0·072	0	−0·052
2	−7·524	11·314	−3·359	0	−0·298	0	−0·133	0
3	0	−4·389	8·659	−3·154	0	−0·389	0	−0·242
4	−0·586	0	−3·414	8·000	−3·414	0	−0·586	0
5	0	−0·389	0	−3·154	8·659	−4·389	0	−1·212
6	−0·133	0	−0·298	0	−3·359	11·314	−7·524	0
7	0	−0·072	0	−0·224	0	−4·072	20·905	−33·022

TABLE 5

$s_{\mu\nu}^{(2)}$ *for* $N = 8$

μ	ν						
	1	2	3	4	5	6	7
1	6·309	4·993	−1·531	0·828	−0·634	0·664	−1·082
2	−17·048	1·414	4·718	−2·000	1·405	−1·414	2·266
3	8·922	−8·055	0·448	4·828	−2·613	2·398	−3·696
4	−5·657	4·000	−5·657	0	5·657	−4·000	5·657
5	3·696	−2·398	2·613	−4·828	−0·448	8·055	−8·922
6	−2·266	1·414	−1·405	2·000	−4·718	−1·414	17·048
7	1·082	−0·664	0·634	−0·828	1·531	−4·993	−6·309

TABLE 6

$s_{\mu\nu}^{(3)}$ *for* $N = 8$

μ	ν							
	1	2	3	4	5	6	7	8
1	20·905	1·955	0	1·190	0	0·729	0	0·627
2	−10·786	11·314	−1·179	0	0·351	0	0·301	0
3	0	−6·057	8·659	−1·740	0	0·108	0	0·150
4	−1·127	0	−4·721	8·000	−2·107	0	−0·045	0
5	0	−0·886	0	−4·568	8·659	−2·721	0	−0·335
6	−0·567	0	−0·947	0	−5·539	11·314	−4·262	0
7	0	−0·873	0	−1·638	0	−10·099	20·905	−15·858
8	−0·130	0	−0·181	0	−0·405	0	−3·284	—

TABLE 7

$s_{\mu\nu}^{(1)}$ *for* $N = 16$

μ	ν															
	1	2	3	4	5	6	7	8	9	10	11	12	13	14	15	16
1	82·013	−15·061	0	−0·651	0	−0·136	0	−0·051	0	−0·026	0	−0·017	0	−0·013	0	−0·012
2	−29·544	41·810	−11·203	0	−0·705	0	−0·180	0	−0·076	0	−0·044	0	−0·031	0	−0·026	0
3	0	−16·265	28·799	−8·980	0	−0·690	0	−0·201	0	−0·094	0	−0·059	0	−0·045	0	−0·041
4	−2·360	0	−11·430	22·627	−7·698	0	−0·674	0	−0·217	0	−0·111	0	−0·075	0	−0·062	0
5	0	−1·532	0	−9·052	19·243	−6·954	0	−0·673	0	−0·236	0	−0·130	0	−0·095	0	−0·086
6	−0·646	0	−1·147	0	−7·727	17·318	−6·563	0	−0·692	0	−0·262	0	−0·157	0	−0·124	0
7	0	−0·462	0	−0·935	0	−6·968	16·314	−6·442	0	−0·735	0	−0·301	0	−0·196	0	−0·172
8	−0·260	0	−0·362	0	−0·810	0	−6·569	16·000	−6·569	0	−0·810	0	−0·362	0	−0·260	0
9	0	−0·196	0	−0·301	0	−0·735	0	−6·442	16·314	−6·968	0	−0·935	0	−0·462	0	−0·378
10	−0·124	0	−0·157	0	−0·262	0	−0·692	0	−6·563	17·318	−7·727	0	−1·147	0	−0·646	0
11	0	−0·095	0	−0·130	0	−0·236	0	−0·673	0	−6·954	19·243	−9·052	0	−1·532	0	−1·052
12	−0·062	0	−0·075	0	−0·111	0	−0·217	0	−0·674	0	−7·698	22·627	−11·430	0	−2·360	0
13	0	−0·045	0	−0·059	0	−0·094	0	−0·201	0	−0·690	0	−8·980	28·799	−16·265	0	−4·890
14	−0·026	0	−0·031	0	−0·044	0	−0·076	0	−0·180	0	−0·705	0	−11·203	41·810	−29·544	0
15	0	−0·013	0	−0·017	0	−0·026	0	−0·051	0	−0·136	0	−0·651	0	−15·061	82·013	−132·103

TABLE 8

$s_{\mu\nu}^{(2)}$ *for* $N = 16$

μ	ν														
	1	2	3	4	5	6	7	8	9	10	11	12	13	14	15
1	25·769	17·917	−4·703	2·016	−1·104	0·706	−0·506	0·398	−0·338	0·310	−0·305	0·327	−0·388	0·535	−1·020
2	−68·941	6·309	14·908	−4·993	2·499	−1·531	1·071	−0·828	0·697	−0·634	0·622	−0·664	0·785	−1·082	2·060
3	38·144	−31·420	2·694	12·636	−4·844	2·680	−1·780	1·336	−1·104	0·991	−0·963	1·021	−1·203	1·654	−3·143
4	−26·486	17·048	−20·468	1·414	11·224	−4·718	2·816	−2·000	1·598	−1·405	1·347	−1·414	1·654	−2·266	4·295
5	20·046	−11·798	10·849	−15·519	0·804	10·411	−4·704	2·993	−2·259	1·918	−1·800	1·862	−2·158	2·937	−5·548
6	−15·836	8·922	−7·411	8·054	−12·854	0·448	10·043	−4·828	3·261	−2·613	2·369	−2·398	2·739	−3·696	6·946
7	12·797	−7·033	5·548	−5·418	6·546	−11·318	0·203	10·055	−5·126	3·675	−3·143	3·075	−3·439	4·581	−8·551
8	−10·453	5·657	−4·330	4·000	−4·330	5·657	−10·453	0	10·453	−5·657	4·330	−4·000	4·330	−5·657	10·453
9	8·551	−4·581	3·439	−3·075	3·143	−3·675	5·126	−10·055	−0·203	11·318	−6·546	5·418	−5·548	7·033	−12·797
10	−6·946	3·696	−2·739	2·398	−2·369	2·613	−3·261	4·828	−10·043	−0·448	12·854	−8·054	7·411	−8·922	15·836
11	5·548	−2·937	2·158	−1·862	1·800	−1·918	2·259	−2·993	4·704	−10·411	−0·804	15·519	−10·849	11·798	−20·046
12	−4·295	2·266	−1·654	1·414	−1·347	1·405	−1·598	2·000	−2·816	4·718	−11·224	−1·414	20·468	−17·048	26·486
13	3·143	−1·654	1·203	−1·021	0·963	−0·991	1·104	−1·336	1·780	−2·680	4·844	−12·636	−2·694	31·420	−38·144
14	−2·060	1·082	−0·785	0·664	−0·622	0·634	−0·697	0·828	−1·071	1·531	−2·499	4·993	−14·908	−6·309	68·941
15	1·020	−0·535	0·388	−0·327	0·305	−0·310	0·338	−0·398	0·506	−0·706	1·104	−2·016	4·703	−17·917	−25·769

TABLE 9

$s_{\mu\nu}^{(3)}$ *for* $N = 16$

μ	ν															
	1	2	3	4	5	6	7	8	9	10	11	12	13	14	15	16
1	82·013	7·458	0	4·031	0	2·006	0	1·256	0	0·914	0	0·742	0	0·659	0	0·635
2	−41·024	41·810	−4·134	0	1·068	0	0·716	0	0·507	0	0·398	0	0·341	0	0·317	0
3	0	−21·134	28·799	−5·362	0	0·313	0	0·340	0	0·276	0	0·234	0	0·211	0	0·204
4	−3·562	0	−14·273	22·627	−5·365	0	0·016	0	0·175	0	0·169	0	0·155	0	0·147	0
5	0	−2·349	0	−11·036	19·243	−5·215	0	−0·132	0	0·084	0	0·108	0	0·108	0	0·107
6	−1·098	0	−1·750	0	−9·293	17·318	−5·121	0	−0·224	0	0·026	0	0·066	0	0·074	0
7	0	−0·811	0	−1·433	0	−8·326	16·314	−5·136	0	−0·293	0	−0·019	0	0·032	0	0·042
8	−0·515	0	−0·662	0	−1·260	0	−7·850	16·000	−5·287	0	−0·360	0	−0·061	0	−0·005	0
9	0	−0·424	0	−0·584	0	−1·176	0	−7·749	16·314	−5·609	0	−0·437	0	−0·112	0	−0·062
10	−0·323	0	−0·380	0	−0·551	0	−1·160	0	−8·006	17·318	−6·162	0	−0·544	0	−0·193	0
11	0	−0·298	0	−0·369	0	−0·557	0	−1·215	0	−8·694	19·243	−7·068	0	−0·716	0	−0·376
12	−0·271	0	−0·305	0	−0·391	0	−0·609	0	−1·365	0	−10·031	22·627	−8·587	0	−1·068	0
13	0	−0·301	0	−0·351	0	−0·465	0	−0·742	0	−1·692	0	−12·599	28·799	−11·395	0	−2·220
14	−0·369	0	−0·403	0	−0·485	0	−0·660	0	−1·076	0	−2·479	0	−18·273	41·810	−18·064	0
15	0	−0·686	0	−0·776	0	−0·966	0	−1·357	0	−2·279	0	−5·334	0	−37·580	82·013	−65·410
16	−0·063	0	−0·068	0	−0·080	0	−0·105	0	−0·155	0	−0·281	0	−0·742	0	−6·505	

TABLE 10

$s_{\mu\nu}^{(1)}$ *for* $N = 32$

μ	ν															
	1	2	3	4	5	6	7	8	9	10	11	12	13	14	15	16
1	326·474	−59·103	0	−2·410	0	−0·457	0	−0·148	0	−0·063	0	−0·033	0	−0·019	0	−0·012
2	−117·636	164·027	−42·889	0	−2·495	0	−0·565	0	−0·203	0	−0·094	0	−0·051	0	−0·031	0
3	0	−63·816	110·237	−33·198	0	−2·305	0	−0·581	0	−0·225	0	−0·110	0	−0·063	0	−0·040
4	−9·409	0	−43·765	83·620	−27·171	0	−2·102	0	−0·571	0	−0·234	0	−0·119	0	−0·070	0
5	0	−6·029	0	−33·470	67·883	−23·149	0	−1·928	0	−0·553	0	−0·236	0	−0·125	0	−0·076
6	−2·591	0	−4·411	0	−27·287	57·599	−20·321	0	−1·788	0	−0·536	0	−0·237	0	−0·129	0
7	0	−1·837	0	−3·484	0	−23·207	50·442	−18·258	0	−1·677	0	−0·520	0	−0·237	0	−0·133
8	−1·065	0	−1·416	0	−2·892	0	−20·350	45·255	−16·717	0	−1·591	0	−0·509	0	−0·238	0
9	0	−0·805	0	−1·153	0	−2·488	0	−18·275	41·397	−15·552	0	−1·525	0	−0·501	0	−0·240
10	−0·538	0	−0·645	0	−0·976	0	−2·198	0	−16·728	38·486	−14·669	0	−1·477	0	−0·496	0
11	0	−0·425	0	−0·538	0	−0·850	0	−1·984	0	−15·560	36·284	−14·008	0	−1·444	0	−0·496
12	−0·308	0	−0·350	0	−0·463	0	−0·758	0	−1·823	0	−14·674	34·637	−13·527	0	−1·425	0
13	0	−0·251	0	−0·298	0	−0·408	0	−0·688	0	−1·700	0	−14·010	33·440	−13·199	0	−1·420
14	−0·192	0	−0·211	0	−0·260	0	−0·367	0	−0·635	0	−1·606	0	−13·529	32·627	−13·010	0
15	0	−0·160	0	−0·182	0	−0·231	0	−0·335	0	−0·594	0	−1·535	0	−13·201	32·155	−12·948
16	−0·126	0	−0·137	0	−0·161	0	−0·209	0	−0·311	0	−0·563	0	−1·483	0	−13·011	32·000
17	0	−0·107	0	−0·119	0	−0·144	0	−0·192	0	−0·291	0	−0·538	0	−1·448	0	−12·948
18	−0·087	0	−0·092	0	−0·106	0	−0·131	0	−0·178	0	−0·276	0	−0·520	0	−1·427	0
19	0	−0·074	0	−0·081	0	−0·095	0	−0·120	0	−0·167	0	−0·264	0	−0·508	0	−1·420
20	−0·061	0	−0·064	0	−0·072	0	−0·086	0	−0·112	0	−0·158	0	−0·255	0	−0·500	0
21	0	−0·052	0	−0·057	0	−0·065	0	−0·079	0	−0·105	0	−0·151	0	−0·248	0	−0·496
22	−0·043	0	−0·045	0	−0·050	0	−0·059	0	−0·073	0	−0·099	0	−0·145	0	−0·243	0
23	0	−0·037	0	−0·040	0	−0·045	0	−0·054	0	−0·068	0	−0·093	0	−0·140	0	−0·240
24	−0·031	0	−0·032	0	−0·035	0	−0·040	0	−0·049	0	−0·064	0	−0·089	0	−0·136	0
25	0	−0·026	0	−0·028	0	−0·031	0	−0·036	0	−0·045	0	−0·059	0	−0·085	0	−0·133
26	−0·021	0	−0·022	0	−0·024	0	−0·027	0	−0·032	0	−0·041	0	−0·055	0	−0·080	0
27	0	−0·017	0	−0·018	0	−0·020	0	−0·023	0	−0·029	0	−0·037	0	−0·051	0	−0·076
28	−0·013	0	−0·013	0	−0·015	0	−0·017	0	−0·020	0	−0·025	0	−0·032	0	−0·046	0
29	0	−0·010	0	−0·010	0	−0·011	0	−0·013	0	−0·016	0	−0·020	0	−0·027	0	−0·040
30	−0·006	0	−0·007	0	−0·007	0	−0·008	0	−0·009	0	−0·012	0	−0·015	0	−0·021	0
31	0	−0·003	0	−0·003	0	−0·004	0	−0·004	0	−0·005	0	−0·007	0	−0·009	0	−0·012

TABLE 10—*continued*

μ	ν															
	17	18	19	20	21	22	23	24	25	26	27	28	29	30	31	32
1	0	−0·009	0	−0·007	0	−0·005	0	−0·004	0	−0·004	0	−0·003	0	−0·003	0	−0·003
2	−0·021	0	−0·015	0	−0·012	0	−0·009	0	−0·008	0	−0·007	0	−0·007	0	−0·006	0
3	0	−0·027	0	−0·020	0	−0·016	0	−0·013	0	−0·011	0	−0·010	0	−0·010	0	−0·009
4	−0·046	0	−0·032	0	−0·025	0	−0·020	0	−0·017	0	−0·015	0	−0·013	0	−0·013	0
5	0	−0·051	0	−0·037	0	−0·029	0	−0·023	0	−0·020	0	−0·018	0	−0·017	0	−0·017
6	−0·080	0	−0·055	0	−0·041	0	−0·032	0	−0·027	0	−0·024	0	−0·022	0	−0·021	0
7	0	−0·085	0	−0·059	0	−0·045	0	−0·036	0	−0·031	0	−0·028	0	−0·026	0	−0·025
8	−0·136	0	−0·089	0	−0·064	0	−0·049	0	−0·040	0	−0·035	0	−0·032	0	−0·031	0
9	0	−0·140	0	−0·093	0	−0·068	0	−0·054	0	−0·045	0	−0·040	0	−0·037	0	−0·036
10	−0·243	0	−0·145	0	−0·099	0	−0·073	0	−0·059	0	−0·050	0	−0·045	0	−0·043	0
11	0	−0·248	0	−0·151	0	−0·105	0	−0·079	0	−0·065	0	−0·057	0	−0·052	0	−0·051
12	−0·500	0	−0·255	0	−0·158	0	−0·112	0	−0·086	0	−0·072	0	−0·064	0	−0·061	0
13	0	−0·508	0	−0·264	0	−0·167	0	−0·120	0	−0·095	0	−0·081	0	−0·074	0	−0·072
14	−1·427	0	−0·520	0	−0·276	0	−0·178	0	−0·131	0	−0·106	0	−0·092	0	−0·087	0
15	0	−1·448	0	−0·538	0	−0·291	0	−0·192	0	−0·144	0	−0·119	0	−0·107	0	−0·103
16	−13·011	0	−1·483	0	−0·563	0	−0·311	0	−0·209	0	−0·161	0	−0·137	0	−0·126	0
17	32·155	−13·201	0	−1·535	0	−0·594	0	−0·335	0	−0·231	0	−0·182	0	−0·160	0	−0·153
18	−13·010	32·627	−13·529	0	−1·606	0	−0·635	0	−0·367	0	−0·260	0	−0·211	0	−0·192	0
19	0	−13·199	33·440	−14·010	0	−1·700	0	−0·688	0	−0·408	0	−0·298	0	−0·251	0	−0·237
20	−1·425	0	−13·527	34·637	−14·674	0	−1·823	0	−0·758	0	−0·463	0	−0·350	0	−0·308	0
21	0	−1·444	0	−14·008	36·284	−15·560	0	−1·984	0	−0·850	0	−0·538	0	−0·425	0	−0·395
22	−0·496	0	−1·477	0	−14·669	38·486	−16·728	0	−2·198	0	−0·976	0	−0·645	0	−0·538	0
23	0	−0·501	0	−1·525	0	−15·552	41·397	−18·275	0	−2·488	0	−1·153	0	−0·805	0	−0·723
24	−0·238	0	−0·509	0	−1·591	0	−16·717	45·255	−20·350	0	−2·892	0	−1·416	0	−1·065	0
25	0	−0·237	0	−0·520	0	−1·677	0	−18·258	50·442	−23·207	0	−3·484	0	−1·837	0	−1·539
26	−0·129	0	−0·237	0	−0·536	0	−1·788	0	−20·321	57·599	−27·287	0	−4·411	0	−2·591	0
27	0	−0·125	0	−0·236	0	−0·553	0	−1·928	0	−23·149	67·883	−33·470	0	−6·029	0	−4·226
28	−0·070	0	−0·119	0	−0·234	0	−0·571	0	−2·102	0	−27·171	83·620	−43·765	0	−9·409	0
29	0	−0·063	0	−0·110	0	−0·225	0	−0·581	0	−2·305	0	−33·198	110·237	−63·816	0	−19·572
30	−0·031	0	−0·051	0	−0·094	0	−0·203	0	−0·565	0	−2·495	0	−42·889	164·027	−117·636	0
31	0	−0·019	0	−0·033	0	−0·063	0	−0·148	0	−0·457	0	−2·410	0	−59·103	326·474	−528·400

TABLE 11

$s_{\mu\nu}^{(2)}$ *for* $N = 32$

μ	ν															
	1	2	3	4	5	6	7	8	9	10	11	12	13	14	15	16
1	103·586	69·783	−17·658	7·184	−3·671	2·155	−1·391	0·962	−0·703	0·536	−0·424	0·346	−0·291	0·250	−0·220	0·197
2	−276·452	25·769	56·370	−17·917	8·372	−4·703	2·960	−2·016	1·457	−1·104	0·869	−0·706	0·590	−0·506	0·444	−0·398
3	154·876	−124·802	11·356	45·888	−16·417	8·329	−4·976	3·286	−2·328	1·740	−1·356	1·094	−0·910	0·777	−0·679	0·607
4	−109·508	68·941	−79·750	6·309	38·696	−14·908	7·997	−4·993	3·420	−2·499	1·918	−1·531	1·262	−1·071	0·931	−0·828
5	84·923	−48·880	43·293	−58·716	3·969	33·636	−13·645	7·627	−4·927	3·474	−2·604	2·044	−1·665	1·400	−1·209	1·069
6	−69·243	38·144	−30·507	31·420	−46·720	2·694	29·961	−12·635	7·293	−4·844	3·499	−2·680	2·146	−1·780	1·522	−1·336
7	58·263	−31·301	23·764	−21·976	24·713	−39·066	1·921	27·227	−11·841	7·018	−4·770	3·518	−2·747	2·238	−1·889	1·641
8	−50·084	26·487	−19·500	17·048	−17·161	20·469	−33·826	1·414	25·160	−11·224	6·803	−4·718	3·546	−2·816	2·333	−2·000
9	43·717	−22·878	16·512	−13·956	13·250	−14·120	17·581	−30·069	1·062	23·589	−10·755	6·648	−4·695	3·588	−2·896	2·437
10	−38·592	20·046	−14·273	11·798	−10·809	10·849	−12·055	15·519	−27·292	0·804	22·401	−10·411	6·551	−4·704	3·652	−2·993
11	34·356	−17·749	12·514	−10·186	9·115	−8·817	9·218	−10·583	13·999	−25·202	0·606	21·521	−10·177	6·509	−4·747	3·742
12	−30·778	15·836	−11·084	8·922	−7·851	7·411	−7·462	8·055	−9·496	12·854	−23·617	0·448	20·898	−10·043	6·522	−4·828
13	27·700	−14·207	9·890	−7·893	6·862	−6·365	6·250	−6·493	7·195	−8·677	11·982	−22·420	0·317	20·499	−10·002	6·593
14	−25·013	12·797	−8·866	7·033	−6·059	5·548	−5·350	5·418	−5·776	6·545	−8·050	11·318	−21·533	0·203	20·305	−10·055
15	22·634	−11·557	7·983	−6·298	5·386	−4·885	4·648	−4·621	4·800	−5·232	6·044	−7·568	10·818	−20·905	0·099	20·306
16	−20·503	10·453	−7·200	5·657	−4·811	4·330	−4·078	4·000	−4·078	4·330	−4·811	5·657	−7·200	10·453	−20·503	0
17	18·575	−9·457	6·499	−5·090	4·309	−3·854	3·602	−3·496	3·516	−3·663	3·963	−4·482	5·356	−6·924	10·202	−20·306
18	−16·813	8·551	−5·866	4·581	−3·864	3·439	−3·193	3·075	−3·059	3·142	−3·337	3·675	−4·223	5·126	−6·725	10·055
19	15·190	−7·718	5·286	−4·119	3·464	−3·071	2·837	−2·714	2·678	−2·721	2·849	−3·078	3·445	−4·020	4·953	−6·593
20	−13·682	6·946	−4·752	3·696	−3·100	2·739	−2·520	2·398	−2·350	2·369	−2·453	2·613	−2·869	3·261	−3·862	4·828
21	12·270	−6·226	4·254	−3·303	2·765	−2·437	2·234	−2·117	2·063	−2·066	2·121	−2·235	2·420	−2·698	3·113	−3·742
22	−10·940	5·548	−3·788	2·937	−2·454	2·158	−1·973	1·863	−1·808	1·800	−1·836	1·918	−2·054	2·259	−2·557	2·993
23	9·679	−4·906	3·347	−2·593	2·163	−1·898	1·732	−1·630	1·576	−1·563	1·585	−1·645	1·747	−1·900	2·121	−2·437
24	−8·476	4·295	−2·928	2·266	−1·888	1·654	−1·506	1·414	−1·364	1·347	−1·361	1·405	−1·482	1·598	−1·765	2·000
25	7·321	−3·708	2·527	−1·954	1·626	−1·423	1·294	−1·212	1·166	−1·149	1·156	−1·188	1·247	−1·336	1·464	−1·641
26	−6·206	3·143	−2·140	1·654	−1·376	1·203	−1·091	1·021	−0·981	0·963	−0·967	0·991	−1·035	1·104	−1·201	1·336
27	5·124	−2·594	1·766	−1·364	1·134	−0·990	0·898	−0·839	0·804	−0·789	0·790	−0·807	0·840	−0·893	0·967	−1·069
28	−4·069	2·060	−1·402	1·082	−0·899	0·785	−0·711	0·664	−0·635	0·622	−0·622	0·634	−0·659	0·697	−0·753	0·828
29	3·034	−1·536	1·045	−0·807	0·670	−0·584	0·529	−0·493	0·472	−0·462	0·461	−0·469	0·486	−0·514	0·553	−0·607
30	−2·015	1·020	−0·694	0·535	−0·444	0·388	−0·351	0·327	−0·313	0·305	−0·305	0·310	−0·321	0·338	−0·363	0·398
31	1·005	−0·509	0·346	−0·266	0·222	−0·194	0·175	−0·163	0·156	−0·152	0·152	−0·154	0·159	−0·167	0·180	−0·197

TABLE 11—*continued*

μ	ν														
	17	18	19	20	21	22	23	24	25	26	27	28	29	30	31
1	−0·180	0·167	−0·159	0·154	−0·152	0·152	−0·156	0·163	−0·175	0·194	−0·222	0·266	−0·346	0·509	−1·005
2	0·363	−0·338	0·321	−0·310	0·305	−0·305	0·313	−0·327	0·351	−0·388	0·444	−0·535	0·694	−1·020	2·015
3	−0·553	0·514	−0·486	0·469	−0·461	0·462	−0·472	0·493	−0·529	0·584	−0·670	0·807	−1·045	1·536	−3·034
4	0·753	−0·697	0·659	−0·634	0·622	−0·622	0·635	−0·664	0·711	−0·785	0·899	−1·082	1·402	−2·060	4·069
5	−0·967	0·893	−0·840	0·807	−0·790	0·789	−0·804	0·839	−0·898	0·990	−1·134	1·364	−1·766	2·594	−5·124
6	1·201	−1·104	1·035	−0·991	0·967	−0·963	0·981	−1·021	1·091	−1·203	1·376	−1·654	2·140	−3·143	6·206
7	−1·464	1·336	−1·247	1·188	−1·156	1·149	−1·166	1·212	−1·294	1·423	−1·626	1·954	−2·527	3·708	−7·321
8	1·765	−1·598	1·482	−1·405	1·361	−1·347	1·364	−1·414	1·506	−1·654	1·888	−2·266	2·928	−4·295	8·476
9	−2·121	1·900	−1·747	1·645	−1·585	1·563	−1·576	1·630	−1·732	1·898	−2·163	2·593	−3·347	4·906	−9·679
10	2·557	−2·259	2·054	−1·918	1·836	−1·800	1·808	−1·863	1·973	−2·158	2·454	−2·937	3·788	−5·548	10·940
11	−3·113	2·698	−2·420	2·235	−2·121	2·066	−2·063	2·117	−2·234	2·437	−2·765	3·303	−4·254	6·226	−12·270
12	3·862	−3·261	2·869	−2·613	2·453	−2·369	2·350	−2·398	2·520	−2·739	3·100	−3·696	4·752	−6·946	13·682
13	−4·953	4·020	−3·445	3·078	−2·849	2·721	−2·678	2·714	−2·837	3·071	−3·464	4·119	−5·286	7·718	−15·190
14	6·725	−5·126	4·223	−3·675	3·337	−3·142	3·059	−3·075	3·193	−3·439	3·864	−4·581	5·866	−8·551	16·813
15	−10·202	6·924	−5·356	4·482	−3·963	3·663	−3·516	3·496	−3·602	3·854	−4·309	5·090	−6·499	9·457	−18·575
16	20·503	−10·453	7·200	−5·657	4·811	−4·330	4·078	−4·000	4·078	−4·330	4·811	−5·657	7·200	−10·453	20·503
17	−0·099	20·905	−10·818	7·568	−6·044	5·232	−4·800	4·621	−4·648	4·885	−5·386	6·298	−7·983	11·557	−22·634
18	−20·305	−0·203	21·533	−11·318	8·050	−6·545	5·776	−5·418	5·350	−5·548	6·059	−7·033	8·866	−12·797	25·013
19	10·002	−20·499	−0·317	22·420	−11·982	8·677	−7·195	6·493	−6·250	6·365	−6·862	7·893	−9·890	14·207	−27·700
20	−6·522	10·043	−20·898	−0·448	23·617	−12·854	9·496	−8·055	7·462	−7·411	7·851	−8·922	11·084	−15·836	30·778
21	4·747	−6·509	10·177	−21·521	−0·606	25·202	−13·999	10·583	−9·218	8·817	−9·115	10·186	−12·514	17·749	−34·356
22	−3·652	4·704	−6·551	10·411	−22·401	−0·804	27·292	−15·519	12·055	−10·849	10·809	−11·798	14·273	−20·046	38·592
23	2·896	−3·588	4·695	−6·648	10·755	−23·589	−1·062	30·069	−17·581	14·120	−13·250	13·956	−16·512	22·878	−43·717
24	−2·333	2·816	−3·546	4·718	−6·803	11·224	−25·160	−1·414	33·826	−20·469	17·161	−17·048	19·500	−26·487	50·084
25	1·889	−2·238	2·747	−3·518	4·770	−7·018	11·841	−27·227	−1·921	39·066	−24·713	21·976	−23·764	31·301	−58·263
26	−1·522	1·780	−2·146	2·680	−3·499	4·844	−7·293	12·635	−29·961	−2·694	46·720	−31·420	30·507	−38·144	69·243
27	1·209	−1·400	1·665	−2·044	2·604	−3·474	4·927	−7·627	13·645	−33·636	−3·969	58·716	−43·293	48·880	−84·923
28	−0·931	1·071	−1·262	1·531	−1·918	2·499	−3·420	4·993	−7·997	14·908	−38·696	−6·309	79·750	−68·941	109·508
29	0·679	−0·777	0·910	−1·094	1·356	−1·740	2·328	−3·286	4·976	−8·329	16·417	−45·888	−11·356	124·802	−154·876
30	−0·444	0·506	−0·590	0·706	−0·869	1·104	−1·457	2·016	−2·960	4·703	−8·372	17·917	−56·370	−25·769	276·452
31	0·220	−0·250	0·291	−0·346	0·424	−0·536	0·703	−0·962	1·391	−2·155	3·671	−7·184	17·658	−69·783	−103·586

TABLE 12

$s_{\mu\nu}^{(3)}$ *for* $N = 32$

μ	ν															
	1	2	3	4	5	6	7	8	9	10	11	12	13	14	15	16
1	326·474	29·462	0	15·475	0	7·333	0	4·279	0	2·838	0	2·049	0	1·575	0	1·269
2	−162·133	164·027	−16·018	0	3·986	0	2·519	0	1·647	0	1·164	0	0·877	0	0·695	0
3	0	−81·875	110·237	−20·176	0	1·127	0	1·143	0	0·848	0	0·640	0	0·502	0	0·410
4	−13·990	0	−53·644	83·620	−19·386	0	0·063	0	0·557	0	0·488	0	0·397	0	0·326	0
5	0	−8·711	0	−39·790	67·883	−17·893	0	−0·411	0	0·260	0	0·295	0	0·261	0	0·225
6	−3·965	0	−6·204	0	−31·747	57·599	−16·472	0	−0·646	0	0·089	0	0·179	0	0·178	0
7	0	−2·785	0	−4·790	0	−26·578	50·442	−15·269	0	−0·771	0	−0·015	0	0·104	0	0·122
8	−1·679	0	−2·124	0	−3·903	0	−23·032	45·255	−14·286	0	−0·841	0	−0·085	0	0·051	0
9	0	−1·272	0	−1·712	0	−3·309	0	−20·499	41·397	−13·501	0	−0·883	0	−0·133	0	0·015
10	−0·880	0	−1·020	0	−1·437	0	−2·889	0	−18·635	38·486	−12·883	0	−0·910	0	−0·167	0
11	0	−0·703	0	−0·851	0	−1·244	0	−2·585	0	−17·244	36·284	−12·410	0	−0·931	0	−0·195
12	−0·529	0	−0·586	0	−0·734	0	−1·105	0	−2·361	0	−16·199	34·637	−12·063	0	−0·950	0
13	0	−0·440	0	−0·504	0	−0·649	0	−1·001	0	−2·192	0	−15·424	33·440	−11·827	0	−0·970
14	−0·351	0	−0·378	0	−0·446	0	−0·588	0	−0·926	0	−2·067	0	−14·868	32·627	−11·697	0
15	0	−0·302	0	−0·334	0	−0·402	0	−0·541	0	−0·869	0	−1·976	0	−14·495	32·155	−11·667
16	−0·252	0	−0·268	0	−0·303	0	−0·371	0	−0·508	0	−0·828	0	−1·914	0	−14·286	32
17	0	−0·223	0	−0·242	0	−0·279	0	−0·348	0	−0·483	0	−0·799	0	−1·877	0	−14·229
18	−0·194	0	−0·203	0	−0·224	0	−0·263	0	−0·332	0	−0·467	0	−0·783	0	−1·862	0
19	0	−0·177	0	−0·189	0	−0·211	0	−0·251	0	−0·321	0	−0·458	0	−0·777	0	−1·870
20	−0·159	0	−0·165	0	−0·179	0	−0·203	0	−0·245	0	−0·316	0	−0·456	0	−0·781	0
21	0	−0·150	0	−0·159	0	−0·174	0	−0·199	0	−0·243	0	−0·317	0	−0·461	0	−0·797
22	−0·140	0	−0·144	0	−0·155	0	−0·172	0	−0·199	0	−0·245	0	−0·323	0	−0·473	0
23	0	−0·137	0	−0·144	0	−0·156	0	−0·175	0	−0·204	0	−0·252	0	−0·335	0	−0·495
24	−0·135	0	−0·138	0	−0·146	0	−0·159	0	−0·181	0	−0·214	0	−0·266	0	−0·357	0
25	0	−0·138	0	−0·144	0	−0·154	0	−0·169	0	−0·193	0	−0·229	0	−0·289	0	−0·388
26	−0·144	0	−0·148	0	−0·155	0	−0·167	0	−0·185	0	−0·214	0	−0·256	0	−0·322	0
27	0	−0·159	0	−0·165	0	−0·175	0	−0·190	0	−0·213	0	−0·247	0	−0·297	0	−0·377
28	−0·183	0	−0·187	0	−0·196	0	−0·209	0	−0·230	0	−0·259	0	−0·301	0	−0·366	0
29	0	−0·232	0	−0·239	0	−0·252	0	−0·272	0	−0·301	0	−0·341	0	−0·400	0	−0·490
30	−0·330	0	−0·338	0	−0·351	0	−0·373	0	−0·406	0	−0·453	0	−0·519	0	−0·615	0
31	0	−0·648	0	−0·668	0	−0·702	0	−0·753	0	−0·827	0	−0·933	0	−1·080	0	−1·293
32	−0·031	0	−0·032	0	−0·033	0	−0·035	0	−0·038	0	−0·042	0	−0·048	0	−0·057	0

TABLE 13

Example of the Calculation of the Pressure Coefficient

Section : RAE 101, $t/c = 0{\cdot}12$

						$\varphi = 45$ deg $\cos\varphi = 0{\cdot}7071$					$\alpha = 4$ deg $\cos\alpha = 0{\cdot}9976$ $\sin\alpha = 0{\cdot}0698$ $\cos^2\alpha\sin^2\varphi = 0{\cdot}4976$			C_p upper surface		C_p lower surface
	(1)	(2)	(3)	(4)	(5)	(6)	(7)	(8)	(9)	(10)	(11)	(12)	(13)	(14)	(15)	(16)
ν	x_ν	z_ν	$S^{(1)}$	$S^{(2)}$	$S^{(3)}$	$\sqrt{\left\{1+\left[\frac{(4)}{\cos\varphi}\right]^2\right\}}$	$\frac{\cos\varphi+(3)}{(6)}$	$\sqrt{\left\{\frac{1-x}{x}\right\}}$	$1+\frac{(5)}{\cos\varphi}$	$\frac{(8)\,.\,(9)}{(6)}$	$\cos\alpha$ (7)	$\sin\alpha$ (10)	(11) + (12)	$1-\cos^2\alpha\sin^2\varphi$ $-(13)^2$	(11) − (12)	$1-\cos^2\alpha\sin^2\varphi$ $-(15)^2$
1	0·9904	0·00103	−0·1191	−0·1017	−0·2510	1·0104	0·5819	0·0984	0·6450	0·0628	0·5805	0·0044	0·5849	0·160	0·5761	0·171
2	0·9619	0·00408	−0·0671	−0·1082	−0·1670	1·0117	0·6326	0·1990	0·7638	0·1502	0·6311	0·0105	0·6416	0·091	0·6206	0·117
3	0·9157	0·00905	−0·0352	−0·1073	−0·1267	1·0115	0·6643	0·3034	0·8208	0·2462	0·6627	0·0172	0·6799	0·040	0·6455	0·086
4	0·8536	0·01571	−0·0096	−0·1070	−0·0932	1·0115	0·6896	0·4141	0·8682	0·3554	0·6879	0·0248	0·7127	−0·006	0·6631	0·063
5	0·7778	0·02385	0·0155	−0·1078	−0·0652	1·0116	0·7143	0·5345	0·9078	0·4797	0·7126	0·0335	0·7461	−0·054	0·6791	0·041
6	0·6913	0·03308	0·0438	−0·1050	−0·0335	1·0110	0·7427	0·6682	0·9526	0·6296	0·7409	0·0439	0·7848	−0·114	0·6970	0·017
7	0·5975	0·04261	0·0758	−0·0969	0·0034	1·0093	0·7757	0·8207	1·0048	0·8170	0·7738	0·0570	0·8308	−0·188	0·7168	−0·011
8	0·5000	0·05120	0·1092	−0·0774	0·0372	1·0060	0·8114	1·0000	1·0526	1·0463	0·8095	0·0730	0·8825	−0·276	0·7365	−0·040
9	0·4025	0·05749	0·1423	−0·0496	0·0740	1·0024	0·8474	1·2183	1·1047	1·3426	0·8454	0·0937	0·9391	−0·380	0·7517	−0·063
10	0·3087	0·06000	0·1736	0·0017	0·1119	1·0000	0·8807	1·4963	1·1583	1·7332	0·8786	0·1210	0·9996	−0·497	0·7576	−0·072
11	0·2222	0·05713	0·1773	0·0641	0·1222	1·0040	0·8809	1·8709	1·1728	2·1854	0·8788	0·1525	1·0313	−0·561	0·7263	−0·025
12	0·1464	0·05021	0·1776	0·1220	0·1274	1·0148	0·8718	2·4146	1·1802	2·8082	0·8697	0·1960	1·0657	−0·633	0·6736	0·049
13	0·08427	0·04028	0·1774	0·2061	0·1305	1·0416	0·8492	3·2971	1·1846	3·7498	0·8472	0·2617	1·1089	−0·727	0·5855	0·160
14	0·03806	0·02811	0·1777	0·3456	0·1332	1·1131	0·7949	5·0269	1·1884	5·3670	0·7930	0·3746	1·1676	−0·861	0·4184	0·327
15	0·00961	0·01443	0·1772	0·7430	0·1340	1·4506	0·6096	10·152	1·1895	8·3247	0·6081	0·5811	1·1892	−0·912	0·0270	0·502
16	0	(*0·07414)	0·1777	—	0·1348	—	0	—	1·1906	**16·059	0	1·1209	1·1209	−0·754	−1·1209	−0·754

*Value of $\sqrt{\left(\frac{\varrho}{2c}\right)}$

** $= \frac{(9)}{(2)}$

TABLE 12—*continued*

μ	ν															
	17	18	19	20	21	22	23	24	25	26	27	28	29	30	31	32
1	0	1·062	0	0·920	0	0·818	0	0·745	0	0·694	0	0·662	0	0·642	00	0·636
2	0·573	0	0·489	0	0·429	0	0·388	0	0·357	0	0·337	0	0·324	0	0·318	0
3	0	0·346	0	0·301	0	0·269	0	0·246	0	0·230	0	0·219	0	0·212	0	0·211
4	0·274	0	0·237	0	0·209	0	0·190	0	0·175	0	0·166	0	0·161	0	0·157	0
5	0	0·195	0	0·173	0	0·155	0	0·144	0	0·135	0	0·129	0	0·125	0	0·124
6	0·162	0	0·146	0	0·132	0	0·121	0	0·113	0	0·107	0	0·104	0	0·102	0
7	0	0·119	0	0·111	0	0·103	0	0·097	0	0·092	0	0·088	0	0·086	0	0·086
8	0·084	0	0·088	0	0·086	0	0·083	0	0·079	0	0·076	0	0·074	0	0·073	0
9	0	0·055	0	0·066	0	0·068	0	0·067	0	0·065	0	0·064	0	0·063	0	0·063
10	−0·013	0	0·033	0	0·047	0	0·053	0	0·054	0	0·055	0	0·054	0	0·054	0
11	0	−0·035	0	0·015	0	0·033	0	0·041	0	0·044	0	0·045	0	0·046	0	0·045
12	−0·219	0	−0·054	0	0	0	0·021	0	0·031	0	0·035	0	0·037	0	0·037	0
13	0	−0·239	0	−0·070	0	−0·013	0	0·011	0	0·021	0	0·027	0	0·029	0	0·029
14	−0·992	0	−0·257	0	−0·085	0	−0·024	0	0·001	0	0·012	0	0·019	0	0·020	0
15	0	−1·019	0	−0·277	0	−0·099	0	−0·036	0	−0·009	0	0·004	0	0·009	0	0·011
16	−11·736	0	−1·052	0	−0·298	0	−0·114	0	−0·047	0	−0·019	0	−0·006	0	0	0
17	32·155	−11·907	0	−1·094	0	−0·319	0	−0·129	0	−0·060	0	−0·030	0	−0·018	0	−0·014
18	−14·324	32·627	−12·190	0	−1·145	0	−0·344	0	−0·146	0	−0·074	0	−0·044	0	−0·033	0
19	0	−14·571	33·440	−12·596	0	−1·208	0	−0·375	0	−0·167	0	−0·092	0	−0·062	0	−0·053
20	−1·900	0	−14·991	34·637	−13·149	0	−1·285	0	−0·411	0	−0·192	0	−0·114	0	−0·087	0
21	0	−1·957	0	−15·606	36·284	−13·876	0	−1·383	0	−0·456	0	−0·225	0	−0·147	0	−0·126
22	−0·825	0	−2·044	0	−16·455	38·486	−14·821	0	−1·507	0	−0·515	0	−0·270	0	−0·196	0
23	0	−0·869	0	−2·167	0	−17·603	41·397	−16·051	0	−1·667	0	−0·594	0	−0·338	0	−0·281
24	−0·528	0	−0·933	0	−2·341	0	−19·148	45·255	−17·668	0	−1·881	0	−0·708	0	−0·451	0
25	0	−0·578	0	−1·025	0	−2·583	0	−21·247	50·442	−19·836	0	−2·178	0	−0·889	0	−0·671
26	−0·436	0	−0·653	0	−1·161	0	−2·930	0	−24·170	57·599	−22·827	0	−2·618	0	−1·217	0
27	0	−0·511	0	−0·767	0	−1·366	0	−3·445	0	−28·405	67·883	−27·150	0	−3·347	0	−1·981
28	−0·466	0	−0·635	0	−0·956	0	−1·699	0	−4·267	0	−34·956	8 83·620	−33·891	0	−4·828	0
29	0	−0·628	0	−0·860	0	−1·298	0	−2·305	0	−5·737	0	−46·220	110·237	−45·757	0	−9·569
30	−0·757	0	−0·979	0	−1·352	0	−2·053	0	−3·649	0	−8·976	0	−69·760	164·027	−73·139	0
31	0	−1·613	0	−2·115	0	−2·964	0	−4·575	0	−8·247	0	−20·295	0	−147·668	326·474	−263·566
32	−0·069	0	−0·088	0	−0·118	0	−0·171	0	−0·275	0	−0·529	0	−1·451	0	−12·979	—

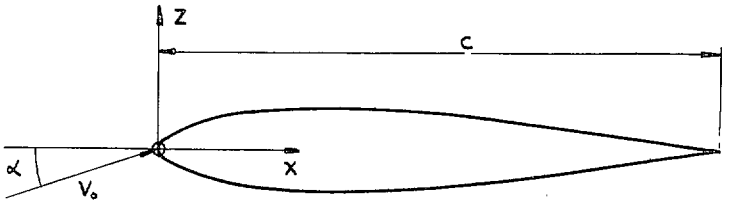

FIG. 1. Nomenclature.

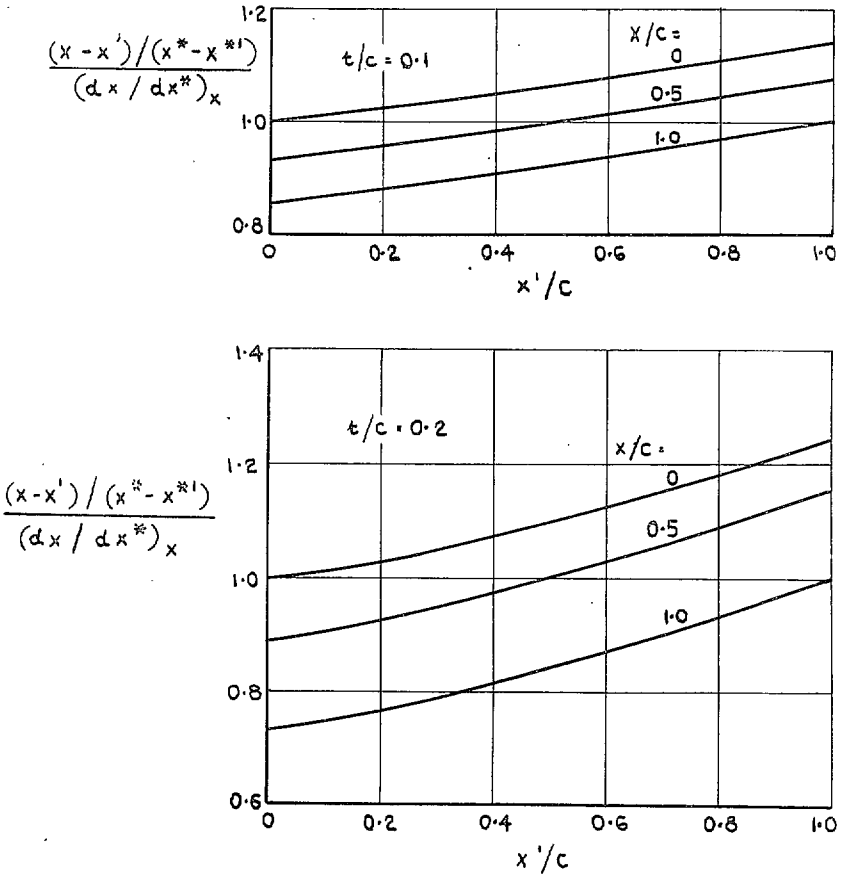

FIG. 2. Coefficient in equation (2–12) for Joukowski profiles.

EI

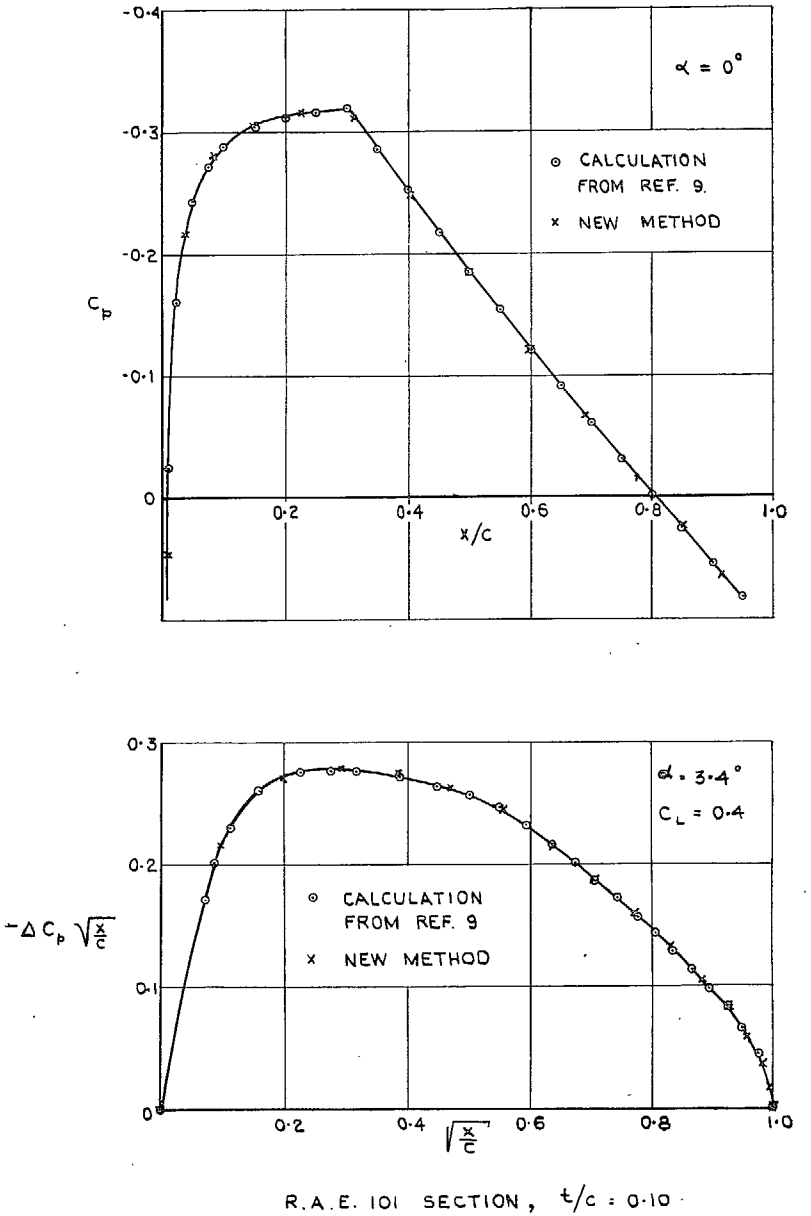

FIG. 3. Calculated pressure distributions for two-dimensional flow.

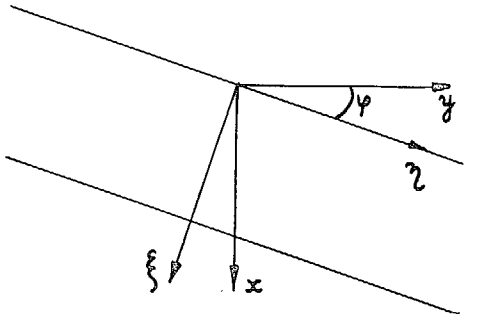

FIG. 4 Co-ordinate systems for sheared wing.

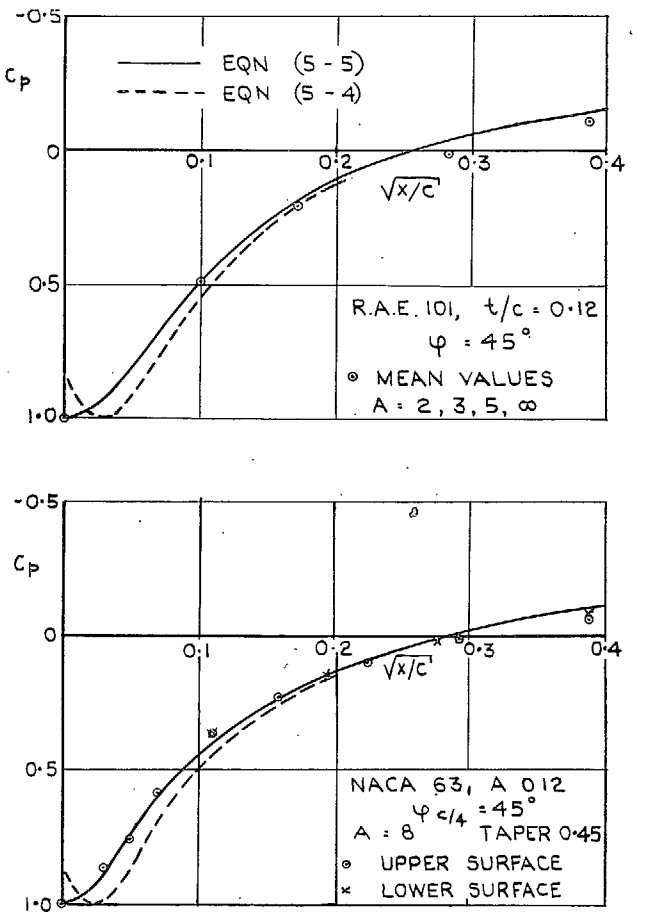

FIG. 5 Pressure distributions near the leading edge at the centre-section of swept-back wings at zero lift.

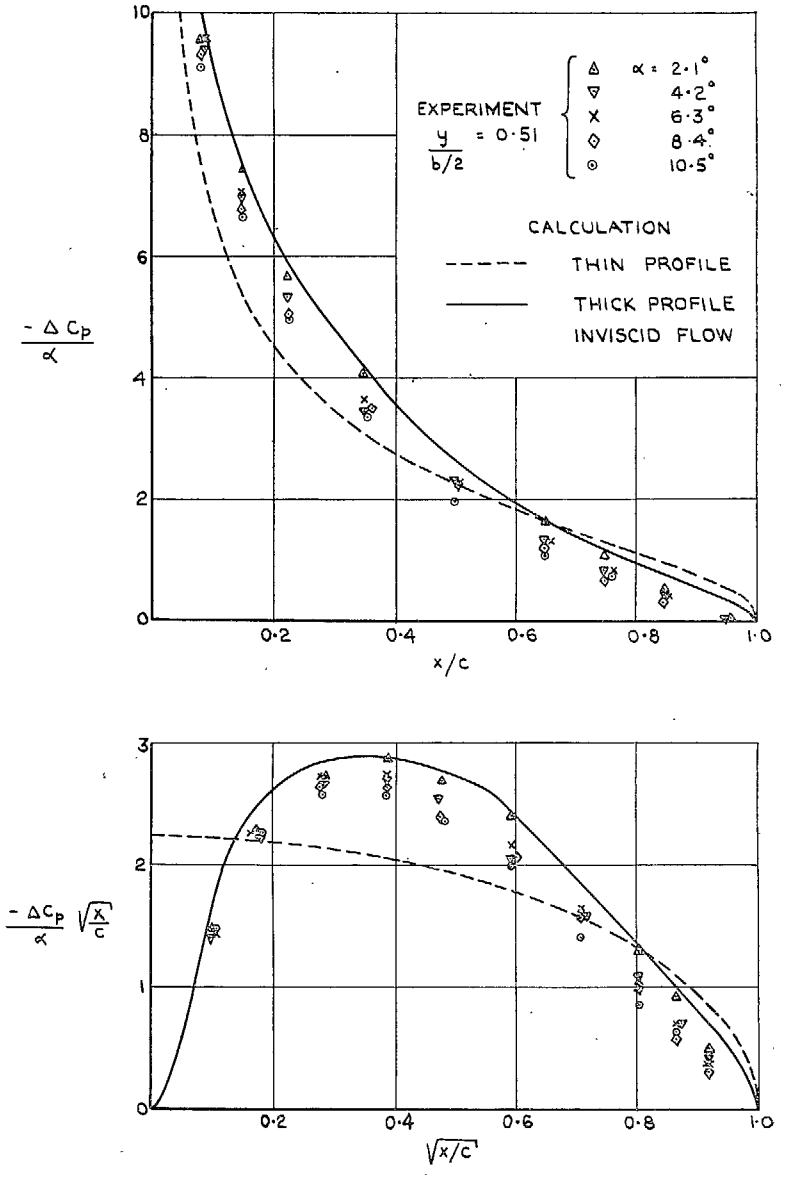

45° SWEPTBACK WING, A = 5, CONSTANT CHORD,
SECTION R.A.E. 101, t/c = 0·12

FIG. 6. Measured and culculated load distribtions at mid-semi-span.

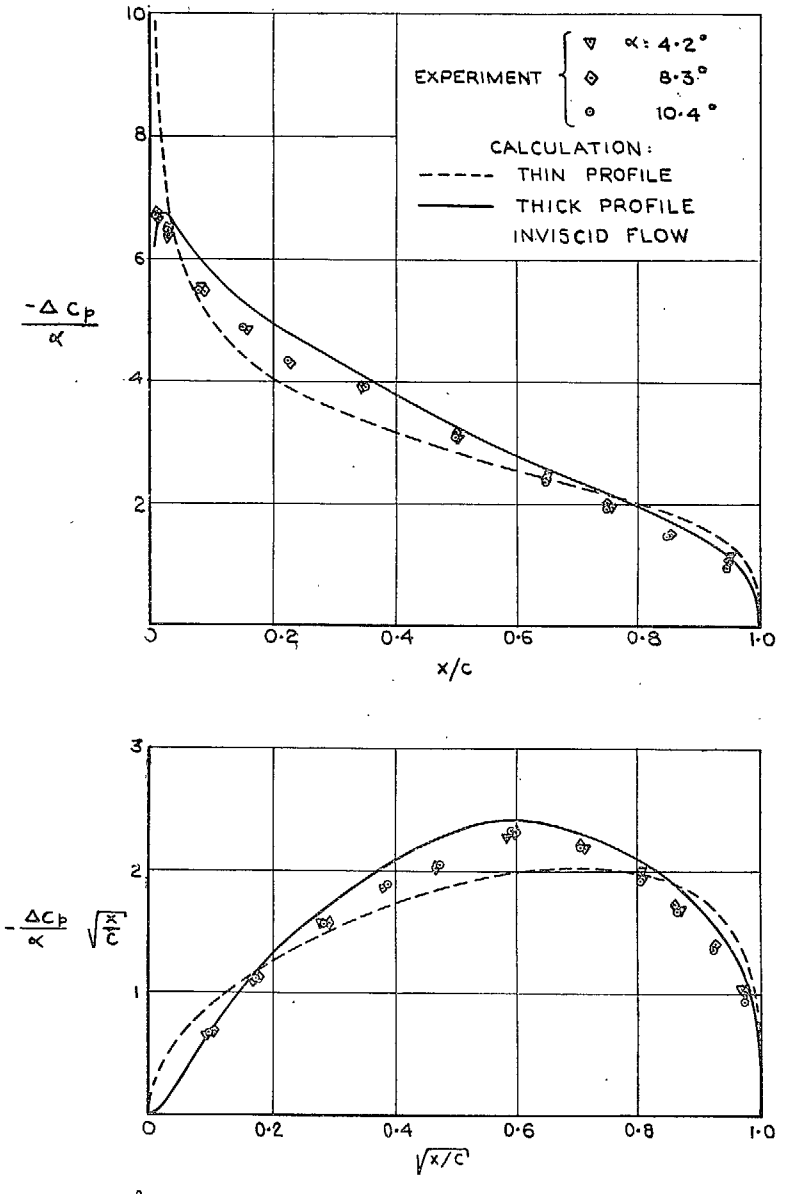

45° SWEPTBACK WING, A = 5, CONSTANT CHORD,
SECTION R.A.E. 101, t/c = 0·12

FIG. 7. Measured and calculated load distributions at the centre-section.

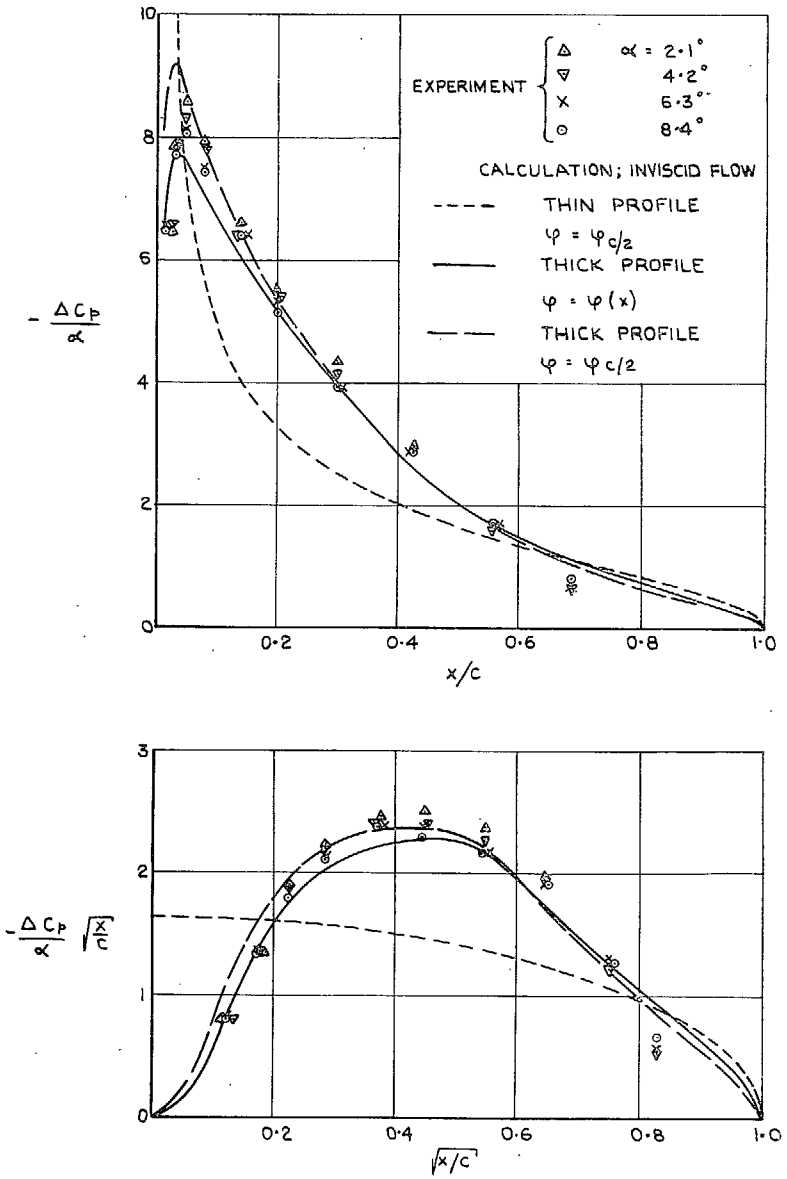

59° SWEPTBACK WING, A = 3·6, TAPER RATIO 0·25,
SECTION R.A.E. 101, t/c = 0·14.

FIG. 8. Measured and calculated load distributions at mid-semi-span.

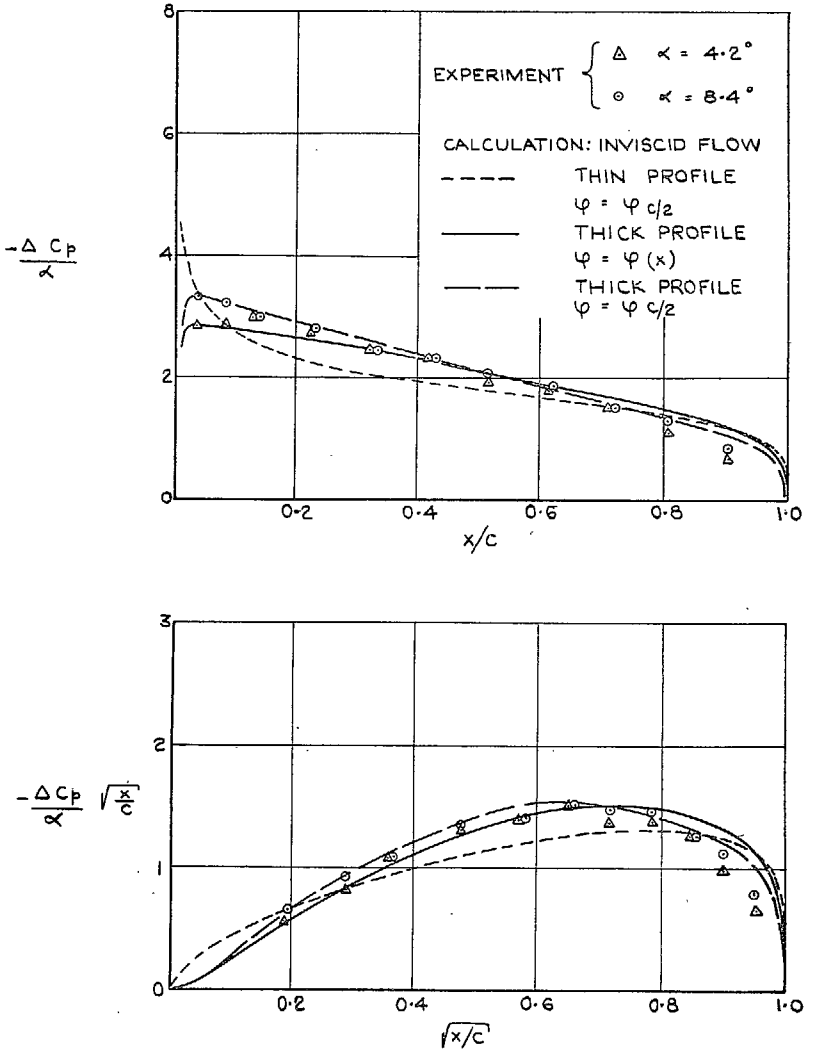

59° SWEPTBACK WING; A = 3·6; TAPER RATIO 0·25;
SECTION R.A.E. 101; t/c = 0·14.

FIG. 9. Measured and calculated load distributions at the centre-section.

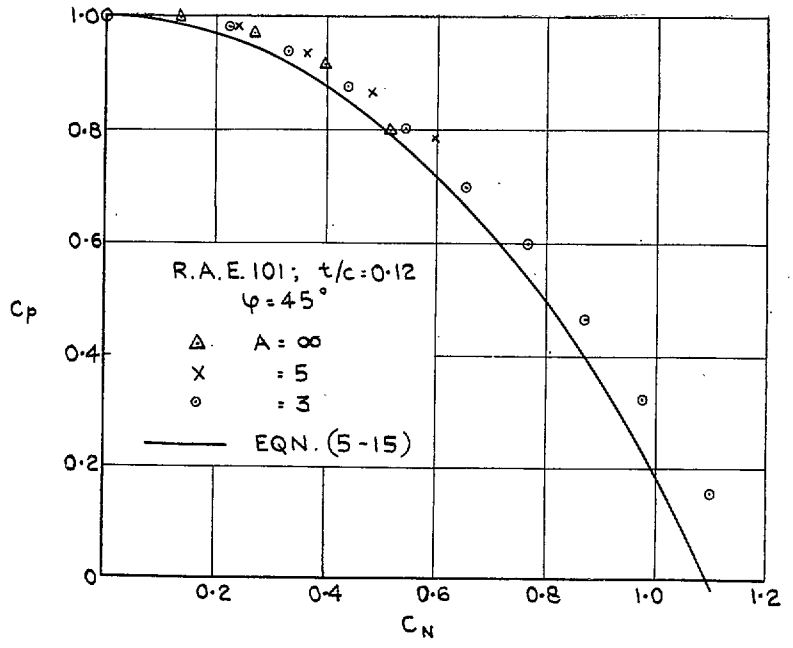

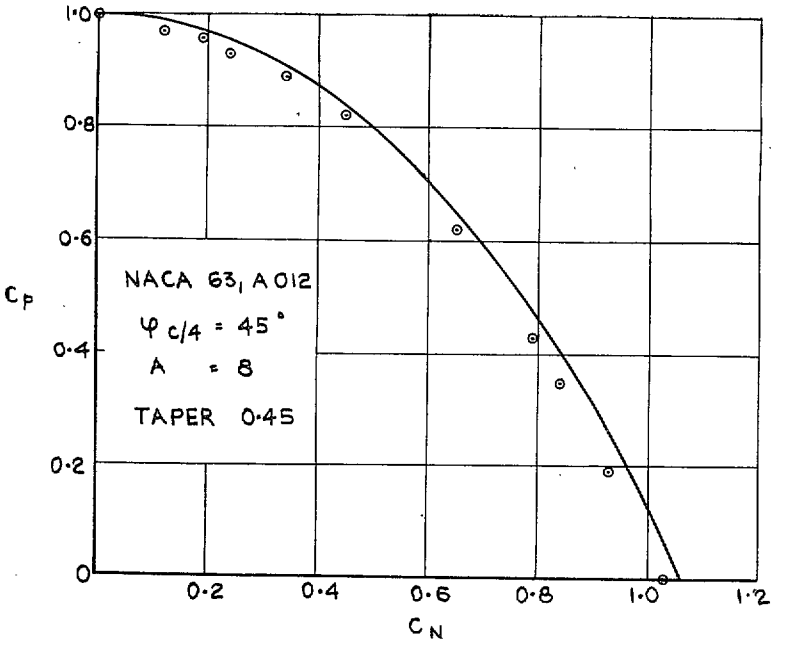

FIG. 10. Pressure coefficient at the leading edge at the centre-section of swept-back wings.

J4348 Wt.19/8411 K9 9/55 D&Co. 34/263

PRINTED IN GREAT BRITAIN

Publications of the Aeronautical Research Council

ANNUAL TECHNICAL REPORTS OF THE AERONAUTICAL RESEARCH COUNCIL (BOUND VOLUMES)

1938 Vol. I. Aerodynamics General, Performance, Airscrews. 50*s.* (51*s.* 8*d.*)
Vol. II. Stability and Control, Flutter, Structures, Seaplanes, Wind Tunnels, Materials. 30*s.* (31*s.* 8*d.*)

1939 Vol. I. Aerodynamics General, Performance, Airscrews, Engines. 50*s.* (51*s.* 8*d.*)
Vol. II. Stability and Control, Flutter and Vibration, Instruments, Structures, Seaplanes, etc. 63*s.* (64*s.* 8*d.*)

1940 Aero and Hydrodynamics, Aerofoils, Airscrews, Engines, Flutter, Icing, Stability and Control, Structures, and a miscellaneous section. 50*s.* (51*s.* 8*d.*)

1941 Aero and Hydrodynamics, Aerofoils, Airscrews, Engines, Flutter, Stability and Control, Structures. 63*s.* (64*s.* 8*d.*)

1942 Vol. I. Aero and Hydrodynamics, Aerofoils, Airscrews, Engines. 75*s.* (76*s.* 8*d.*)
Vol. II. Noise, Parachutes, Stability and Control, Structures, Vibration, Wind Tunnels. 47*s.* 6*d.* (49*s.* 2*d.*)

1943 Vol. I. Aerodynamics, Aerofoils, Airscrews. 80*s.* (81*s.* 8*d.*)
Vol. II. Engines, Flutter, Materials, Parachutes, Performance, Stability and Control, Structures. 90*s.* (91*s.* 11*d.*)

1944 Vol. I. Aero and Hydrodynamics, Aerofoils, Aircraft, Airscrews, Controls. 84*s.* (86*s.* 9*d.*)
Vol. II. Flutter and Vibration, Materials, Miscellaneous, Navigation, Parachutes, Performance, Plates and Panels, Stability, Structures, Test Equipment, Wind Tunnels. 84*s.* (86*s.* 9*d.*)

ANNUAL REPORTS OF THE AERONAUTICAL RESEARCH COUNCIL—

1933–34	1*s.* 6*d.* (1*s.* 8½*d.*)	1937	2*s.* (2*s.* 2½*d.*)
1934–35	1*s.* 6*d.* (1*s.* 8½*d.*)	1938	1*s.* 6*d.* (1*s.* 8½*d.*)
April 1, 1935 to Dec. 31, 1936	4*s.* (4*s.* 5½*d.*)	1939–48	3*s.* (3*s.* 3½*d.*)

INDEX TO ALL REPORTS AND MEMORANDA PUBLISHED IN THE ANNUAL TECHNICAL REPORTS, AND SEPARATELY—

April, 1950 – – – – – R. & M. No. 2600. 2*s.* 6*d.* (2*s.* 7½*d.*)

AUTHOR INDEX TO ALL REPORTS AND MEMORANDA OF THE AERONAUTICAL RESEARCH COUNCIL—

1909–January, 1954 – – – R. & M. No. 2570. 15*s.* (15*s.* 5½*d.*)

INDEXES TO THE TECHNICAL REPORTS OF THE AERONAUTICAL RESEARCH COUNCIL—

December 1, 1936 — June 30, 1939.	R. & M. No. 1850.	1*s.* 3*d.* (1*s.* 4½*d.*)
July 1, 1939 — June 30, 1945. –	R. & M. No. 1950.	1*s.* (1*s.* 1½*d.*)
July 1, 1945 — June 30, 1946. –	R. & M. No. 2050.	1*s.* (1*s.* 1½*d.*)
July 1, 1946 — December 31, 1946.	R. & M. No. 2150.	1*s.* 3*d.* (1*s.* 4½*d.*)
January 1, 1947 — June 30, 1947. –	R. & M. No. 2250.	1*s.* 3*d.* (1*s.* 4½*d.*)

PUBLISHED REPORTS AND MEMORANDA OF THE AERONAUTICAL RESEARCH COUNCIL—

Between Nos. 2251–2349. – –	R. & M. No. 2350.	1*s.* 9*d.* (1*s.* 10½*d.*)
Between Nos. 2351–2449. – –	R. & M. No. 2450.	2*s.* (2*s.* 1½*d.*)
Between Nos. 2451–2549. – –	R. & M. No. 2550.	2*s.* 6*d.* (2*s.* 7½*d.*)
Between Nos. 2551–2649. – –	R. & M. No. 2650.	2*s.* 6*d.* (2*s.* 7½*d.*)

Prices in brackets include postage

HER MAJESTY'S STATIONERY OFFICE

York House, Kingsway, London W.C.2; 423 Oxford Street, London W.1 (Post Orders: P.O. Box 569, London S.E.1); 13a Castle Street, Edinburgh 2; 39 King Street, Manchester 2; 2 Edmund Street, Birmingham 3; 109 St. Mary Street, Cardiff; Tower Lane, Bristol 1; 80 Chichester Street, Belfast, *or through any bookseller*

S.O. Code No. 23-2918